CHALMERS UNIVERSITY OF TECHNOLOGY **CHARMEC**

Mechanics and Maritime Sciences **Chalmers Railway Mechanics**

Tore Vernersson
Anders Ekberg
Roger Lundén

2020-10-09
79 pages

Report for
Mikael Aho
Transportstyrelsen

Swedish tests of block brake performance in winter conditions Winter 2019–2020

Summary

The Swedish Transport agency have arranged testing of LL brake blocks in the northern part of Sweden. These tests were performed from January through to April 2020, using a train built-up by one locomotive and five unloaded (empty) test wagons (2Bgu block configuration). Stop braking was performed from 100 km/h. The locomotive was unbraked during the tests.

The present report contains two parts. In Part 1 the focus is on braking distances of the test train when having uniform brake block types on the test wagons. In Part 2 the focus is on measured forces in hanger links, brake triangles, and on the braking performance also for a train with mixed block types. Measured data utilized in Part 1 include train speed and pneumatic pressure of the main brake pipe and of a brake cylinder. These were the only sampled signals for the first phase of the measurements (from January up to mid-February) for which a small data acquisition (DAQ) system was employed. After these tests, a large DAQ system was mounted that could acquire brake cylinder pressures of all wagons, and brake block temperatures, hanger link forces and brake triangle forces for about half of the wagons. Data from the large DAQ system are analysed in Part 2. In addition, metrological data from the Swedish Transport Administration (Trafikverket) have been merged with the on-train sampled information for tests on the Boden to Haparanda line for which a set of tests sites had been defined.

A total of 221 stop braking cycles were performed by the test train with uniform brake block types (either organic composite or sinter blocks) on the wagons. Of the braking cycle data, 18 were discarded because of brake valve malfunctioning. After braking with uniform block types, 163 additional stops were performed with cast iron blocks mounted in one bogie (replacing sinter). Of these 163 stops, the last 100 stops also had organic composite brake block in another bogie (again replacing sinter).

The results on braking distances for the test train when equipped with uniform brake blocks of either sinter type or organic type, indicate that the sintered brake blocks provide consistent braking performance irrespective of weather conditions. However, for the organic brake blocks, the weather conditions are found to be important for the braking performance, manifested as prolonged braking distances for situations with high UIC winter indices

(defined in UIC 541-4). For high UIC indices, with lots of snow whirling around the wagons, there is a trend with increasing braking distances for lowering of temperatures. This implies, presuming the identified trend continues for even lower temperatures, that unacceptably long braking distances would result for a temperature of around –30 ºC. However, since no such low temperatures were encountered during the present test campaign, this remains to be investigated.

The investigations of brake friction using data from instrumented hanger links and brake triangles show mixed results when it comes to dependencies on air temperature and UIC winter index. Some identified trends coincide with those found in the brake distance study pf Part 1, but this is not always the case. A general problem is that the test results are for a narrow range of temperatures, especially for the cast iron blocks and (even more) for the organic composite blocks. No data for these materials correspond to temperatures below -8 ºC, as the testing with these brake blocks were at the end of the test campaign when winter was giving place for spring season.

A study of the metrological winter conditions during the four latest winters is also provided in the present report. It shows that the winter season 2019–2020 was a very mild one, with substantially higher temperatures than for earlier winters and that it provided less duration of snowfall. Especially, the combination of snowfall and really low temperatures are less common than during previous years. Thus, the results should be judged with care, keeping in mind the relatively mild winter weather experienced during the test campaign, and the tentative braking performance problems that might occur at lower temperatures than studied so far. In fact, additional data from field tests performed at much lower temperatures than the ones studied here are necessary for demonstrating the suitability of LL brake blocks in general winter conditions.

Contents

1. BACKGROUND AND AIM

Reported safety incidents and general problems with winter braking performance for novel types of freight wagon brake blocks (read "not cast iron brake blocks") in Sweden (but also Norway and Finland) have drawn the attention of the Swedish Transport Agency (Transportstyrelsen). For this reason, the agency has arranged winter testing of LL type brake blocks in the northern part of Sweden for three consecutive years. Tests during the winter 2017–2018 were performed using wagons with a mix of cast iron and LL-type brake blocks, meaning that a comparison of braking distances resulting from the different types of brake blocks was not possible. The winter test performed 2018–2019, again employing wagons with mixed blocks types, were unfortunately delayed until April 2019, just after the winter had ended. Only a few days of testing were performed as a precursor for the tests during winter 2019–2020, when a large campaign was launched. The campaign was performed in line with the test specification issued by the Swedish Transport Agency[1].

From January through to April 2020, a dedicated test train, built-up by one locomotive and five unloaded test wagons (wagon type Habbins having 2Bgu block configuration) was employed for winter testing. The locomotive (Green Cargo locomotive of RD type) was unbraked during the brake tests.

Part 1 of the present report focusses on braking distances of the test train when having one single brake block type on the test wagons. Measured data include train speed, pneumatic pressure of the main brake pipe (connection between locomotive and trailing wagon) and of one brake cylinder. These were the only sampled signals for the first part of the measurements (from January up to mid-February) for which a small data acquisition (DAQ) system was employed. After this a large DAQ system was mounted that was capable of acquiring brake cylinder pressures of all wagons, and also hanger link forces and brake triangle forces for about half the wagons. Also brake block temperatures could be acquired. The measuring systems employed during the test campaign are detailed in a separate report[2]. The analyses are based on data provided on Excel data sheets by on-train test engineers and the data files that were generated during the tests[3]. To this end, data were imported into Matlab[4] to allow for straightforward processing, structuring and visualization of results. In addition to the sampled data, metrological data[5] from weather stations (VViS, supplied by the Swedish Transport Administration, Trafikverket) adjacent to test sites have been merged with the on-train sampled information.

Part 2 of the report focusses on analysis of data from the large DAQ system. Early in these tests, there was one single brake block type in the wagons (sinter), but later cast iron blocks were installed in one bogie and organic composite blocks in another bogie. The detailed

---

[1] M. Aho, Test Specification: Brake equipment for freight wagons, TSJ 2019-5343, *Transportstyrelsen*, 2019

[2] I. Brottare, Brake performance tests of brake blocks in winter conditions, *AFRY Test Center*, Report No 6190113:01, 2020-10-09

[3] Nominal braking information in xlsx-format and time history data files in DeWeSoft-format supplied by AFRY Test Center, uploaded to common SharePoint drive.

[4] Matlab, version R2019b, *The MathWorks, Inc.*, Natick, Massachusetts, USA, 2019

[5] Personal communication, V. Moberg (Trafikverket) and M. Aho (Transportstyrelsen), 2020-04-07.

measurements allow for calculation of for instance braking energy of an entire bogie or the braking energy related to a single brake block insert.

The general aim of the Swedish winter tests is to objectively investigate winter performance of LL brake blocks and to find specific weather conditions for which the braking performance may be deteriorated. The work presented in this report aims at revealing the braking performance of the winter train in an objective way. Another aim has been to find possible causes for deteriorated braking based on measured data.

2. TEST TRAIN, TEST SITES AND DATA ACQUISITION SYSTEM

The test train was provided by Green Cargo, see Figure 1. The five wagons of type Habbins-15, see Figure 2, have Y25 bogies and are equipped with one brake cylinder per wagon. The brake block configuration of the wagon is 2Bgu. The wheel diameters of the wagons range from 884 mm to 923 mm[6]. The tare weight of a wagon is about 26 metric tonnes. The wagons were subjected to maintenance prior to testing at which the brake rigging system was lubricated. The efficiency of the wagons after this was measured by DB Systemtechnik (supported by UIC), see details in Section 4.1.6. The wagons were completely de-iced every two to three weeks during the test campaign.

The test train is powered by an RD type locomotive, equipped with the novel ERTMS signalling system. The mass of the locomotive[7] is 78 tonnes and its dynamic mass is 89 tonnes. The locomotive had no operating brakes[8] during the test runs.

Figure 1 Test train consisting of locomotive and five freight wagons an early morning in Haparanda, March 2020.

---

[6] New wheels having diameter 923 mm on 17 out of 20 wheelsets. Worn wheelset diameters were 914 mm for axle 4 of wagon 2, 890 mm for axle 1 of wagon 3 and 884 mm for axle 2 of wagon 3.

[7] Järnvägsföretagets säkerhetsbestämmelser, del A, *Green Cargo*, Document Number C82-08 A, second edition.

[8] A pneumatic valve was operated to immobilize the locomotive brakes. The locomotive has no ED braking.

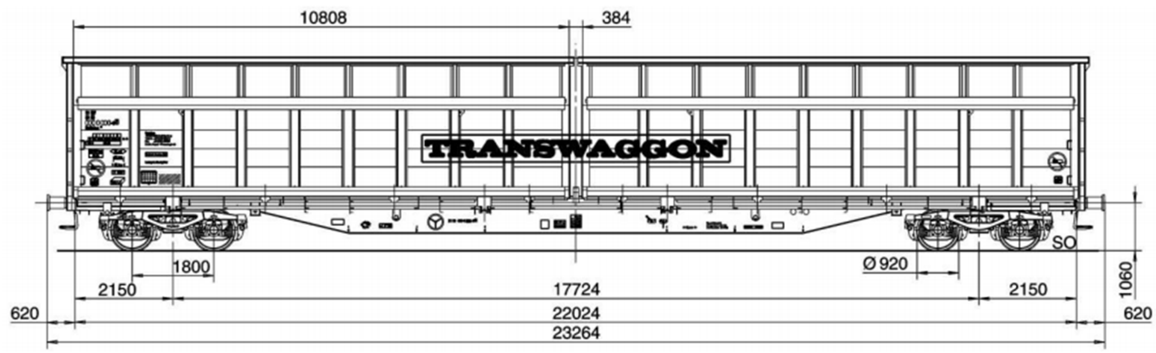

Figure 2 Test wagon of type Habbiins-15, extract from https://transwaggon.com/images/pdf/wagons-specs/HB_15.pdf.

The reported tests in Part 1 of the report (with focus on braking distances) were all performed on the line between Boden and Haparanda. An overview of the test sites is given in Figure 3. Also marked on the map are weather stations from which metrological data are extracted. Regarding Part 2 of this report (with focus on measured forces), the early phase was performed on the same line, while the last part was performed on the Iron Ore Line. Note that the large DAQ system was installed during the tests when the wagons had one single type of brake blocks. Thus, some brake cycles are reported in both Part 1 and Part 2 of the report. An overview of the two data acquisition systems employed during the testing period are given in Figure 4. A laptop in the locomotive was plugged in to the data bus that connected the separate measurement systems located on wagons (not detailed here). Not shown in the overview are 1) The GPS sensor which supplied speed signal and GPS coordinates, and 2) The video camera that was mounted outside of the locomotive and provided a view of trailing wagons. Sensor data were sampled using the DEWESoft software[9] at a rate of 100 Hz.

Figure 3 Map of test track between Boden and Haparanda with test sites indicated by encircled site numbers 1 - 6. Red markers show locations of relevant weather stations (positioned along roads). Inset indicates the test region via the red square.

---

[9] DEWESoft X3 SP10, DEWESoft d.o.o, Gabrsko 11a, 1420 Trbovlje, Republic of Slovenia, see www.dewesoft.com

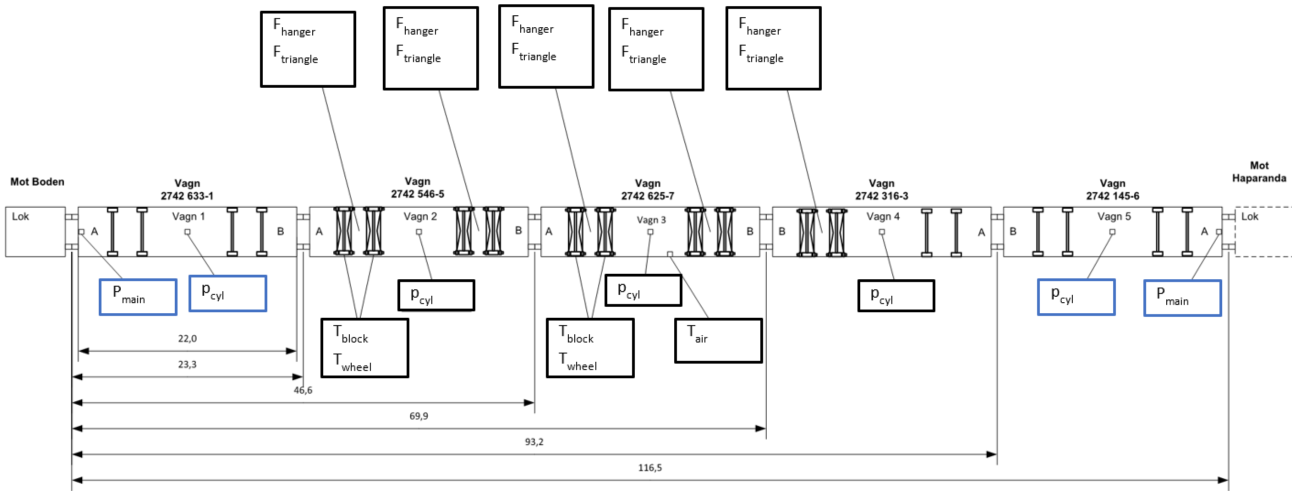

Figure 4 Overview of train and DAQ systems, adapted from AFRY-report, indicating positions of sensors for main pipe pressures (p_{main}), brake cylinder pressures (p_{cyl}), hanger link forces (F_{hanger}) and brake triangle forces ($F_{triangle}$). Sensors in blue squares are for the part of the measurement campaign when using the small DAQ system (reported in Part 1) and the ones in black squares were added when the large DAQ system was introduced.

3. METHOD OF DATA ANALYSIS

3.1. Part 1: Braking distances for uniform blocks

Firstly, the nominal data, i.e. data according to the test plan and noted in Excel sheets on the train during testing, were read into Matlab, providing the following information for the individual brake cycles: test run number of day, date and time, test site no, track distance mark, average track gradient (always nil for test sites), initial speed of braking, nominal main pipe braking pressure, outdoor temperature and braking distance. For each test run, information is also given on prevailing snow whirling conditions employing the UIC snow whirling index, as defined in Appendix G of UIC 541-4[10]. After this, acquired time data were imported. In the acquired time data, each individual brake cycle was identified by a graphical on-screen procedure based on 1) finding the approximate time period using supplied time marks, and 2) manually introducing one mark prior to start of braking and one mark after end of each brake cycle. After completion of this procedure a more exact numerical analysis of the brake data was carried out.

The chosen start of braking was taken as the time point (and related distance mark) when the brake cylinder pressure starts to increase, which is manifested as a distinct pressure peak in the data, see example in Figure 5, at time 4.7 s. This procedure was chosen instead of an alternative method to make detection based on decrease in the main pipe pressure, since this would give a less distinct start of the braking and thus could introduce an error in braking distances.

The end of the braking cycle should ideally be taken as the time (and related distance mark) when the train was at full stop. However, on one of the first days of field testing it was detected by in-track wheel impact load detectors that small wheel flats had formed on the wheels on some wagons of the test train. The reason for this was the increasing coefficient of friction at lower speeds, intrinsic to the LL type blocks. Consequently, it was decided that the locomotive driver should abort the braking at a speed of approximately 30 km/h, which has the effect that the main brake pipe pressure starts to increase and that the brake cylinder pressure accordingly slowly decreases, see Figure 5. Depending on the overall conditions, this operating procedure meant that the train deceleration towards lower speeds was modified by the lowered brake block normal force and that the train rather frequently did not come to a full stop at end of the brake cycle. An extrapolation scheme needed to be introduced to numerically estimate a stopping distance of the train that could be used for comparison of braking performance. Methods for performing this extrapolation are discussed in Section 4.1.1.

The stop braking distances are corrected for differences in initial speed by employing a correcting factor being the square of the ratio between actual initial speed and nominal speed (100 km/h), in accordance with UIC leaflet 544-1[11]. The correction should according to the leaflet only be used for braking cycles with speed deviations lower than 4 km/h. In the present report the correction factor has however been used for all braking cycles, irrespective of initial speed deviations. All brake cycles are performed at the same nominal pneumatic settings with a main pipe reduction of the pressure to 3.3 bar, with a resulting brake cylinder pressure of about 1.3 bar, corresponding to full service braking of the train.

---

[10] UIC CODE 541-4, Composite brake blocks – General conditions for certification and use, 5th edition, *UIC*, November 2018.
[11] UIC CODE 544-1, Brakes – Braking power, 4th edition, *UIC*, October 2004.

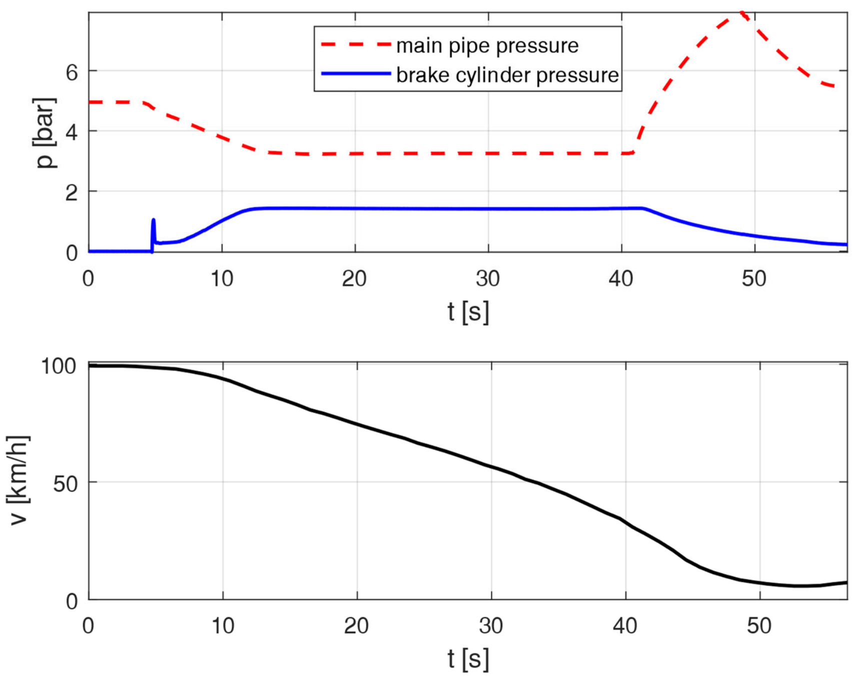

Figure 5 Example history of main pipe pressure, brake cylinder pressure and speed.

In addition to the sensor data, metrological information from weather stations at sites near to the sites for brake testing, see Figure 3, has been added to the database. The locations of the test sites have been added to the map using GPS data from some chosen brake cycles. The data include the following metrics:

1. Air temperature T_{air} [°C]
2. Surface temperature T_{surf} [°C]
3. Air dew point temperature $T_{air,dew}$ [°C]
4. Surface dew point temperature $T_{surf,dew}$ [°C]
5. Air humidity RH [%]
6. Wind speed, average v_{wind} [m/s]
7. Wind speed, maximum $v_{wind,\ max}$ [m/s]
8. Snow precipitation P_{snow} [mm/30 min]
9. Rain precipitation P_{rain} [mm/30 min]
10. Melting P_{melt} [mm/30 min]

Based on air temperature and snow precipitation, a metric that describes the possibility for snow drift D_{snow} could be calculated based on a report developed for assessing risks of winter problems in road traffic[12]. According to the report, snow is prone to drifting if all of the following conditions are fulfilled:

[12] S. Möller, Calculation model for VädErsKombi (in Swedish), version 1.00, VTI notat 38-2003, *The Swedish national Road and Transport Research Institute*, Linköping Sweden, 2003

1. Snow has fallen during the 14 recent days. The snow precipitation[13] shall be at least 2.0 cm (solid form) under a period of 24 h.
2. **During** the last snowfall with at least 2.0 cm snowfall the air temperature (half-hour readings) has been higher than +0.5 ºC at the most 6 times (3 h totally, does not have to be in succession).
3. **After** the last snowfall with at least 2.0 cm snowfall, rain (half-hour readings) has occurred no more than 3 times (1.5 h totally, does not have to be in succession).
4. **After** the last snowfall with at least 2.0 cm snowfall, the air temperature (half-hour readings) has been higher than +0.5 ºC at the most 12 times (6 h totally, does not have to be in succession).

Metrological data were received for the past four years, which also allows for a statistical comparison between different winter seasons, see Section 4.3.

3.2. Part 2: Braking forces, braking energies and friction coefficients

Here, the data from the large DAQ system is analysed. As explained previously, in the first phase of the tests, there were sinter brake blocks on all of the wagons. In a second phase of the tests, bogie 1 of wagon 2 was equipped with cast iron blocks and, finally, in the third phase bogie 2 of wagon 2 was equipped with organic composite blocks. Braking distances for the first phase are analysed in Part 1 of the report.

In addition to the analyses performed in Part 1, also measured forces in brake triangles, denoted F_t, and hanger links, F_h, are exploited. These additional data make possible a detailed analysis of the friction conditions at brake block inserts. The friction force at a block insert (or for a wheel or a bogie) can be calculated (using measured hanger link angles and estimated height of brake force application).

Based on the geometry of the wagon brake rigging system, the braking normal force on an insert and the pertaining friction force can straightforwardly be calculated for hangers 3 to 14 (that is all hanger links except those mounted at both ends of the wagon, being hangers 1, 2, 15 and 16) from measured forces in the brake triangle and hanger link forces. For these hangers, the riggings system provides a brake normal force that is acting approximately in the horizontal plane. However, the brake triangles will be in a rotated position, thus not in the horizontal plane as depicted in Figure 6. The actual positions will depend on wheel sizes, that are used to prescribe the proper adjustments settings for the brake rigging system for the Y25 bogie, but also the wear states of the brake blocks will have an influence. This means that these brake triangles (all triangles except the two at the ends of the wagon) are positioned so that the brake normal force is acting in a plane that is below the wheel centres. The effect of this is that the measured hanger link forces are directly affected by the brake normal force in such a way that tensile forces are added to the hanger link force. This produces a tensile offset force that is superimposed on the friction force measured by a hanger link.

[13] A requirement on wind speed given in the report has been neglected. It is assumed that the running train provides the required speed for drifting of the snow.

For the hanger links at the ends if the wagon, the brake triangles are mounted so that they are positioned above the plane of the wheel centres. The brake force is here transmitted via a lever arm that has a fixed upper point, see Figure 6, as compared to the floating arrangements for the ones discussed above. Similar as above, this means that the measured hanger link force is affected by an offsetting force, because of the brake normal force, that here is being acting in compression.

Based on force and moment equilibrium equations, the brake block normal forces and brake block friction forces can be determined for all brake block inserts.

The time delay until a particular brake block insert starts to contribute "significantly" to the total braking power is also assessed. Here, some different assumptions have been made on how to define the meaning of a "significant" part of each brake cycle. Firstly, an analysis was performed based on the instantaneous friction force and secondly a criterion based on (accumulated) braking energy was employed.

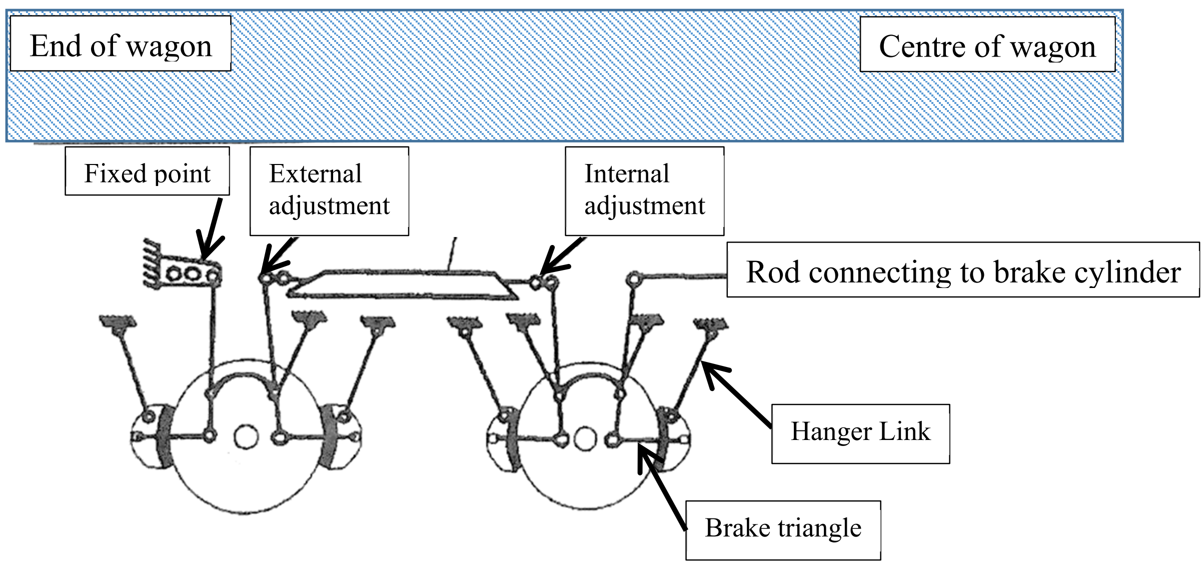

Figure 6 Schematic view of brake rigging system and possibilities for adjustments to various wheel sizes. The specific sketch shows the system for a situation with all brake triangles being horizontal[14].

[14] Schematic figure of brake rigging from Swemaint wagon manual.

4. Results and discussion

In Part 1 the focus is on braking distances for brake cycles having the wagons equipped with uniform brake block types. In Part 2 the focus is on measured forces and braking energies.

No temperature results for brake blocks are presented because of almost immediate failure of the thermocouple measurements. Most likely, it was the massive build-up of ice and snow around the brake blocks that caused the thermocouple wires to break due to falling off of larger pieces of ice or snow.

4.1. Part 1: Braking distances for uniform block configuration

A total of 221 stop braking cycles were performed by the test train, out of which 18 were removed because of malfunctioning of pneumatic brake cylinder valve(s) on one or two wagons. These 18 stops are shortly discussed in Appendix C. Remaining are 203 stop braking cycles, of which 94 are for reference conditions R0, and 109 stops for winter conditions W1–W5. There were sinter blocks on the wagons for 130 of the stops and organic composites for the remaining 73 stops.

In the following, an extrapolation scheme for finding comparable braking distances is introduced and this is followed by a presentation of results from the brake tests. Finally, explanatory relationships for deteriorated braking performance are explored using linear regression modelling.

4.1.1. Extrapolation of braking distance

The result shown in Figure 5 is an example of a brake cycle for which the train is not stopping completely at the end of the brake cycle as a consequence of the low-speed brake abortion procedure employed to avoid wheel flats. As discussed above, an extrapolation scheme is required for calculating an estimated stop braking distance of the train. This has been explored by implementing four different proposed methods that were implemented and explored in sequence:

Version E1

- Extrapolation using mean deceleration during time for which the cylinder pressure is constant.
- Only if lowest speed for cycle is larger than 0.1 m/s

Version E2

- Extrapolation using deceleration at time point at which cylinder pressure starts to decrease.
- Curve fitting of speed signal to find deceleration.
- Only if lowest speed for cycle is larger than 0.1 m/s

Version E3

- Extrapolation using deceleration at time point at which cylinder pressure starts to decrease.
- Curve fitting of speed signal to find deceleration.
- Implemented for all brake cycles regardless of final speed (c.f. Version E2)

Version E4

- Extrapolation for all stops with lowered cylinder pressure.

- Curve fitting of speed signal during time with lowered cylinder pressure to find maximum deceleration.
- Extrapolation of speed using that deceleration until stop used to find total braking distance

A suitable extrapolation scheme should reflect the conditions at the tests as well as possible. Employing Version E1 does not reflect the increase of deceleration that can be perceived from the information in Figure 5. Clearly, there is an increase in deceleration for speeds lower than about 50 km/h as compared to the average reduction between 90 km/h (when the brake cylinder pressure reaches its nominal value) and 28 km/h (when the brake cylinder pressure starts to decrease). This method would mean an over-estimation of the braking distance. Upon this finding, the time variation of the train deceleration was studied in more detail, see Figure 7. Here, only brake cycles which have full cylinder pressure[10] on each of the chosen 4 km/h speed intervals were considered. The figure clearly shows that the train deceleration increases with decreasing speed. Assumption E1 that employs the average friction value for higher speeds will then always give a braking distance to stop that is longer than the distance that would have resulted if the braking pressure would have been constant until train stop.

Extrapolation E2 means an improvement of E1 since it employs the deceleration at the time point the brake cylinder pressure starts to decrease. Consequently, it also gives shorter estimated stop braking distances than scheme E1. In scheme E3 it was additionally chosen to implement the scheme E2 for all brake cycles. Prior to this, focus had been entirely on the 93 brake cycles for which the train was rolling at the end of the brake cycle.

The result of additional investigations of variation of train deceleration using the same methodology as when producing Figure 7, but now considering all the brake cycles, are presented in Figure 8. Here also the dependence on cylinder pressure is indicated by providing also the mean cylinder pressure for each of the 4 km/h intervals. The figure reveals that for low speeds, the deceleration can be even higher for cylinder pressures slightly higher than 1 bar as compare to full brake cylinder pressures at about 1.3 bar. This is not reflected by interpolation schemes E2 (or E3) and leads to the introduction of scheme E4 that employs extrapolation for all stops that have a lowered cylinder pressure at end of the braking cycle. It builds on curve fitting of the speed signal to find the time point with maximum deceleration.

To this end, the stopping distance is found by:

1. integration of the speed signal up to the point of maximum deceleration during the period of decreasing cylinder pressure, yielding the braking distance $S_{\mathrm{fullbrake}}$
2. integration of extrapolated speed variation based on constant (maximum) deceleration until stop, yielding the braking distance S_{extrap}
3. Total braking distance is found as $S_{\mathrm{stop}} = S_{\mathrm{fullbrake}} + S_{\mathrm{extrap}}$

The relationship between the extrapolated part of the braking distance and the total braking distance is shown in Figure 9. The extrapolated distance is lower than 5% of the total distance for 63 % of the brake cycles and less than 10 % for 97 % of the cycles. The mean value of the extrapolated part[15] is 30 m and it has a standard deviation of 24 m, and the mean of the total braking distance is 758 m with a standard deviation of 101 m.

[15] The of the ratio between actual initial speed and nominal speed (100 km/h), in accordance with UIC leaflet 544-1. However, the correction has been used for all braking cycles, not only those with speed deviations lower than 4 km/h.

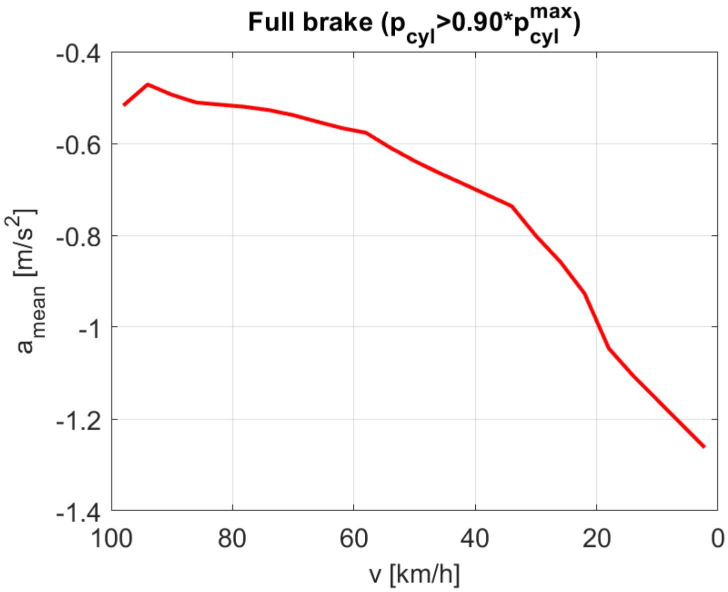

Figure 7 Average acceleration on 4 km/h speed intervals, as function of speed. For each speed interval, all braking cycles are considered which have full braking pressure[16] on that interval.

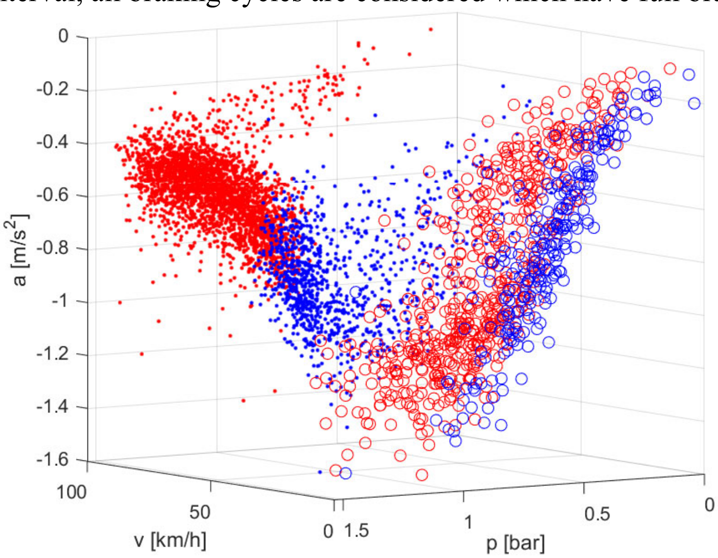

Figure 8 Average acceleration on 4 km/h speed intervals, as function of speed and brake cylinder pressure. For each speed interval, the average braking pressure on that interval was calculated. Red dots are for speeds higher than 40 km/h, blue dots are between 40 and 20 km/h, red circles are between 20 and 10 km/h, and blue circles are between 10 and 0 km/h.

[16] Numerically implemented as if cylinder pressure is higher than 90% of maximum braking pressure for that braking cycle

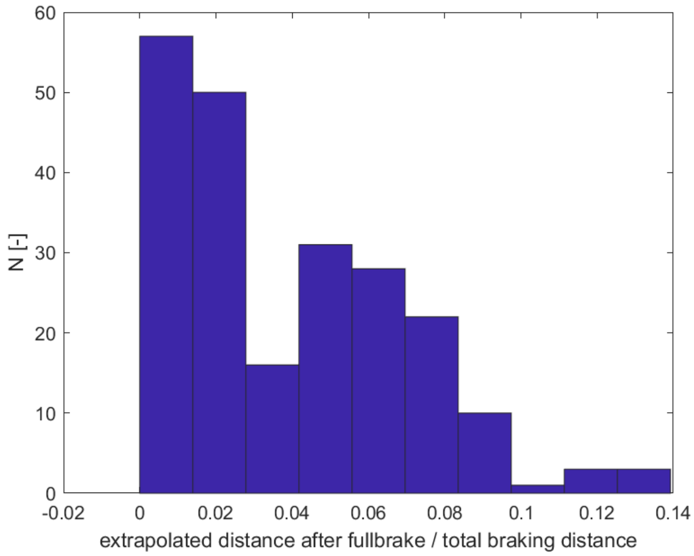

Figure 9 Histogram over ratio of S_{extrap} / S_{stop} showing number N of brake cycles falling into different ranges of extrapolation ratio**.**

4.1.2. General on stop braking cycles

In total 203 brake cycles are available for analysis, 73 for organic composite blocks and 130 for sinter blocks. The initial speeds v_{init} of the studied brake cycles are shown in Figure 10. The average initial speed is 98.6 km/h and the standard deviation is 3.3 km/h. As described earlier, stop braking distances are corrected for differences in initial speed by employing a correcting factor being the square of the ratio between actual initial speed and nominal speed (100 km/h), in accordance with UIC leaflet 544-1. The average brake cylinder pressures for the time duration of full braking pressure[17] are given in Figure 11. The average brake cylinder pressure is 1.35 bar and the standard deviation is 0.06 bar.

[17] Numerically implemented as when cylinder pressure is higher than 90% of maximum braking pressure for that braking cycle

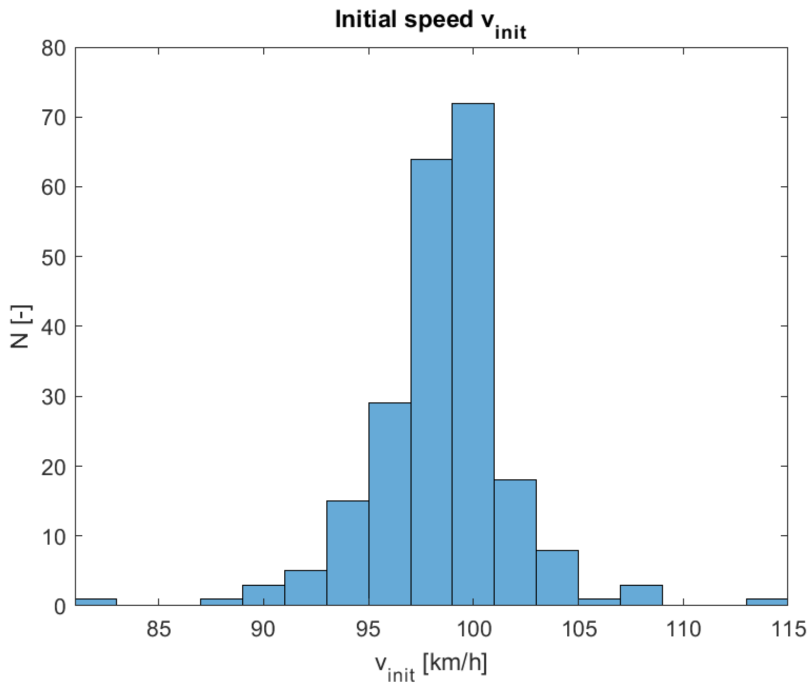

Figure 10 Actual initial test speeds for the studied 203 stop braking cycles.

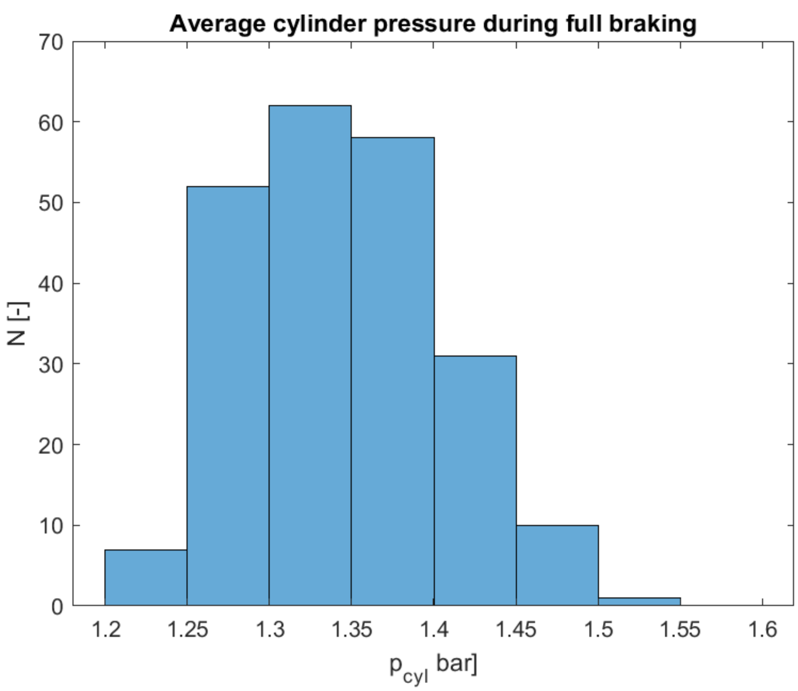

Figure 11 Actual average brake cylinder pressures during the time with full braking pressure for the studied 203 stop braking cycles.

4.1.3. **Braking distances**

A first overview of the braking distances estimated as above of the entire test campaign with uniform blocks on the test wagons is given in Figure 12. These results indicate that the differences between R0 and W1–W5 are rather minor for LL type brake blocks. For R0 conditions, the average braking distance is 772 m with a standard deviation of 80 m whereas for W1–W5 the average is 791 m (a 2.5% increase) with standard deviation 88 m (a 10% increase).

Another overview is given in Figure 13, which shows braking distances as a function of sequential brake cycle number performed per block type. For the sinter blocks, there is a tendency that the first 30 stop braking cycles have prolonged distances and that the distance (on average) decreases for each of those braking cycles. It is noted that 6 out of these 30 cycles are for UIC snow whirling conditions and that they are found between cycle 17 and cycle 30. These results for the sinter blocks indicate that the sinter blocks perhaps still were bedding-in during these first 30 brake cycles.

When splitting the results to study the two block types separately, a different picture appears, see Figure 14 and Figure 15, which show results for sinter and organic composite block, respectively.

For the sinter brake blocks (Figure 14), the bottom figure shows a constant or slight *decrease* in average braking distances for increasing snow whirling conditions (from R0 up to W5). Similarly, there is a trend of decreasing standard deviation of braking distances with increasing snow whirling. The average braking distance is 772 m for R0 and the averages for W1–W5 range between 753 m and 764 m.

For the organic composite brake blocks (Figure 15), the bottom figure shows an increase in average braking distances for conditions with whirling snow (W1–W5) as compared to when no snow whirling is present (R0). The maximum braking distances are found for conditions W3 with an average braking distance being 25 % higher than for R0. Similarly, there is a trend of increase in standard deviation of the braking distances with increasing snow conditions (with exception W3 having low standard deviation). The average braking distance is 724 m for R0 and the averages for W1–W5 range between 792 m and 908 m.

The results in the bottom graphs of Figure 14 and Figure 15 also holds the results of an assessment in which the braking distances were compensated also for the (slight) variations in average braking pressure (see Figure 11). It was found that the introduction of such a compensation did not yield a consistent improvement (decrease) of the standard deviation of the braking distances and for this reason it has *not* been implemented elsewhere in the present report.

A more detailed view of the braking cycles that build up the results are shown in the top five histograms in Figure 14 and Figure 15. It can be noted that for R0 conditions, the sinter blocks are responsible for all but two brake cycles with braking distances longer than 850 m. Moreover, for the sinter blocks there are only four brake cycles that fall into the W4 and W5 conditions, whereas for the organic composite blocks there are 47 braking cycles. For the organic composite block, there are a large number of cycles that have braking distances larger than 850 m for W2–W5 conditions, but none for R0 conditions.

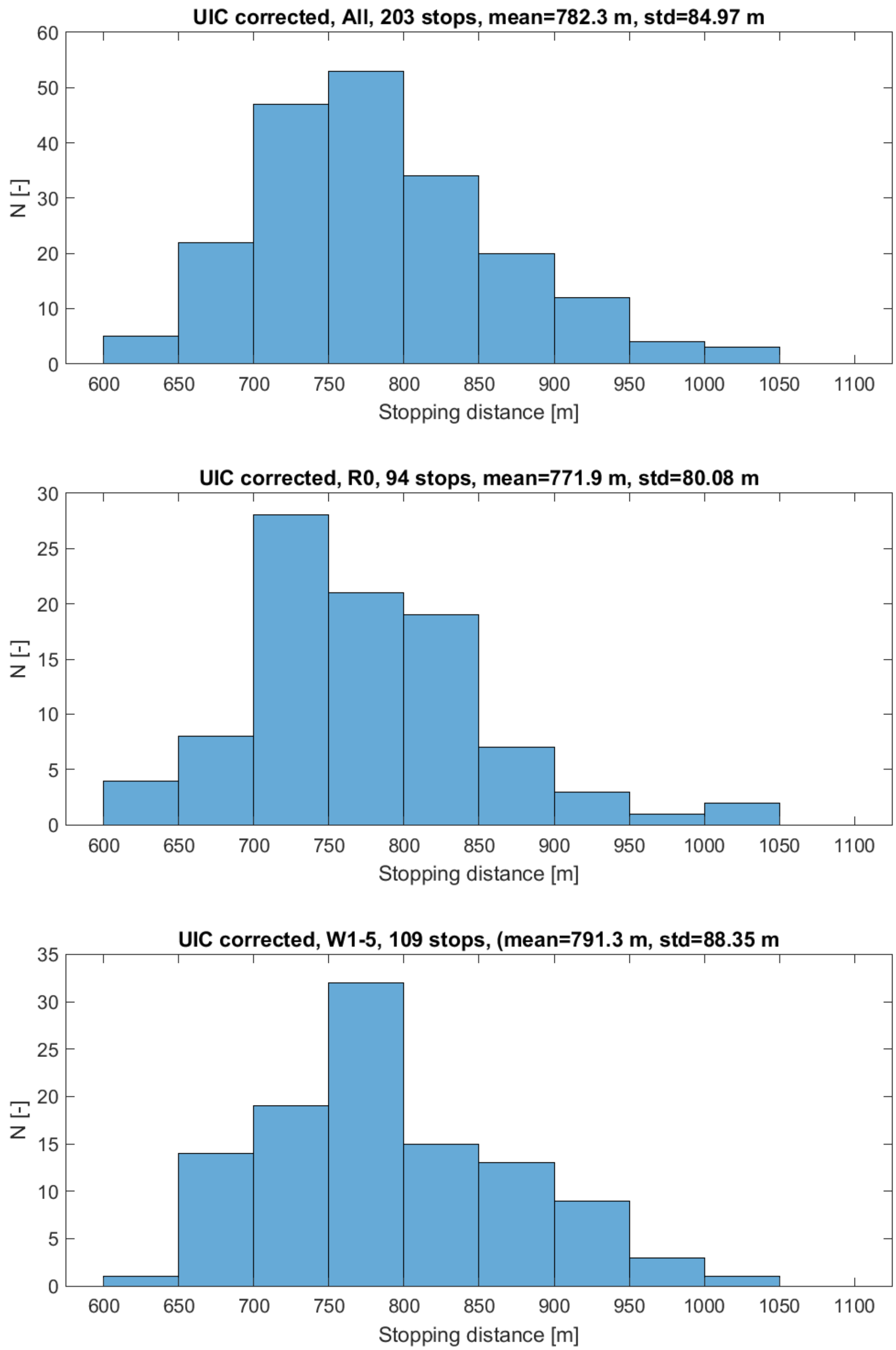

Figure 12 Histogram of braking distances for both types of brake blocks. All braking cycles (top), braking cycles in conditions R0 (middle) and in conditions W1-W5 (bottom).

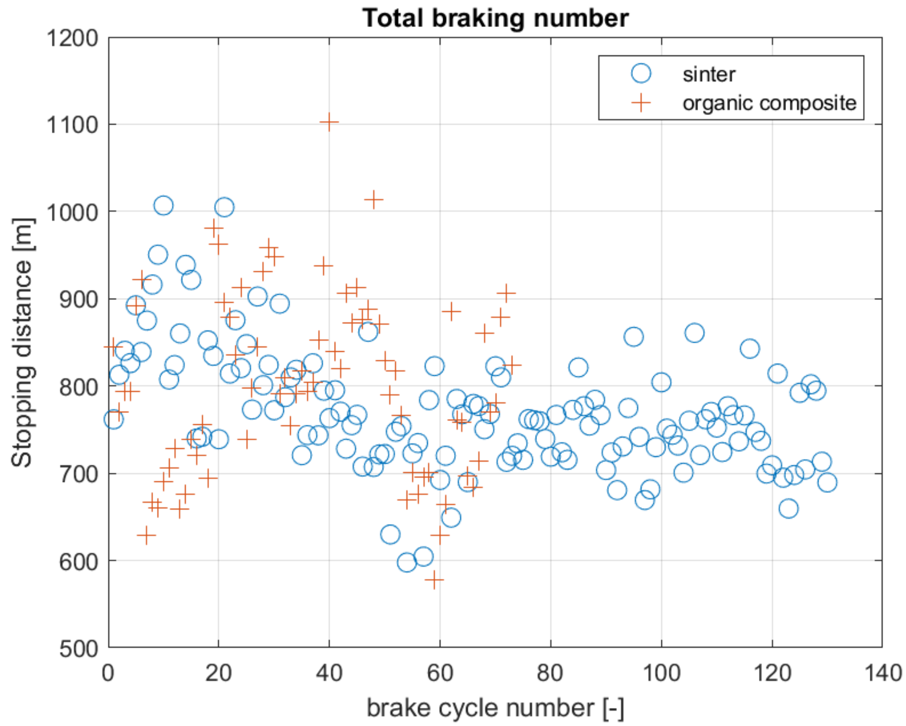

Figure 13 Braking distances for both types of brake blocks as function of brake cycle performed on that block type.

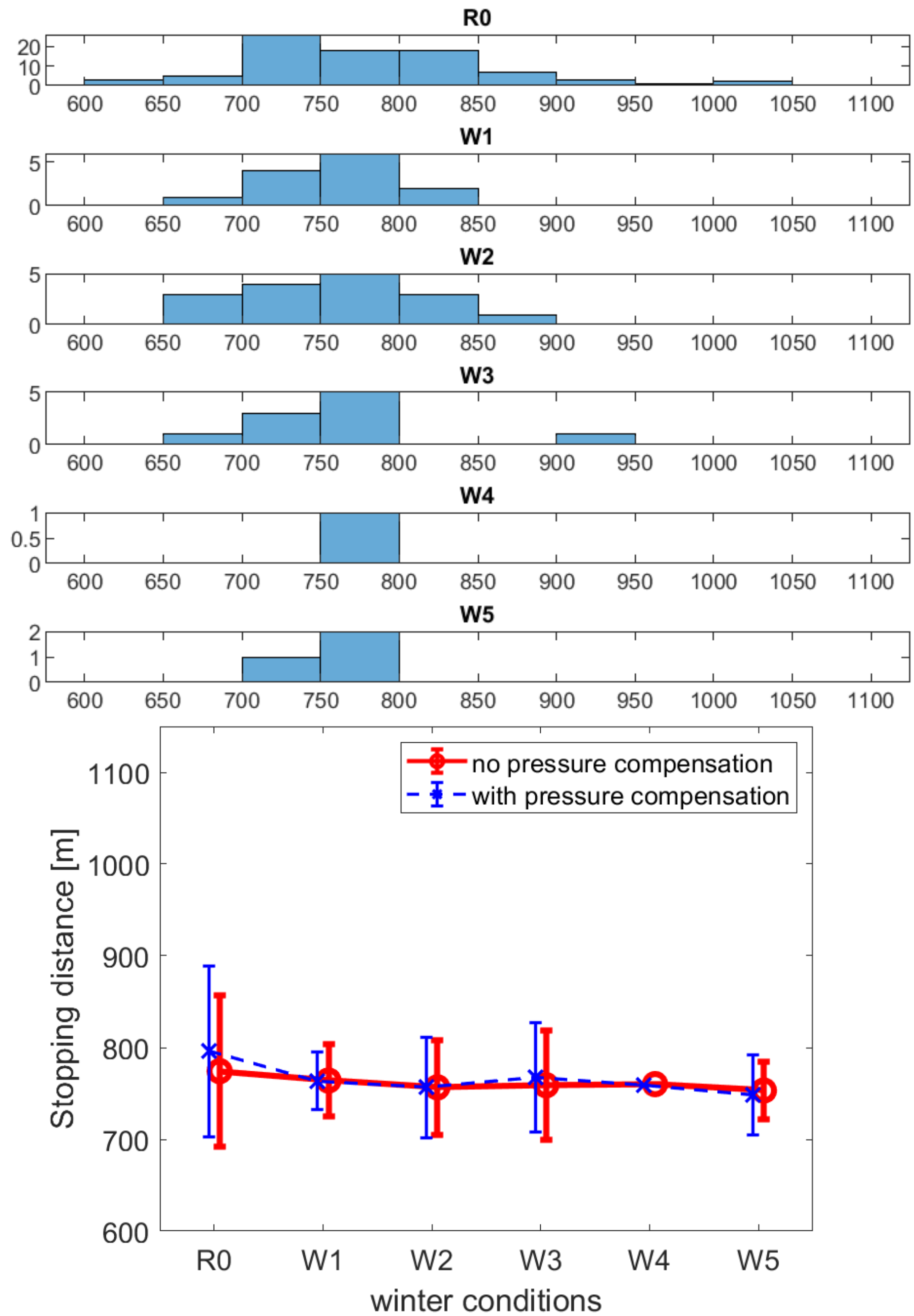

Figure 14 Results for sinter brake blocks. Histograms of braking distances showing number of braking cycles in reference condition R0 and the different UIC winter categories (top six) and a graph over average stopping distance indicated by circles or crosses, with bar indicating standard deviation, as a function of UIC winter conditions (bottom).

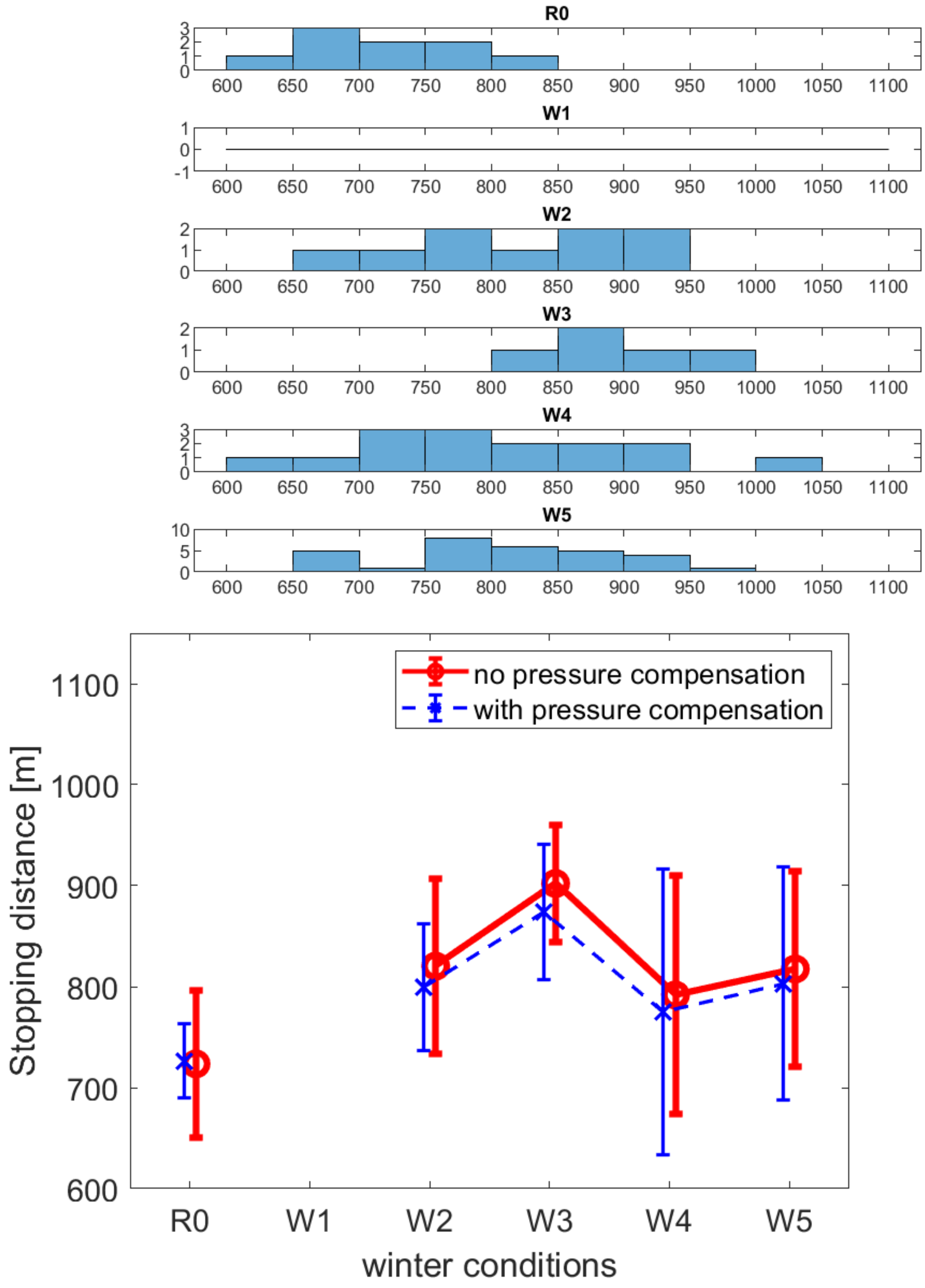

Figure 15 Results for organic composite blocks. Histograms of braking distances showing number of braking cycles in reference condition R0 and the different UIC winter categories (top six) and a graph over average stopping distance indicated by circles or crosses, with bar indicating standard deviation, as a function of UIC winter conditions (bottom).

4.1.4. **Study of specific conditions for general vs longer distance cycles**

The specific conditions for the 203 brake cycles of interest (ignoring the 18 cycles with brake cylinder valve problems) are presented in Appendix A. The results are presented in the form of histograms in which data from sinter and organic composite blocks are given separately. Data are given 1) for all brake cycles, 2) for brake cycles with braking distances larger than 833 m (being 15 % more than the average braking distance for organic composite for R0 conditions), 3) for braking distances > 900 m and 4) braking distances > 950 m. This way of presenting the results aims at providing information on conditions and factors that can explain deteriorated braking performance.

In Figure 49, the time delay for building 90% of the maximum brake cylinder pressure is given for the brake cycles. There is one sinter brake cycle that shows a long initiation time (about 13 s). This brake cycle (number 204 out of total 221), actually has a short braking distance (665 m). The only reason for the detected long delay is that there was an early initiation of the brakes, upon a slight delay until the brakes were fully engaged, most likely since the agreed starting point of the specific test site had not been fully reached. Apart from this one cycle, the cycles are all well grouped around an initiation time ranging from 7 to 8 s (average 7.0 s). There is not significant difference in initiation time for brake cycles showing long braking distances and the average value remains near 7 s. The time delay parameter cannot explain differences in braking distances.

Figure 50 presents the average brake cylinder pressures during the time for which the brakes are fully engaged. There is a spread in pressures between 1.2 bar and 1.52 bar, with mean value being 1.35 bar. One general observation is that braking with sinter blocks is performed at somewhat lower pressures (average 1.33 bar) than those for the organic composite blocks (average 1.38 bar).

Figure 51 shows the initial speeds of the train when braking is initiated (indicated by a spike in brake cylinder pressure). It should here be noted that all presented braking distances have been compensated for differences in initial speeds. Considering all cycles, there are two outliers in the data, one brake cycle at 83 km/h and one at 115 km/h. The remaining cycles can be found between 88 km/h and 110 km/h. From the histogram over brake cycles with distances longer than 833 m it is found that the two outliers in initial speeds are not part of this category. Further, there are only minor differences in average initial speeds as when groups of brake distances is considered. Th initial speed parameter cannot explain differences in braking distances.

Figure 52 shows the relationship between the total braking distance and the extrapolated part of the distance. The average ratio for all cycles is 3.9 %, but the ratio for sinter blocks is 2.6 % and for organic composite it is 6.3 %. For sinter blocks, the trend is that for longer braking distances the ratio is going down. However, for the shortest brake distance category (833 m), two of those cycles are for ratios over 10 %. These two cycles are not present when looking at the even longer distance of 900 m. For organic composite blocks with the overall average being 6.3 %, it is found that they show slightly increasing average ratios for longer braking distances: 7.0 % average for distances longer than 833 m, 7.0 % also for longer than 900 m and 8.5 % for distances longer than 950 m. The extrapolation ratio parameter cannot explain differences in braking distances for the sinter blocks, but it cannot be ruled out for the organic composite blocks as there is some changes in the parameter as the braking distances grow longer.

The results presented in Figure 53, visualize the influence of the brake cycle number during a day on braking distances. It is found for the organic composite blocks that this brake cycle number cannot explain differences since there seem to be a rather similar distribution of braking distances.

For instance, there is nothing that points towards that the braking distance of the first braking of the day should be more prone to longer braking distance than any other cycle, which to some extent was expected. For sinter blocks, it is actually found that longer distances are for "later" brake cycles of the day, where the brake distances longer than 833 m are for cycles 2 and later, brake distances longer than 900 m are for cycle for 4 and later, and longer than 950 m are for brake cycle number 9 and later.

The time from the previous (full) brake cycle until the studied one is presented in Figure 54. If the time is longer than 6 h, then 6 h is presented, indicating that it is the first brake cycle of the day. It is found for the sinter blocks that all brake cycles that have braking distances larger than 833 m all come from brake cycles that have less than 1 h 20 min from the previous brake cycle. For braking with organic composite blocks, there is an overall average time of 1 h for all cycles and for brake cycles having distance larger than 833 it is 1 h 21 min, for > 900 m it is 1 h 34 min and for > 950 m it is 2 h 33 min. This means that brake cycles for which it is a long time since the previous brake cycle is over-represented for longer braking distance.

In Figure 55, the influence of test site number (site 1–6) is presented. For sinter blocks, the parameter cannot explain differences in braking distances for the ranges if all cycles or if cycles >833 m are considered, since even distributions are found. For the longest considered brake cycles, > 950 mm, the three longest cycles are found for site 5 and 6. However, for organic composite blocks, there is an over-representation for brake site number 2 when it comes to braking distances larger than 900 m and 950 m. It can here be mentioned that for a large number of test runs, the train was starting out from Haparanda (near site 6) and was changing running direction at Niemisel (after passing of site 2). After changing of the running direction, site 2 was the first site for brake testing.

Brake cycles directly following after changing of the running direction of the train are depicted in Figure 56. It should be noted that out of the studied 203 stops, 41 are after changing running direction and 162 are for continuing in the same direction. For the sampled cycles this means a ratio of 41 / 162 = 0.25 between cycles after changing direction as compared to the total. The results in Figure 56 show that sinter blocks are not overrepresented for cycles for which directions are changing (the ratio actually goes down).

For organic composite blocks, there is trend of increasing braking distances after changing direction as compared to when not changing directions. For braking distances larger than 833 m, the relation between number of cycles after changing directions and the number of cycles after *not* changing directions is one to three. For distances larger than 900 m the same relation is one to two and larger than 950 m gives two to three.

An overview of metrological data are given in Figure 57 to Figure 61. Air temperatures in Figure 57 show that there seems to be a slight overrepresentation of lower temperatures for longer brake cycles of the organic composite blocks, whereas no such trend can be seen for the sinter blocks. For surface temperatures given in Figure 58 there seems to be no clear trends on temperatures. The influence from relative air humidity on braking distances is shown in Figure 59. There seems not to be a brake distance dependency on this factor. The influence from intensity of snowfall on braking distances is shown in Figure 60. For longer brake cycles of the organic composite blocks there seems to be some overrepresentation of higher snow fall intensities, whereas no such trend can be seen for the sinter blocks. However, it can be noted that for sinter blocks, only 5 brake cycles have been performed for snow fall intensities over 1 mm / 30 min. Finally, the influence from the snow drift parameter is given in Figure 61. For the sinter material there seems to be no dependency, but some influence can be found for the organic composite material with a trend that long distances are more likely for snow drift conditions.

4.1.5. **Investigation of explanatory relationships, including metrological data**

Regression models are explored using visualization of the response surfaces and by linear regression modelling employing so-called stepwise regression. In the latter, terms are added or removed in an automatic stepwise regression procedure[18]. After an initial fit, the procedure examines a set of available terms and adds the best one to the model if the statistics for the analysis of variance for adding the term gives a p-value 0.05 or less. If no terms can be added, it examines the terms currently in the model, and removes the worst one if removing it has a p-value equal to or greater than 0.10. It repeats this process until no terms can be added or removed.

In the present section only results for organic composite brake blocks are investigated, based on the finding from the previous section which indicates that only minor such variations could be expected for sinter blocks. A first fit is made using linear polynomials when also accounting for interactions, see Figure 48. The variation of the braking distance for changes in parameters can be seen for this specific situation (UIC snow index 2.5, air temperature -1ºC, not snowing, no snow drift and an extrapolation ratio of braking distance being 0.79, and the wagon has not changed its running direction).

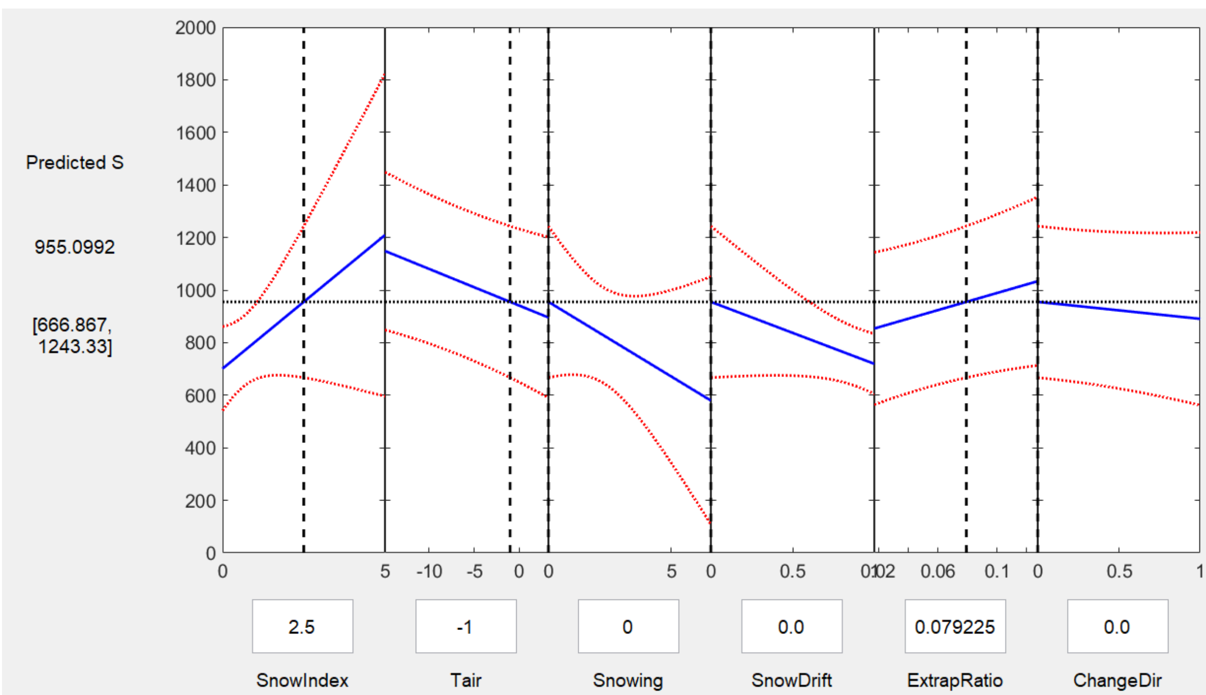

Figure 16 Visualization of dependencies of stopping distance S [m] on vertical axis. Subplots show dependencies on separate influencing parameters. Fit is plotted in blue and 95% simultaneous confidence bands for the fitted response surface are indicated as two red (dotted) curves on each plot.

[18] Matlab function ”stepwiselm” is exploited.

One can also present the surface in the form of a polynomial function where the predictors are on the following form, found from an initially assumed first degree polynomial of the parameters, when also accounting for interactions:

S ~ *1 + ExtrapRatio + SnowIndex***Tair + SnowIndex***SnowDrift + Tair***ChangeDir + Snowing***SnowDrift* Equation (1)

with estimated coefficients given in Table 1 along with relevant information from the fitting procedure[19].

Table 1 Coefficient estimates for fitted model along with standard error of the coefficients SE and pValue being the *t*-statistic of the hypothesis test that the corresponding coefficient is equal to zero or not (e.g. if a *p*-value of is greater than 0.05, the term is not significant at the 5% significance level given the other terms in the model).

	Estimate	SE	tStat	pValue
(Intercept)	584.51	38.966	15	2.6565e-22
SnowIndex	90.851	29.166	3.1149	0.0027854
Tair	13.13	6.0628	2.1657	0.034191
Snowing	-56.676	21.484	-2.6381	0.010528
SnowDrift	157.36	54.181	2.9044	0.0050936
ExtrapRatio	1635.3	421.55	3.8793	0.00025609
ChangeDir	-77.631	41.106	-1.8885	0.063634
SnowIndex:Tair	-10.813	2.4071	-4.4919	3.1403e-05
SnowIndex:SnowDrift	-157.22	35.01	-4.4906	3.1546e-05
Tair:ChangeDir	-13.051	5.4802	-2.3816	0.020322
Snowing:SnowDrift	48.441	22.451	2.1576	0.034839

The results for a chosen less general setting, where the braking distance is assumed to depend only on UIC snow index and on air temperature, is presented in Figure 17 for three chosen combinations of snow indices and air temperatures. Here, the fitting procedure starts out with second degree polynomials with interaction terms. The resulting fit has the following form:

S ~ 1 + *SnowIndex***Tair*, with parameters given below.

	Estimate	SE	tStat	pValue
(Intercept)	754.8	25.557	29.534	6.9894e-41
SnowIndex	-30.13	13.527	-2.2274	0.029187
Tair	-6.1503	5.3979	-1.1394	0.25848
SnowIndex:Tair	-4.1874	2.1832	-1.918	0.059246

Note that the linear parameter *Tair* is here retained by the procedure since the *Tair* is present in the interaction term "*SnowIndex***Tair*". The three examples highlight the rather strong

[19] The procedure fits a model to variables in the dataset. After an initial fit, the function examines a set of available terms, and adds the best one to the model if an F-test for adding the term has a p-value 0.05 or less. If no terms can be added, it examines the terms currently in the model, and removes the worst one if an F-test for removing it has a p-value 0.10 or greater. It repeats this process until no terms can be added or removed.

dependence on air temperature for the situation when the UIC *SnowIndex* is 3 or 5, whereas there is a substantially weaker dependence on temperature for UIC snow index 0, meaning no snow whirling conditions around the test train. This points towards the finding that a combination of low temperatures and snow whirling gives prolonged braking distances.

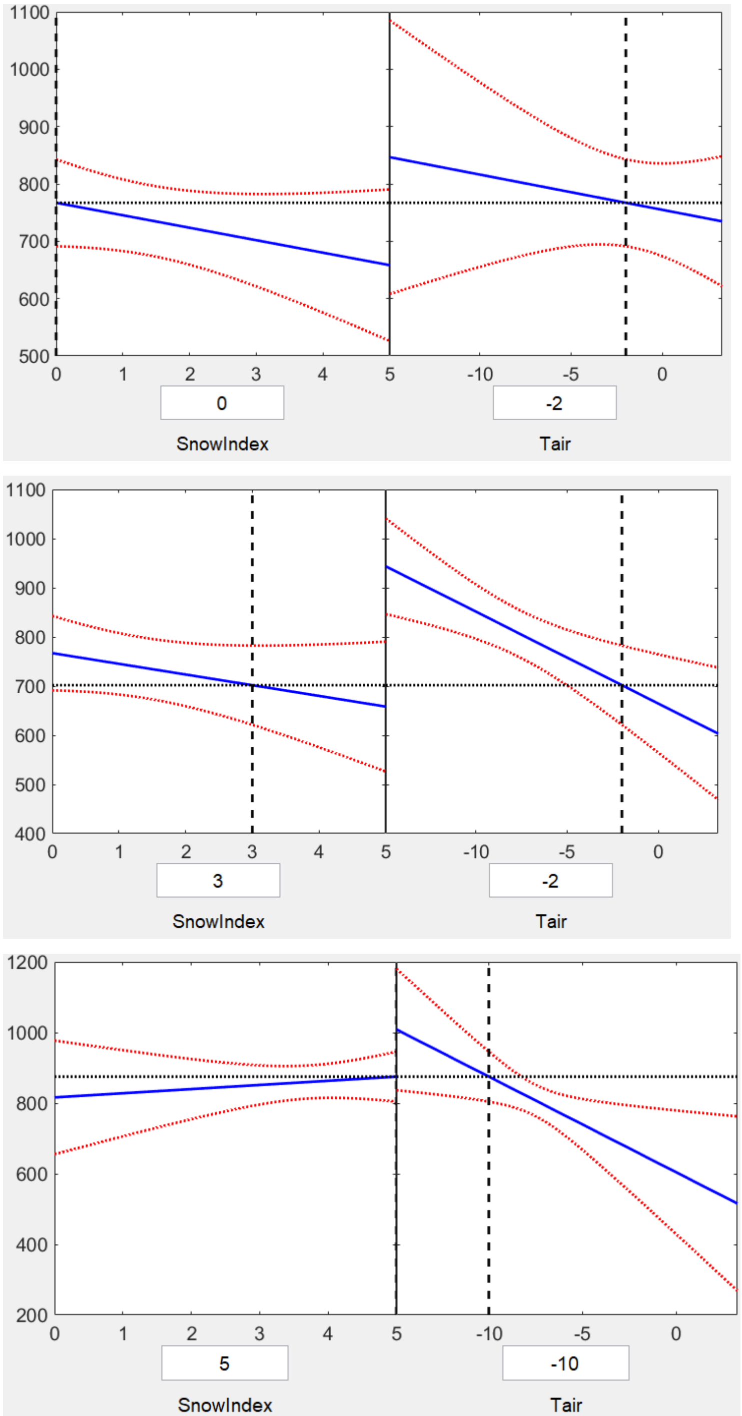

Figure 17 Visualization of the influence of dependencies on stopping distance S [m] (on vertical axis). Subplots show dependencies on separate influencing parameters for the chosen combination of parameter values. Fit is plotted in blue and 95% simultaneous confidence bands for the fitted response surface are indicated as two red (dotted) curves on each plot.

The braking distance results for organic composite blocks can also be represented by a 3D surface as shown in Figure 18, in which also the individual braking distance results have been introduced. Here the tendency that a combination of high UIC winter indices and lower temperatures lead to longer braking distances is clear. For comparison, the same procedure of fitting of a surface to the resulting brake distances has also been employed for sinter brake blocks, see Figure 19. In this figure, the initial 30 stop braking cycles for this block type has been removed, because of the suspicion of insufficiently bedded brake blocks, see Section 4.1.3. Note however the lack of results for sinter blocks when considering the lowest temperatures when combined with high UIC snow indices.

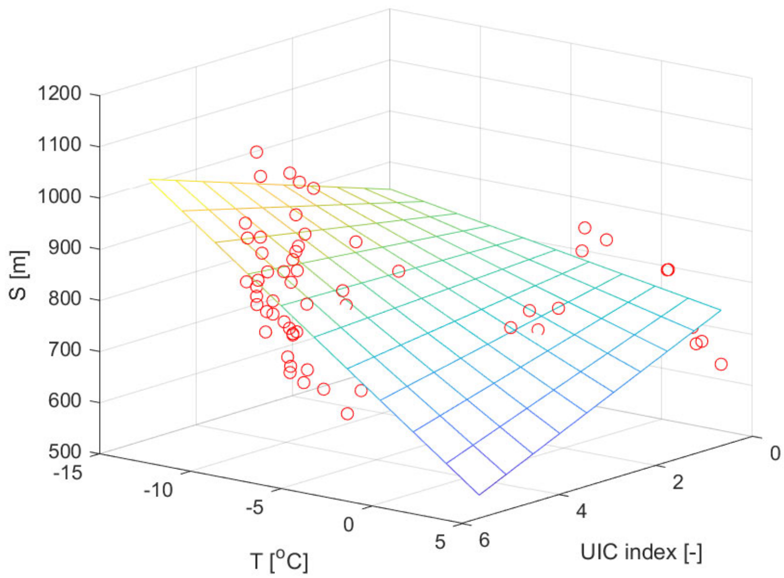

Figure 18 Braking distance results for organic composite blocks as function of air temperature and UIC winter index along with the fitted surface.

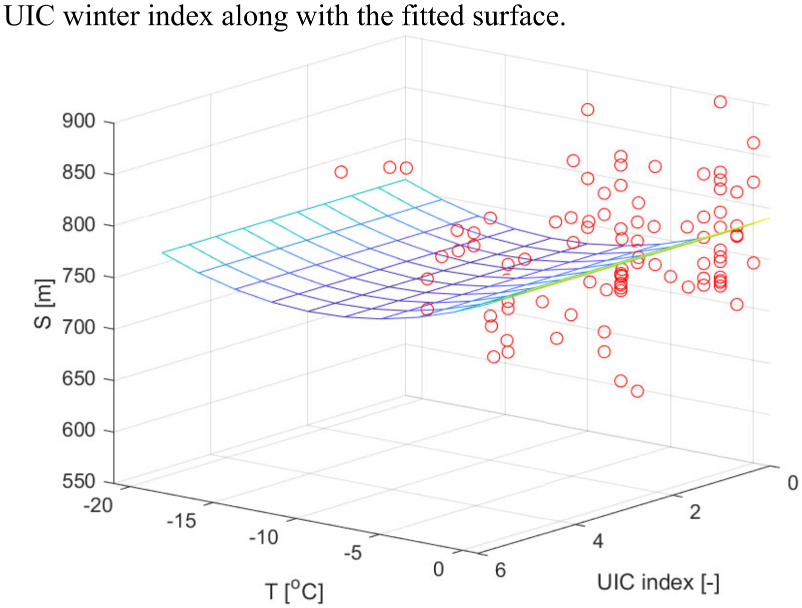

Figure 19 Braking distance results for sinter blocks as function of air temperature and UIC winter index along with the fitted surface.

4.1.6. **Comparison with nominal braking distance based on UIC 544-1**

The nominal braking distances of a complete train and also for a single wagon can be calculated using the information in the UIC leaflet 544-1, based on train mass data and braked percentages. The braked weight for each wagon can be calculated as $B_i = \lambda_{dyn,i} \times m_i$ where $\lambda_{dyn,i}$ is dynamic efficiency and m_i = 26 tonnes is wagon mass[20]. For the train, having an unbraked locomotive, the braked percentage can be found as

$$\lambda_{test} = \frac{B_{loco} + \sum_{i=1}^{5} B_i}{m_{loco} + \sum_{i=1}^{5} m_i}$$

where $B_{loco} = 0$ (unbraked loco) and m_{loco} = 89 tonnes is locomotive dynamic mass. The average dynamic efficiencies were determined by DB Systemtechnik by measurements reported in "Determining the efficiency of five freight car wagons of Habbins type[21]", see Table 2, with an average dynamic efficiency of the wagons being $\bar{\lambda}_{dyn,i} = 0.88$. Based on this information it is found that the braked percentage of the train is $\lambda_{test} = 0.52$.

Table 2 Dynamic brake efficiency for given wagon numbers of train, extracted from report[17]

Wagon	274 2 546-5	274 2 625-7	274 2 316-3	274 2 145-6	274 2 633-1
$\lambda_{dyn,i}$	0.88	0.83	0.88	0.90	0.91

The braking distance s [m] can readily be calculated for a train or a single wagon at speed 100 km/h using UIC544-1 by

$$s = \frac{C}{\lambda_{train}\,[\%] + D}$$

For a train C = 61300 m and D = 8.9 whereas for a single wagon C = 52840 m and D = 10. This gives a braking distance for a train s_{train} = 1003 m and for a wagon s_{wagon} = 849 m, which are, according to the norm, for a wagon braking efficiency of $\bar{\lambda}_{UIC} = 0.83$ and a nominal filling time of $t_{\mathrm{UIC}} = 4$ s.

The filling time of the brake cylinders for the test train is reported in Figure 49, with an average value of 7 s.

A proposal based on the information in the DB document "*On the regulations of technical brake assessment of rail vehicles within the scope of the acceptance according to § 32 EBO - principles of brake evaluation based on UIC 544-1 (in German)*" [22], is that the braking distance of our test train could tentatively be found based on the ratio between train length L_{test} and maximum length L_{max} as

---

[20] Rotational inertia of wagon wheels is neglected.

[21] S. Heinz and C Schmidt, Determining the efficiency of five freight car wagons of Habbiins type, Document 59869-TVP21-192841-PR01, *DB Systemtechnik*, Minden, 2020-02-17.

[22] Anhang IV "*zu den Regelungen für die bremstechnische Beurteilung von Schienenfahrzeugen im Rahmen der Abnahme nach § 32 EBO - Grundsätze der Bremsbewertung in Anlehnung an UIC 544-1*" Stand: Rev. 05, 07.11.2006

$$s_{test} = s_{wagon} + (s_{train} - s_{wagon}) \times \frac{L_{test}}{L_{max}}$$

where L_{test} = 132m is the length of the test train (locomotive being 15.5 m long and five wagons each with length 23.3 m). The maximum train length considered is taken as L_{max} = 500 m which is the longest train length considered in the standard for freight wagons, yielding a stopping distance s_{test}=890 m.

This value is additionally compensated to account for the higher efficiency of the test train ($\lambda_{test} = 0.88$) than what is considered in the standards, stating $\lambda_{UIC} = 0.83$ as dynamic efficiency of wagons. The stopping distance will thus decrease by the following scaling

$s_{test,\lambda} = s_{test} \times \frac{\lambda_{test}}{\lambda_{UIC}}$ = 834 m

Finally, compensating for t_F = 7 s filling time of the brake cylinder as compared to t_{UIC} = 4 s in UIC standard[23]:

$s_{test,\lambda,F} = (\frac{t_F}{2} - \frac{t_{UIC}}{2}) \times v_{nom+} \, s_{test,\lambda}$ = 881 m

The stopping distance of the test train thus has a nominal value of 881 m with the described compensation for 1) the length of the test train, 2) the high efficiency of the wagons, and 3) the longer time delay of building up of the brake cylinder pressure.

[23] This relationship is in the UIC standard strictly only applicable for slipped wagons (i.e. a single vehicle test where the wagon is released from a locomotive by a mechanical coupler) but it is here deemed reasonable to use for our test train which is relatively short.

4.2. Part 2: Braking forces, braking energies and friction coefficients

Results from 228 stop braking cycles are presented in the following. For the first 65 stops sinter blocks were mounted on all wagons. For the remaining 163 stops cast iron blocks were mounted in bogie 1 of wagon 2 and for the last 100 stops there were organic composite blocks in bogie 2 of wagon 2.

4.2.1. General information

The employed brake cylinder pressures are presented in Figure 20. Results for stops when also cast iron blocks and organic composite blocks are mounted are given separately. Note that it has been chosen to only use pressure data from one of the wagons in the analyses. This is motivated by the insignificant time delay between cylinder pressures for the short train, in combination with problems with damaged pressures sensors on wagons during testing. The figure shows that there is a spread in brake pressures, but the distributions are very similar for all three brake block types (as expected). In fact, because of the overlapping of the braking cycles for the three materials, several of considered cycles are identical.

Brake block friction forces and brake block normal forces are, as described in Section 3.2, found from brake triangle forces and hanger link forces. Because of the geometrically based offsetting effect introduced by the braking force from the brake triangle on the hanger link force, a specific balancing analysis is performed to determine the offsetting forces. To this end, the offsetting forces were determined by comparing some specific brake cycles when the wagons were travelling in opposite directions for reference conditions R0. Here, the brake blocks are presumed to be braking with their full (nominal) capacity. The offset of the forces for the two hanger links acting together on each brake triangle, and the pertaining geometries, could thus readily be determined. This procedure was performed using some of the first brake cycles for R0 conditions for each type of brake blocks. It could be noted that the offsetting force acting on a hanger link typically has the same magnitude as the contribution from the brake friction force acting on the brake block.

When it comes to measurement of brake triangle forces, it was discovered that there was a mistake in the strain gauge instrumentation of them. Strain gauge pairs were installed to detect bending strains of the front triangle bars instead of tensile strains, caused by a misunderstanding of the intended principle of measurement. For nominal loading of the brake triangle, with a presumed reaction forces from the block-wheel contact acting at the centre of the brake blocks, there is no difference in results as compared to the intended measuring principle. This was also shown by successful calibration of the brake triangles. However, for a field situation with occasionally less-than perfect contact conditions between blocks and wheel, introduced by wear of blocks (or by mismatching blocks on wheels with different wheel diameters), it has been found that the forces detected by the brake triangles are too high by some 30 % (on an average). For this reason, it was chosen to instead of using the measured brake triangle forces to utilize the brake cylinder pressure and the measured dynamic efficiencies λ_{dyn} for the individual bogies of the wagons as presented in the DB Systemtechnik report. The normal braking force F_{n} [kN] is thus found by

$$F_{\mathrm{n}} = \lambda_{dyn} \times \frac{\left(A_{\mathrm{BZ}} \times p_{\mathrm{cyl}} \times 10 - F_{\mathrm{BZ}}\right) \times i - n \times F_{\mathrm{R}}}{1000 \times n_{\mathrm{BS}}}$$

where A_{BZ} [cm^2] is brake cylinder area, p_{cyl} [bar] is brake cylinder pressure, F_{BZ} [N] is retracting force of brake cylinder, F_R [N] is retracting force of slack adjuster, i [-] is total transmission ratio, n [-] is number of transmissions after central brake leverage and n_{BS} [-] is number of brake block inserts. Thus, the time variations of the braking normal forces are calculated by use of the measured brake cylinder pressures. For information, the dynamic efficiencies presented in the report for the bogies of the wagons range between 0.82 and 0.91. A histogram over resulting brake normal forces are presented in Figure 21.

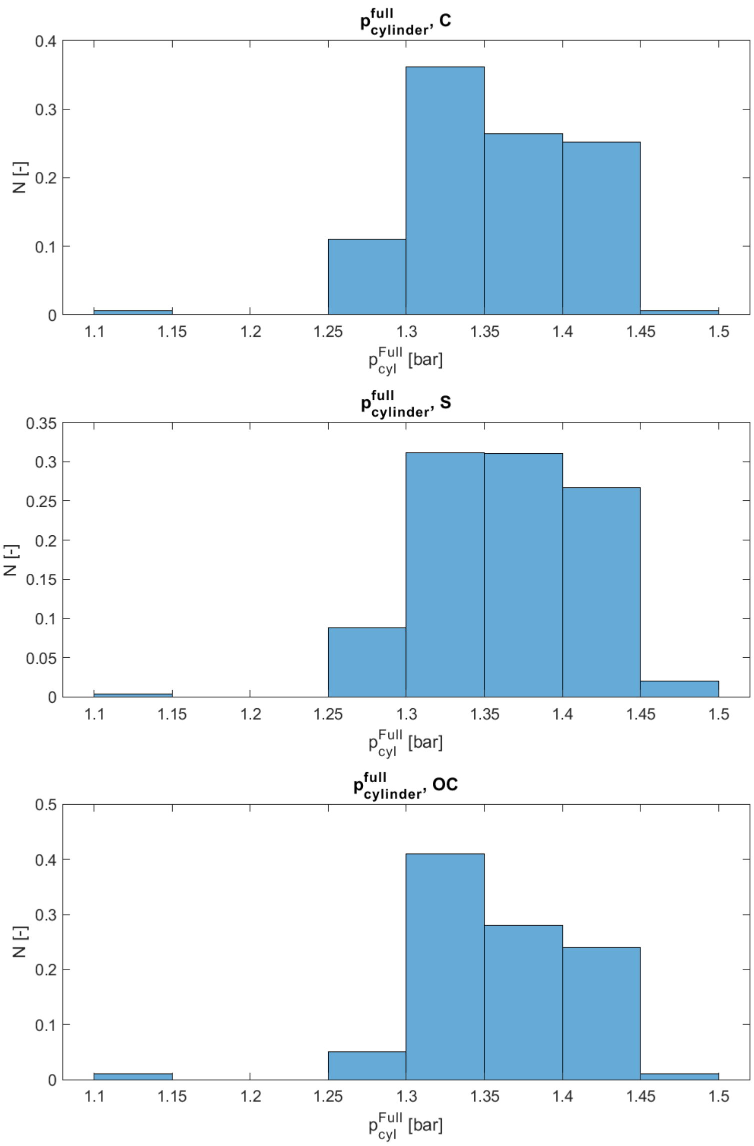

Figure 20 Normalized histograms over average brake pressures during time of full braking pressure for the studied 228 stop braking cycles. Top: results for cast iron blocks, middle for sinter blocks and bottom for organic composite blocks.

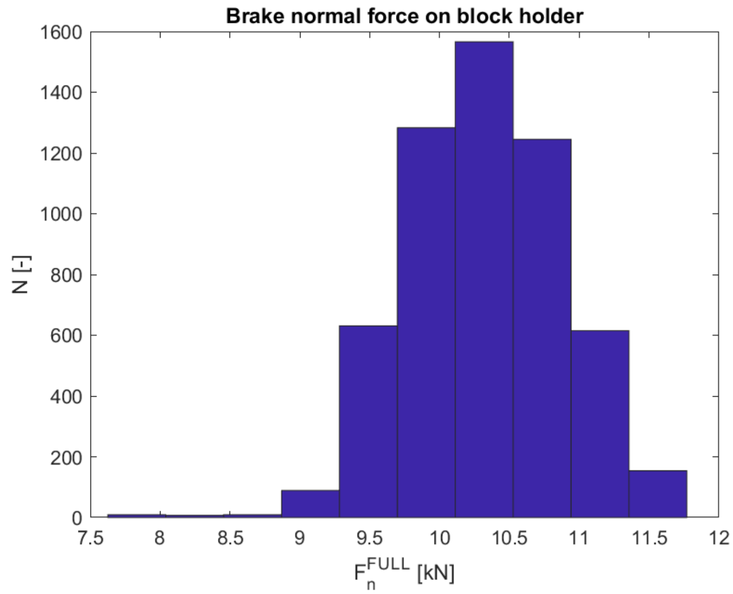

Figure 21 Histogram over average normal forces of individual brake blocks calculated from history of brake pressures. The average is taken over the time for which the brake cylinder produces full braking effort.

4.2.2. **Stopping distances**

An overview of the stopping distances for all considered stops for this part of the report is given in Figure 22. The stopping distances for all braking cycles range between 600 m and 900 m. The middle and bottom subplots show that there is a slight increase in average braking distances when going from R0 winter conditions (Reference – meaning no whirling snow) with an average of 720 m to W1–5 (with increasing amounts of snow whirling around the wagons) with an average of 733 m. The standard deviations are about the same.

In order to put focus on the different UIC winter categories, the average and standard deviation of braking distances are presented in Figure 23. Here, the results have also been separated into brake cycles with only sinter blocks, when also cast iron blocks were added into bogie 1 of wagon 2 and, finally, when organic composite blocks were added into bogie 2 of wagon 2. It can be seen that braking with sinter blocks on all wagons gives average braking distances that are consistent and between 730 m and 760 m, with standard deviation being below some 60 m. For reference (R0) conditions, the introduction of cast blocks in one bogie (instead of sinter blocks), can be seen to decrease the braking distances for R0 conditions by about 30 m, but that for winter conditions W2–W4 they are instead increased, with the largest increase being about 40 m. Note that no data are present for W1 and for W5 for braking with sinter blocks and cast iron blocks on bogie 1 of wagon 2. The changing of sinter blocks in bogie 2 of wagon 2 into organic composite blocks can be seen to lower the braking distances for all conditions. The decrease in average braking distance is between 30 and 50 m as compared to braking with only sinter blocks, then excluding results for W4 when there is only one data point for braking with only sinter blocks.

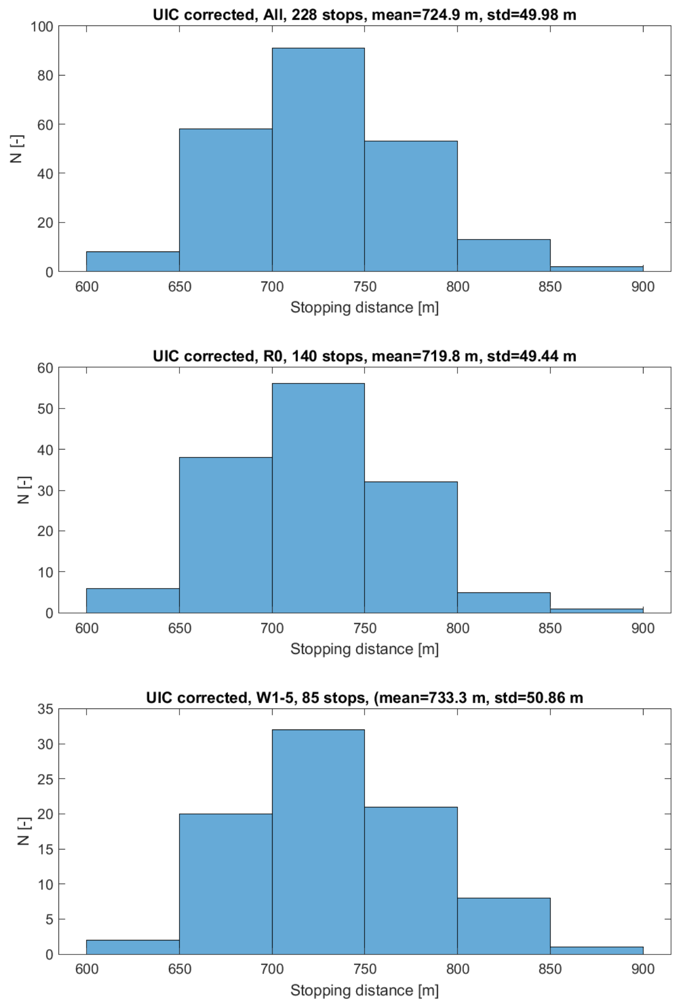

Figure 22 Histogram of braking distances for all stops. All braking cycles (top), braking cycles in conditions R0 (middle) and in conditions W1–W5 (bottom).

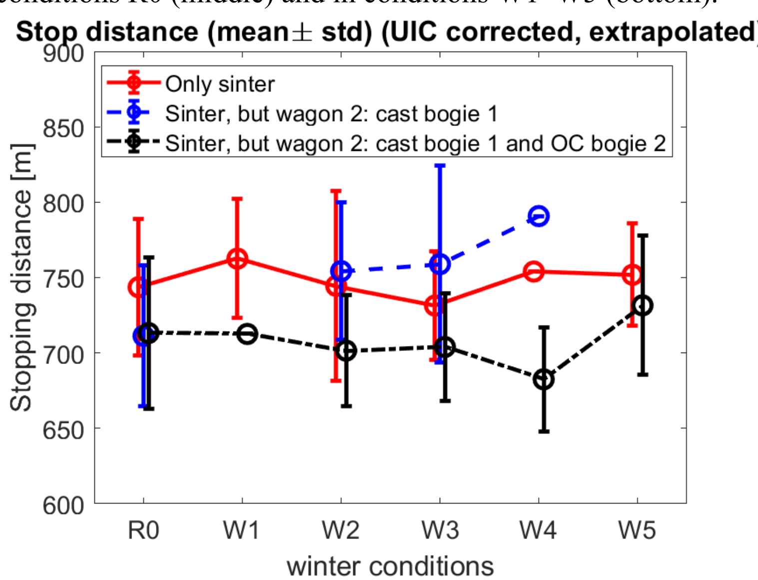

Figure 23 Graph over average stopping distance indicated by circles, with bar indicating standard deviation, as a function of UIC winter conditions (bottom). Results are shown for different brake block installations on the test wagons during testing. OC is organic composite blocks.

4.2.3. **Brake friction force of half a bogie**

Focussing on the differences in braking capacity for the three studied block materials in winter conditions, the braking performance of bogie units with uniform blocks is first studied. The analyses build on *one* hanger link force each at front and back of the two wheelsets in the two bogies in wagon 2 and similarly for the instrumented bogie of wagon 4. Thus, it is *the force of half a bogie* that is studied. The reason for this choice is that there were several hanger links with defect force sensors so that data for the complete bogie could not be established. No set of hanger link forces were available for the bogies of wagon 3 because of break-down of several hanger link force sensors. The friction force that is presented is the time averaged force for the time during which the pneumatic brake pressure is at its nominal level, thus ignoring initial build-up of brake pressure and also the often occurring later phase with decrease in braking pressure.

The results are first presented in histograms and the data are after that analysed with respect to dependencies when it comes to air temperature and UIC snow index. The histograms for sinter material is presented in Figure 24, for cast iron material in Figure 25 and for organic composite material in Figure 26. The results are presented separately for the bogie when it is in leading position in the wagon and when it is trailing, since they might experience different conditions as a result of tentative variations of local snow whirling. The results indicate that the three materials have similar average brake friction forces, with sinter having somewhat lower values than the two others, with 5.7 kN and 6.0 kN respectively for a bogie in leading and trailing positions, respectively. This is to be compared with cast iron blocks 7.1 and 6.8 kN, and organic composite blocks with 6.3 and 7.1 kN. The standard deviations in forces is largest for the cast iron blocks with 1.1 kN for both leading and trailing positions, while the two other materials range between 0.58 and 0.76 kN. The larger spread in forces for the cast iron blocks can also readily be seen when comparing the three figures.

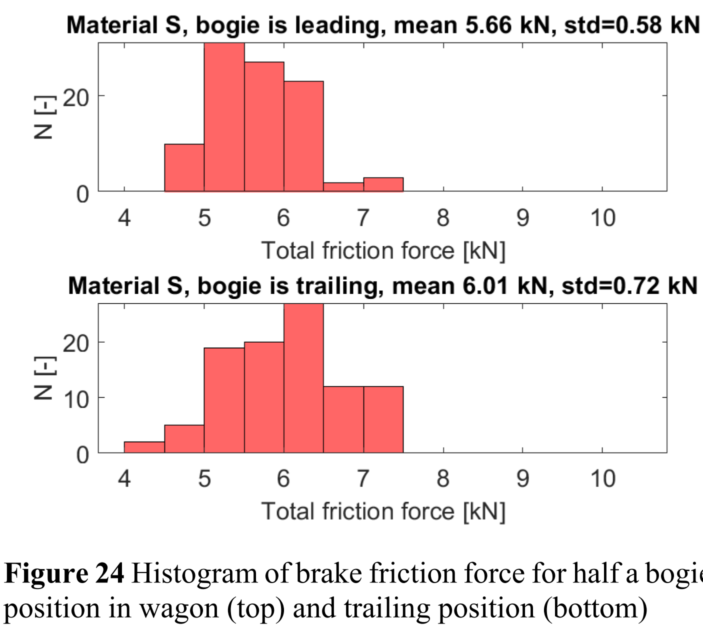

Figure 24 Histogram of brake friction force for half a bogie with sinter brake blocks. Bogie in leading position in wagon (top) and trailing position (bottom)

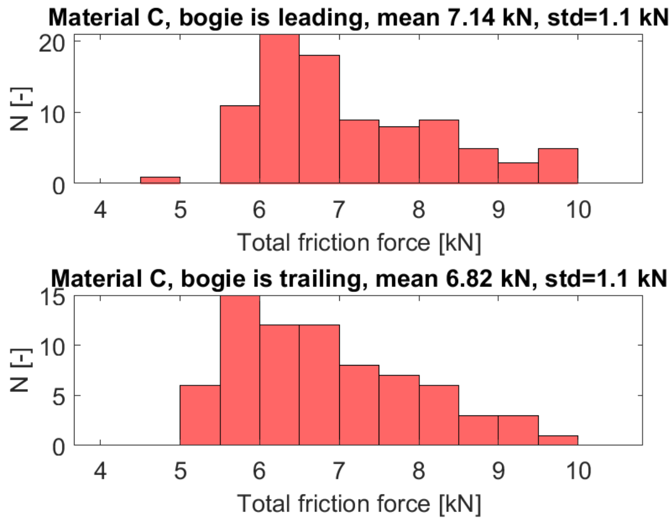

Figure 25 Histogram of brake friction force for half a bogie with cast iron brake blocks. Bogie in leading position in wagon (top) and trailing position (bottom)

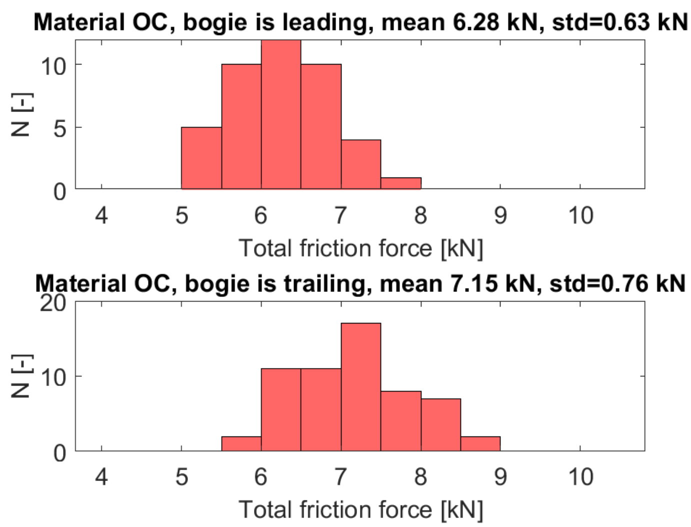

Figure 26 Histogram of brake friction force for half a bogie with organic composite brake blocks. Bogie in leading position in wagon (top) and trailing position (bottom)

Linear regression modelling employing stepwise regression is performed on data as previously performed in Section 4.1.5. Here the only available parameters are UIC snow index and air temperature. A quadratic model is employed in the stepwise regression procedure. The individual friction force results for sinter blocks are presented in Figure 27 along with the surface fitted to the data and the corresponding results for cast iron blocks and for organic blocks are given in Figure 28 and Figure 29, respectively.

The fitted models can be seen to exhibit various behaviours in which often either the air temperature or the UIC winter index parameters are not considered to be explanatory with respect to the data sets. For sinter material there are some trends that points towards decreasing braking performance in the leading bogie for the combination of low temperatures and high UIC indices. However, the apparent lack of data for low temperatures in general (there are only 6 data points that are for temperatures below -10 ºC) and specifically for the combination of low temperatures and high UIC indices is problematic. In the same way, for the trailing position a slight decrease in the friction force is found as the temperature decreases, but again with the same lack of data at lower temperatures.

The lack of data for lower temperatures is also evident for both cast iron and organic composite materials, with lowest temperatures being about -8 ºC, see Figure 28 and Figure 29. The trend for cast iron material is an increasing braking performance with increasing UIC index for the leading bogie and with decreasing temperature for the trailing bogie. For the organic composite material, a similar trend with increasing brake friction force with decreasing temperature is found for the trailing bogie, whereas for the leading bogie no temperature dependence is found. For the leading bogie there is a trend with a decrease in braking performance for the highest UIC index values.

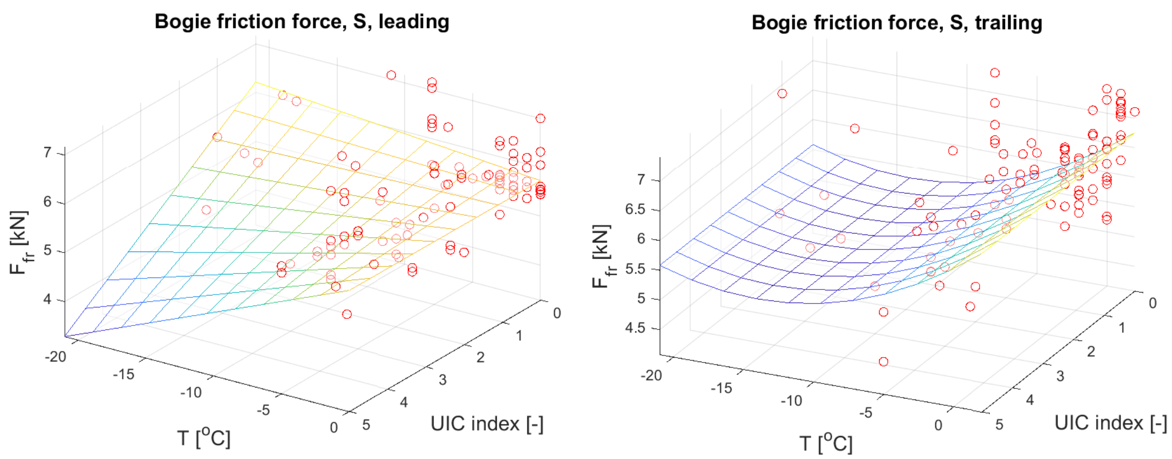

Figure 27 Sinter brake blocks: calculated total brake friction forces for bogie as function of air temperature and UIC winter index. Bogie in leading position in wagon (left) and trailing position (right)

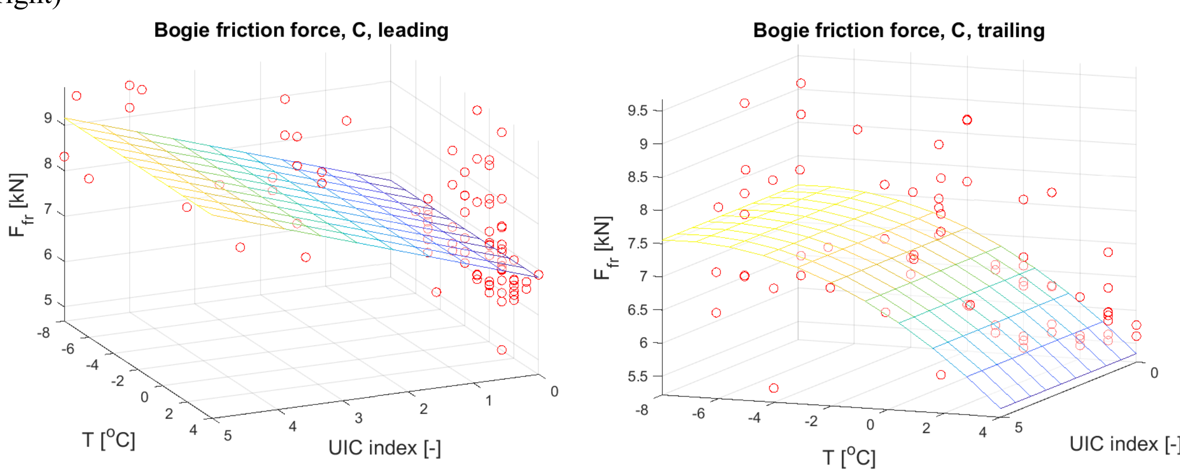

Figure 28 Cast iron blocks: calculated total brake friction forces for bogie as function of air temperature and UIC winter index. Bogie in leading position in wagon (left) and trailing position (right)

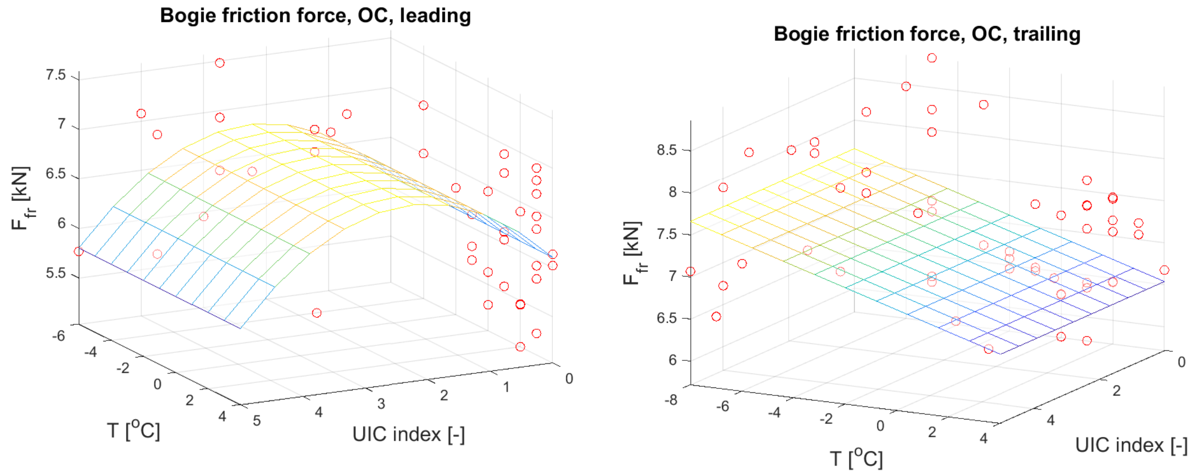

Figure 29 Organic composite blocks: calculated total brake friction forces for bogie as function of air temperature and UIC winter index. Bogie in leading position in wagon (left) and trailing position (right)

4.2.4. Brake friction work of half a bogie

The braking performance of bogie units with uniform blocks is now studied with respect to friction work during the entire braking, from highest speed train speed at initiation of the pneumatic brakes until stop (or train minimum speed). The analyses exploit the same hanger link force as in the previous section, meaning that the energy of only half the bogie is considered in the analysis. The results are first presented in histograms and the data are after that analysed with respect to dependencies when it comes to air temperature and UIC snow index. The histogram for sinter material is presented in Figure 30, cast iron material in Figure 31 organic composite material in Figure 32.

Again the results indicate that the three materials produce similar average brake friction work, with sinter being somewhat lower than the others yielding 3.6 MJ for both bogies, as compared to organic composite blocks being intermediate with 3.7 MJ for leading and 4.1 MJ for trailing bogies, and finally highest for cast iron blocks at about 4.2 MJ for both bogies. The standard deviations are (as for the friction forces in previous section) largest for the cast iron blocks with at 0.6 to 0.7 MJ, while the two other materials are near 0.4 MJ. The larger spread in friction work for the cast iron blocks can also readily be seen when comparing the three figures.

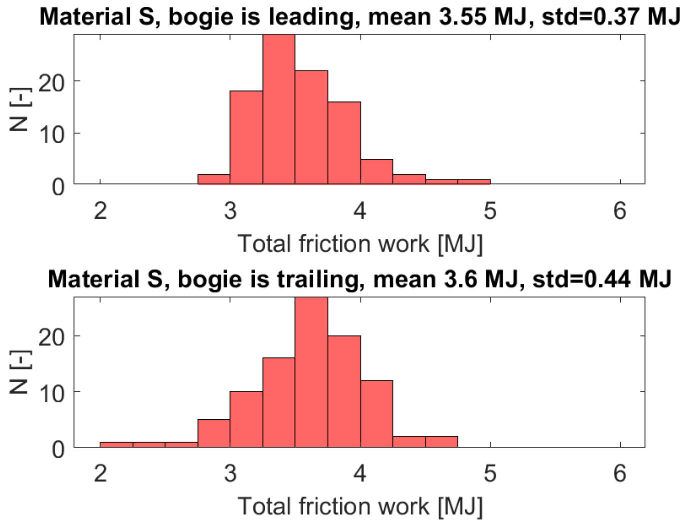

Figure 30 Sinter brake blocks: Histogram of total brake friction work for half a bogie. Bogie in leading position in wagon (top) and trailing position (bottom)

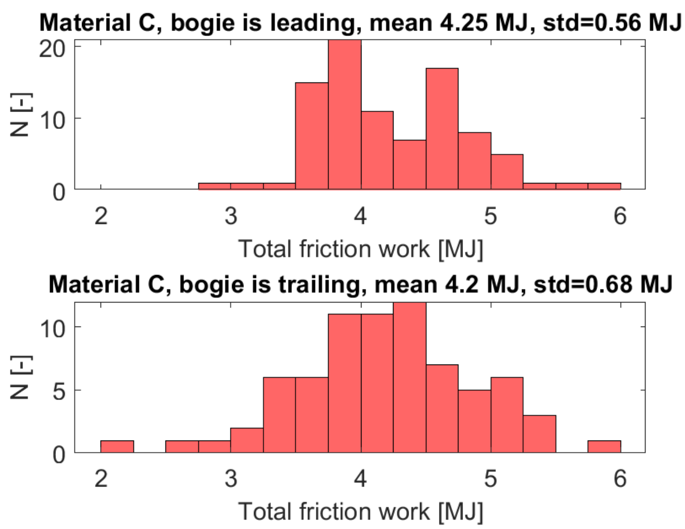

Figure 31 Cast iron brake blocks: Histogram of total brake friction work for half a bogie. Bogie in leading position in wagon (top) and trailing position (bottom)

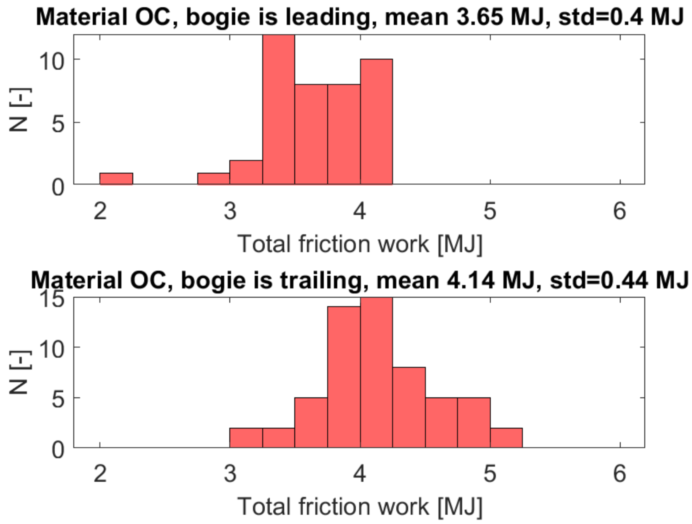

Figure 32 Organic composite brake blocks: Histogram of total brake friction work for half a bogie. Bogie in leading position in wagon (top) and trailing position (bottom)

Linear regression modelling employing stepwise regression is performed on the data with regard to the parameters UIC snow index and air temperature. The individual friction work results for sinter blocks are presented in Figure 33 along with the surface fitted to the data. The corresponding results for cast iron blocks and for organic blocks are given in Figure 34 and Figure 35, respectively.

For sinter material, see Figure 33, the fitted surface indicate somewhat decreasing brake friction work for both bogies for a lowering of temperatures, but with a rather weak dependency on UIC winter indices. The trends for cast iron material, see Figure 34, are complex for the leading bogie with highest brake friction work for intermediate temperatures and UIC indices, while the trailing bogie shows increasing brake friction work with decreasing temperature. For the organic composite blocks, see Figure 35, the leading bogie shows a trend with highest energies at intermediate temperatures (maximum at about -2 ºC) and no variation with the UIC index. For the trailing bogie there is a trend with decreasing the brake friction work at towards higher UIC indices, but also a slight increase of brake work with a lowering of temperatures.

Again, it must be pointed out that there is a lack of data for low temperatures in general, and in particular for the cast iron and the organic composite block materials where no data are available for temperatures below -8 ºC. The models are fitted to a rather narrow range of temperatures.

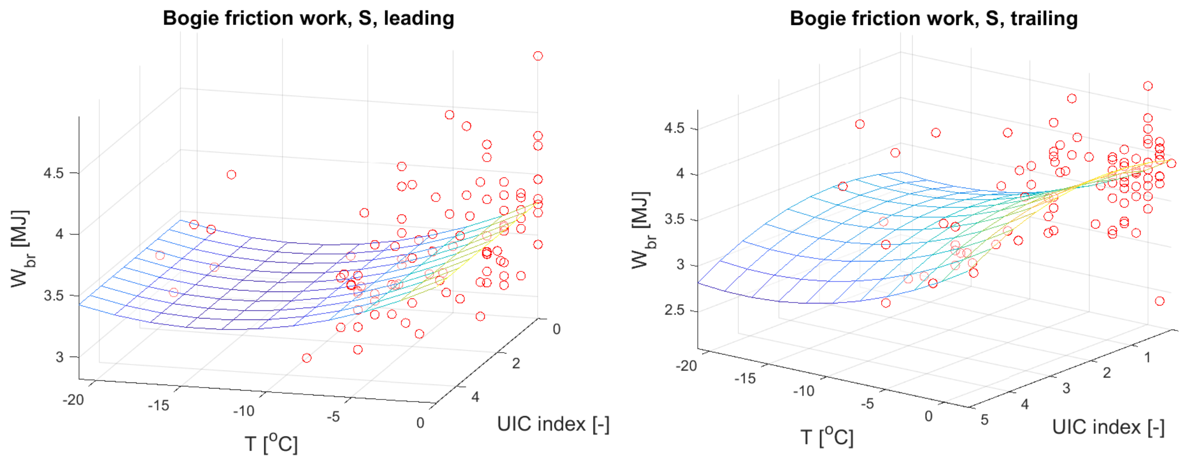

Figure 33 Sinter brake blocks: Calculated total brake friction work for half a bogie as function of air temperature and UIC winter index. Bogie in leading position in wagon (left) and trailing position (right)

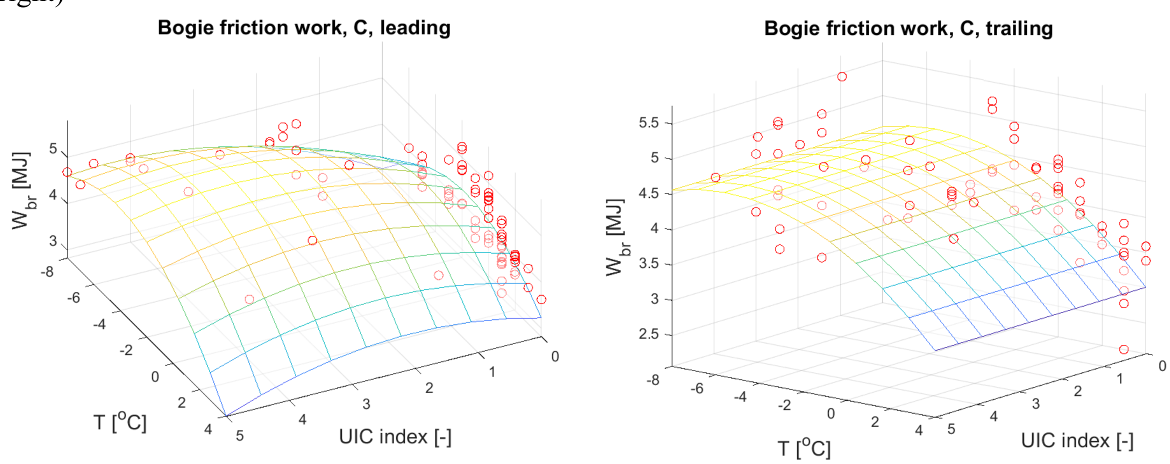

Figure 34 Cast iron blocks: Calculated total brake friction work for half a bogie as function of air temperature and UIC winter index. Bogie in leading position in wagon (left) and trailing position (right)

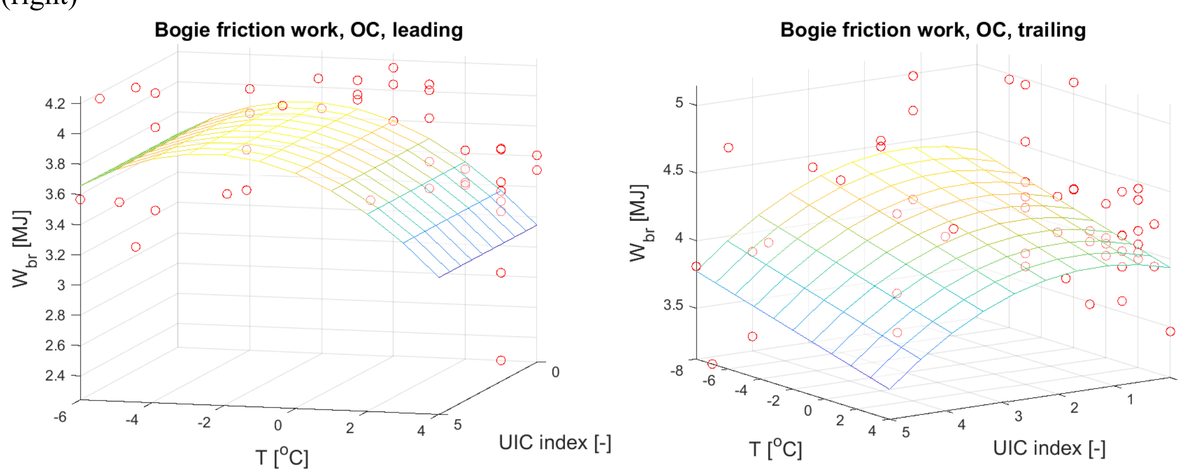

Figure 35 Organic composite blocks: Calculated total brake friction work for half a bogie as function of air temperature and UIC winter index. Bogie in leading position in wagon (left) and trailing position (right)

4.2.5. **Brake friction force of individual hanger links**

The braking performance of block inserts pertaining to single hanger links is now studied with respect to friction force. As previously, the friction force is presented as the time averaged force for the time during which the pneumatic brake pressure is at its nominal level. The same hanger link forces as in the previous sections are studied. The data are analysed with respect to dependencies when it comes to air temperature and UIC snow index. Linear regression modelling employing stepwise regression is performed on data with regard to these two parameters. Data from two of the wagons are presented individually, meaning that data for sinter blocks come both from early tests on wagon 2 and from all tests on wagon 4 (for that one instrumented bogie). In the figures, filled markers indicate that the data point comes from a braking cycle just after the train has changed its travelling direction, whereas the unfilled markers indicate that they are for braking cycles for which the train has previously performed brake cycles in the same travelling direction.

The friction forces for sinter blocks are presented in Figure 36 (for wagon 2) and in Figure 37 (for wagon 4) along with the surfaces fitted to the data. Data are shown for axle one up to four in such a way that axle 1 means the leading axle of the wagon and axle 4 is the trailing[24]. Hangers on the leading side and trailing side of the wheels of the axles are presented separately. Generally, the fitted surfaces indicate that there are only weak dependencies on the studied parameters of temperature and UIC index, showing rather horizontal surfaces. There are some trends that indicate less braking friction forces at lower temperature and higher UIC indices (Wagon 2, axles 1-3, Leading; Wagon 2, axles 3 and 4 trailing; Wagon 4, axle 4 trailing). There is no apparent difference between brake cycles immediately after the test train has changed its traveling direction (filled markers in the plots) and other brake cycles.

For cast iron material, Figure 38, the fitted surfaces generally indicate somewhat increasing braking performance with lower temperatures and/or UIC indices. However, the hanger link on the trailing side of Axle 2 shows a decrease in braking performance for the lowest temperatures.

For the organic composite blocks, see Figure 39, it can first be noticed that the data for axles 1 and 2 are for a very narrow range of temperatures (between -4 ºC and +4 ºC). For these axles, the fitted surfaces generally indicate that there are only weak dependencies on the studied parameters, with the exception being the leading side of axle 1 that shows some decrease at higher UIC indices. Axles 3 and 4 show slightly increasing braking performance with decreasing temperature and only slight variations with UIC indices, except for trailing Axle 4 that shows some weakening at high UIC indices.

Again, it must be pointed out that the models are fitted for a rather narrow range of temperatures.

---

[24] It is thus results for different wheels and blocks that are presented.

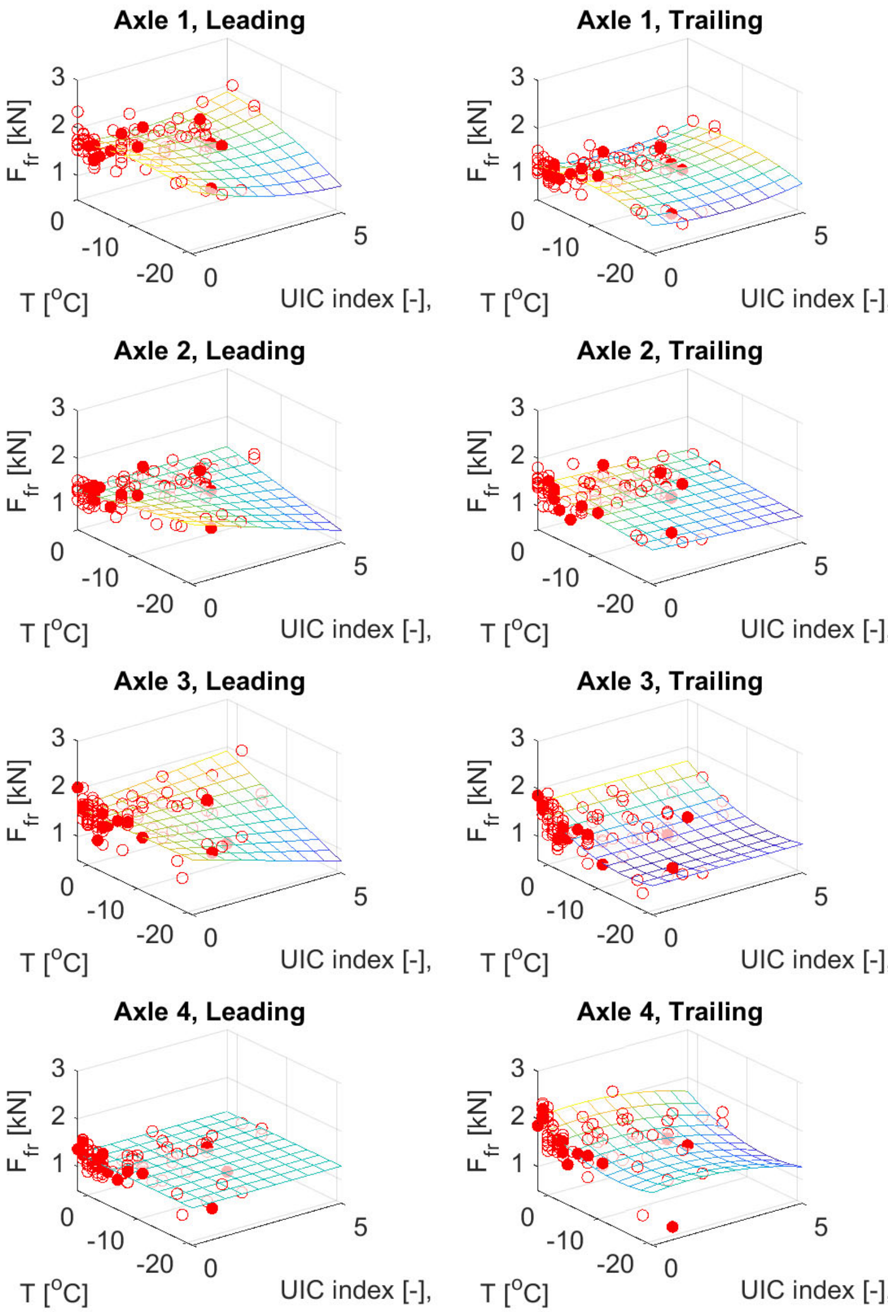

Figure 36 Sinter brake blocks: Calculated average brake friction forces for hanger links pertaining to given axles and positions on wagon 2 when equipped as function of air temperature and UIC winter index. Axle 1 is leading axle of wagon and axle 4 is trailing. A filled marker indicate that the datum point comes from a braking cycle just after the train changed its travelling direction

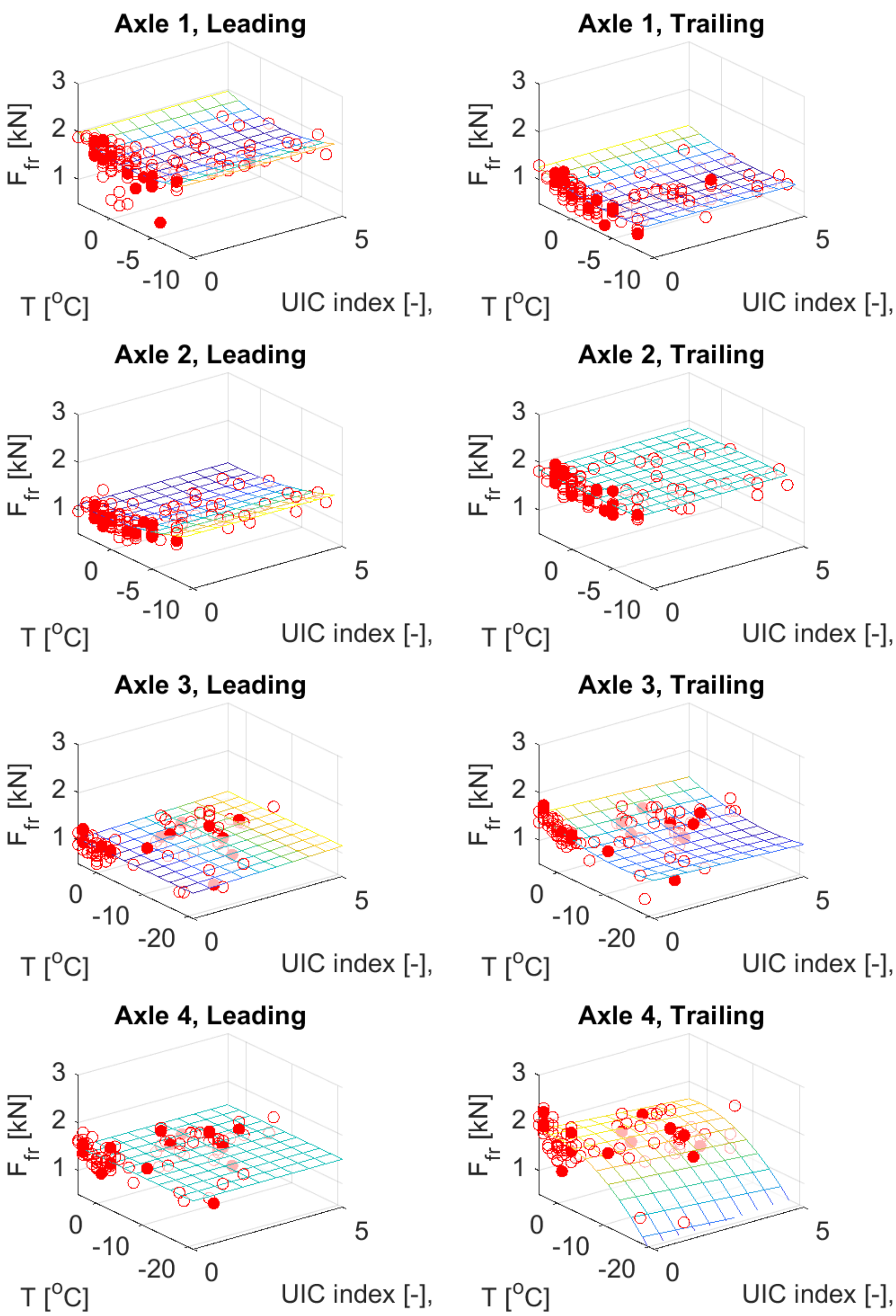

Figure 37 Sinter brake blocks: Calculated average brake friction forces for hanger links pertaining to given axles and positions of wagon 4 when equipped as function of air temperature and UIC winter index. Axle 1 is leading axle of wagon and axle 4 is trailing. A filled marker indicate that the datum point comes from a braking cycle just after the train changed its travelling direction

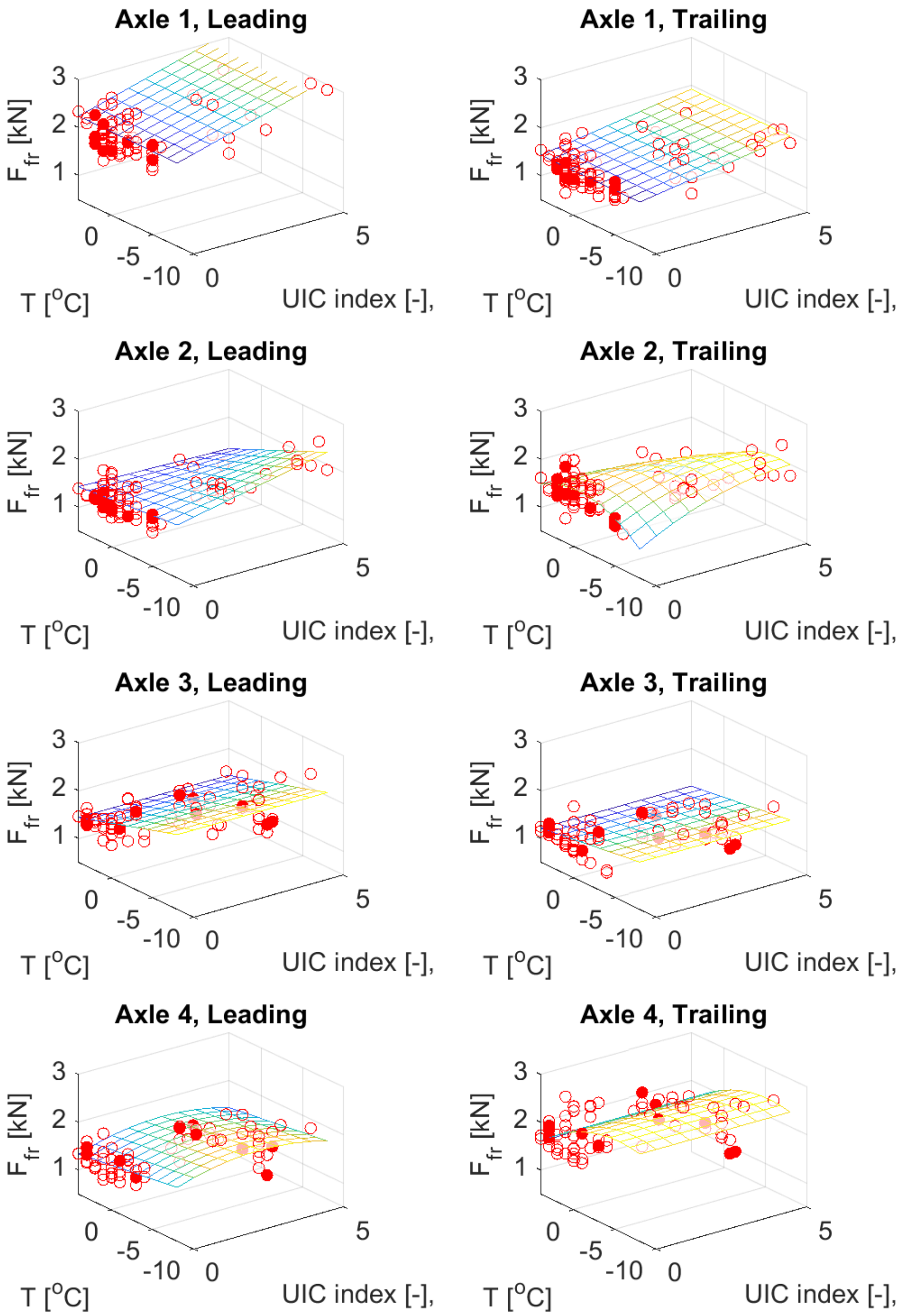

Figure 38 Cast iron brake blocks: Calculated average brake friction forces for hanger links pertaining to given axles and positions of wagon 2 as function of air temperature and UIC winter index. Axle 1 is leading axle of wagon and axle 4 is trailing. A filled marker indicate that the datum point comes from a braking cycle just after the train changed its travelling direction

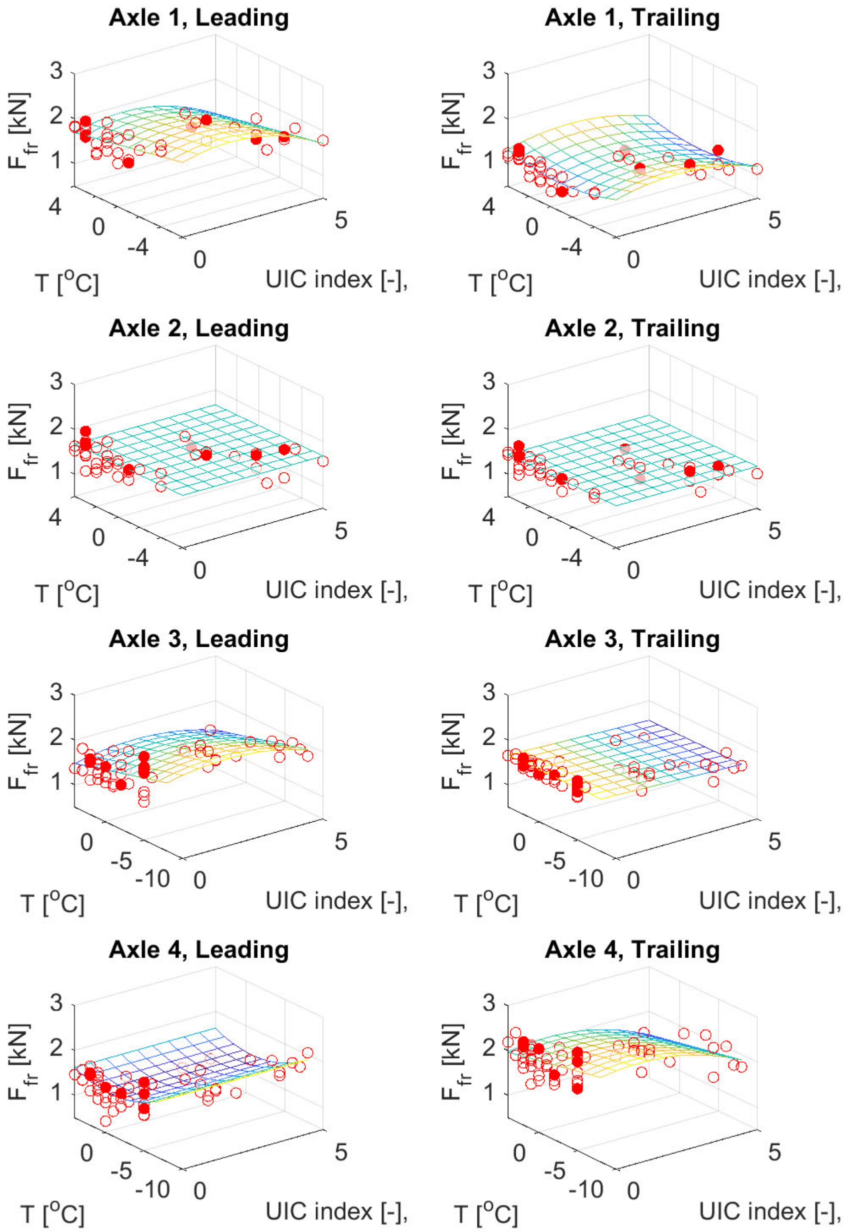

Figure 39 Organic composite brake blocks: Calculated average brake friction forces for hanger links pertaining to given axles and positions of wagon 2 as function of air temperature and UIC winter index. Axle 1 is leading axle of wagon and axle 4 is trailing. A filled marker indicate that the datum point comes from a braking cycle just after the train changed its travelling direction.

4.2.6. **Brake friction work of individual hanger links**

The braking performance of single hanger links is now studied with respect to friction work considered for the entire brake cycle. The data are analysed with respect to dependencies to air temperature and UIC snow index as in the previous section. In the figures, filled markers indicate that the datum point comes from a braking cycle just after the train has changed its travelling direction, whereas the unfilled markers indicate that they are for braking cycles for which the train has previously performed brake cycles in the same travelling direction.

The friction work magnitudes for sinter blocks are presented in Figure 40 (for wagon 2) and Figure 41 (for wagon 4) along with the surfaces fitted to the data. Generally, the fitted surfaces indicate that there are only weak dependencies on the studied parameters being temperature and UIC index, showing rather horizontal surfaces. There are some trends that indicate less braking friction work at lower temperature and higher UIC indices (Wagon 2, axle 3; Wagon 2, axle 4 trailing). A substantial decrease for lowered temperatures is (as for the friction force study) found for Wagon 4, axle 4, trailing. There is also a trend of increasing braking work when the temperature drops, see Wagon 4, axle 2 or leading side of axles 3 and 4. There is no apparent difference between brake cycles immediately after the test train has changed its traveling direction (filled markers in the plots) and other brake cycles.

For cast iron material, see Figure 42, the fitted surfaces generally indicate somewhat increasing brake work with lower temperatures and/or increased UIC indices (as also found for the study of friction force), but there are also indications of decreasing braking work for the very lowest temperatures (about –10 ºC) for axles 1 and 2.

For the organic composite blocks, see Figure 43, it can first (again) be noticed that the data for axles 1 and 2 are for a very narrow range of temperatures (between –4 ºC and +4 ºC). For these axles, the fitted surfaces generally indicate that there are only weak dependencies on the studied parameters, but with some tendencies for decreasing braking work for the lowest temperatures (–4 ºC). Axles 3 and 4 show some tendencies for decreasing braking energy for lower temperatures (Axle 3 Trailing), for higher UIC indices (Axle 4, Trailing), but also a slight increase in energy can be found with the lowering of temperature (Axle 3, Leading).

Again, it must be pointed out that the models are fitted to a rather narrow range of temperatures.

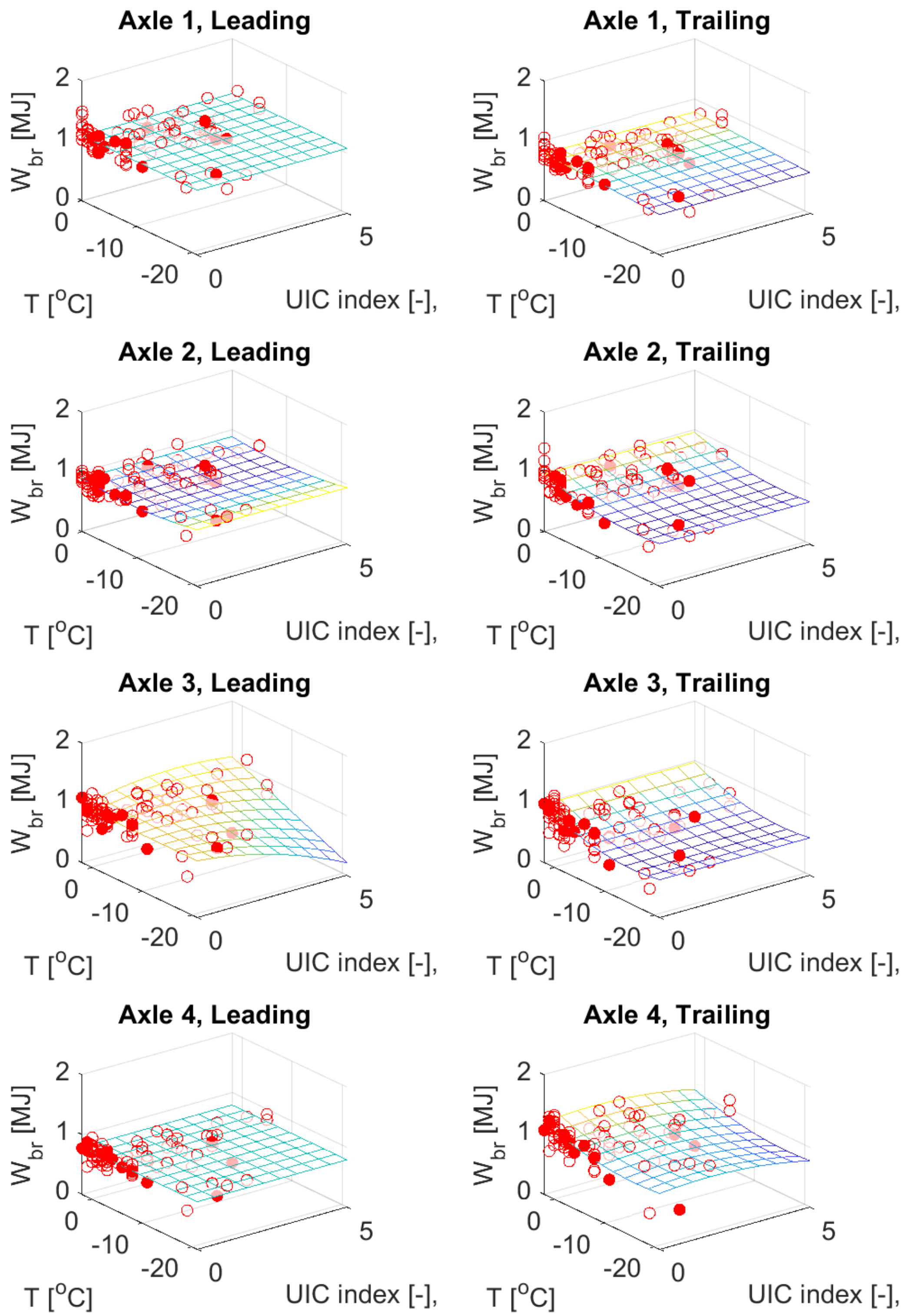

Figure 40 Sinter brake blocks: Calculated average brake friction work for hanger links pertaining to given axles and positions on wagon 2 as function of air temperature and UIC winter index. Axle 1 is leading axle of wagon and axle 4 is trailing. A filled marker indicate that the datum point comes from a braking cycle just after the train changed its travelling direction.

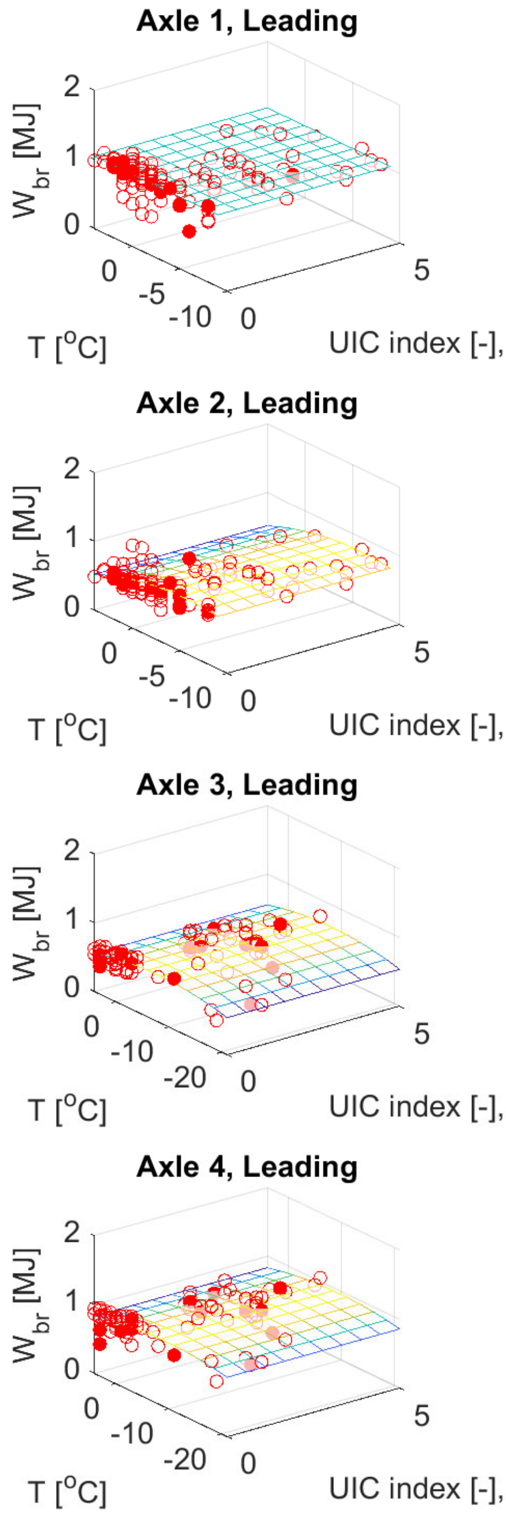

Figure 41 Sinter brake blocks: Calculated average brake friction work for hanger links pertaining to given axles and positions of wagon 4 as function of air temperature and UIC winter index. Axle 1 is leading axle of wagon and axle 4 is trailing. A filled marker indicate that the datum point comes from a braking cycle just after the train changed its travelling direction.

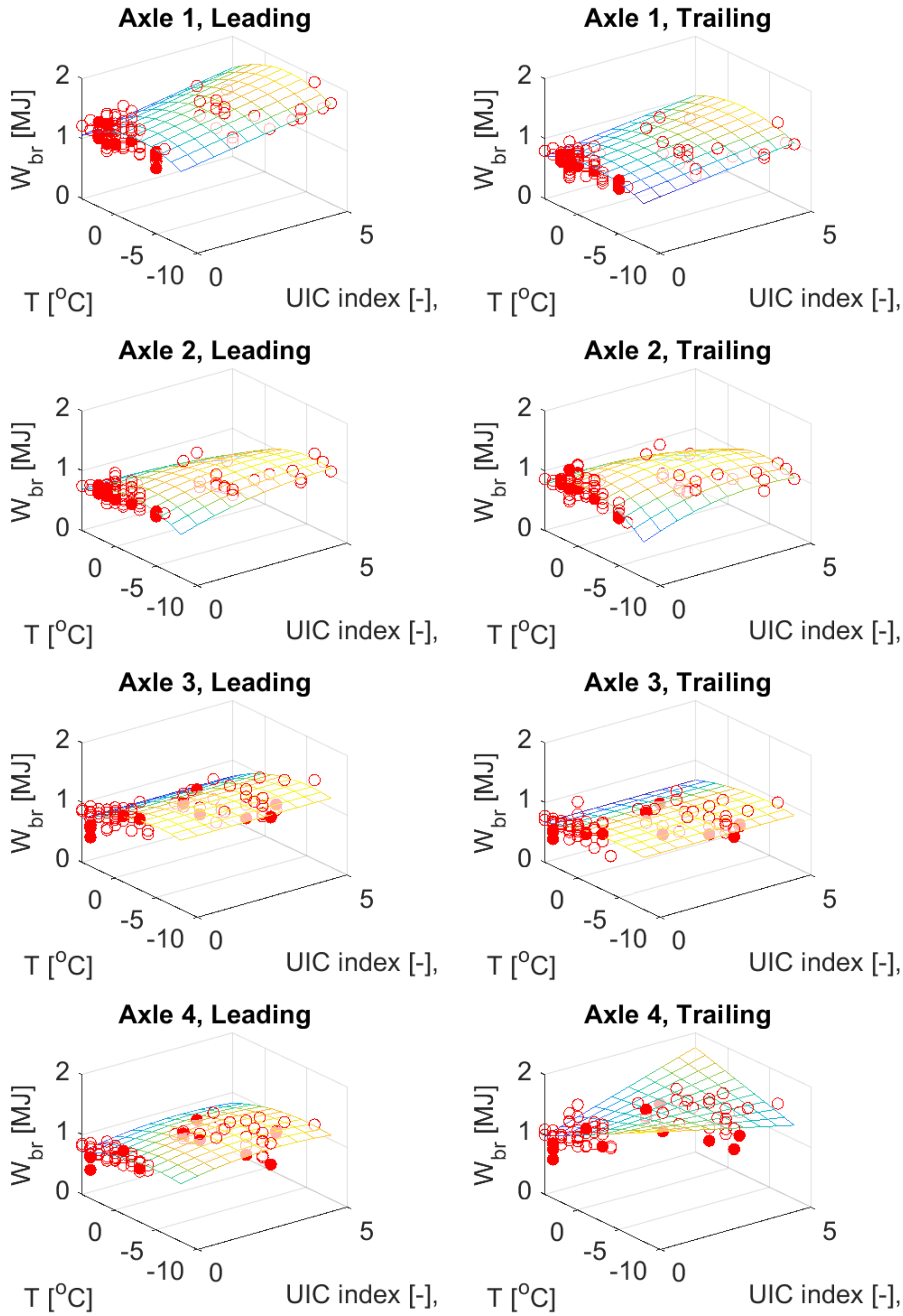

Figure 42 Cast iron brake blocks: Calculated average brake friction work for hanger links pertaining to given axles and positions of wagon 2 as function of air temperature and UIC winter index. Axle 1 is leading axle of wagon and axle 4 is trailing. A filled marker indicate that the datum point comes from a braking cycle just after the train changed its travelling direction.

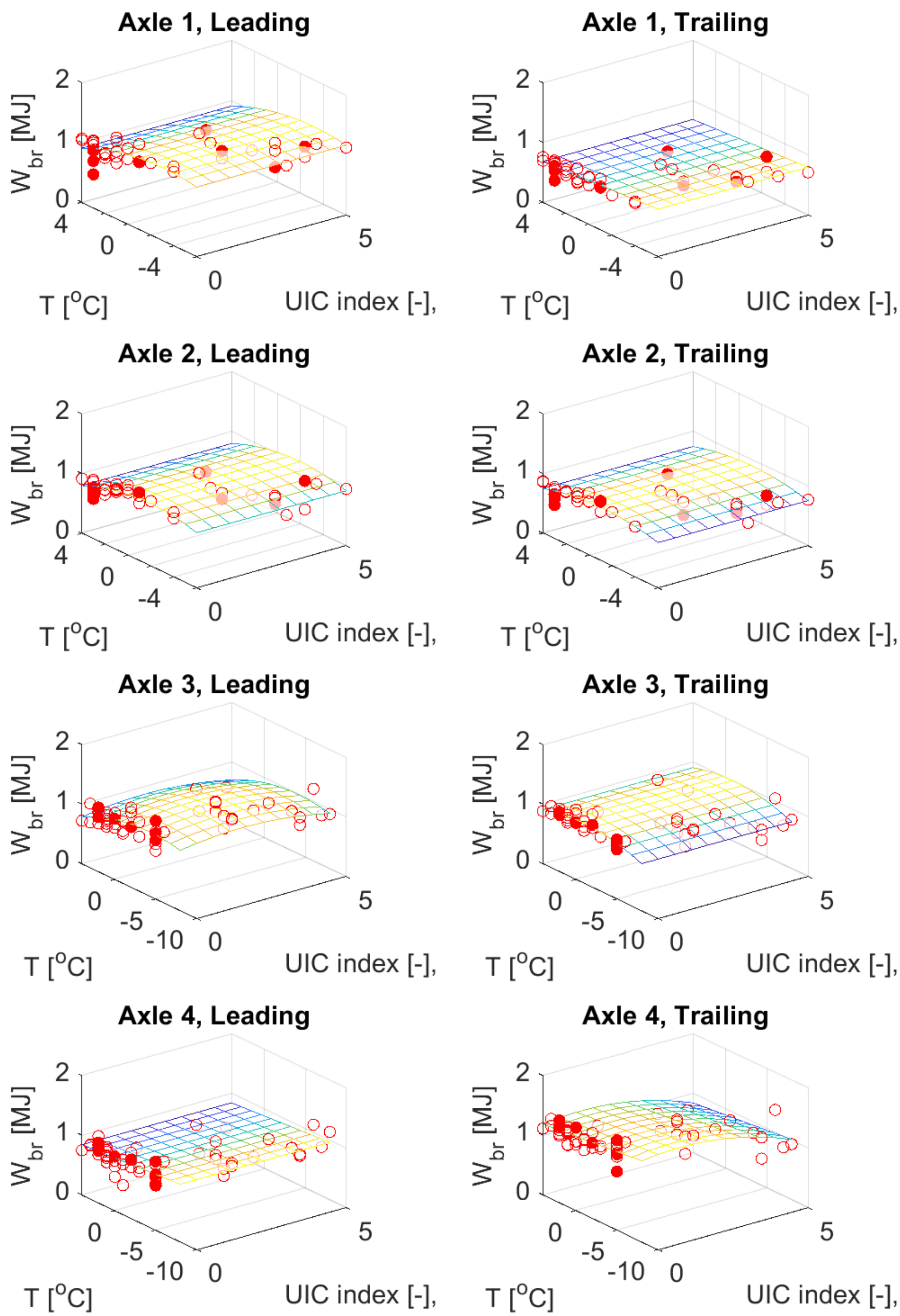

Figure 43 Organic composite brake blocks: Calculated average brake friction work for hanger links pertaining to given axles and positions of wagon 2 as function of air temperature and UIC winter index. Axle 1 is leading axle of wagon and axle 4 is trailing. A filled marker indicate that the datum point comes from a braking cycle just after the train changed its travelling direction.

4.2.7. **Time delay to onset of braking for individual block inserts**

The braking performance is now studied with respect to the time delay until the onset of the braking force for the individual brake block inserts. Here, it has been chosen to employ a criterion based on braking energy supposing that this time delay value is the time from start of pneumatic pressure rise until the time at which the level of 10 % of the maximum friction work for the entire stop of any block insert (for the considered wagon and braking) has been reached by the insert of the individual hangers. The data are analysed with respect to dependencies when it comes to air temperature and UIC snow index as in the previous four section. In the figures, filled markers indicate that the datum point comes from a braking cycle just after the train has changed its travelling direction, whereas the unfilled markers indicate that they are for braking cycles for which the train has previously performed brake cycles in the same travelling direction. Note that the vertical axles here do not have uniform scaling, because of the rather large occasional time delays.

The resulting time delay for sinter blocks are presented in Figure 44 (for wagon 2) and Figure 45 (for wagon 4) along with the surfaces fitted to the data. A first observation is that half of the 8 studied inserts have time until onset ranging between 5 and 10 s, while the remaining ones show some higher time delays. For those, the highest time delays are found for either low temperatures or for high UIC indices (with highest value for any fitted surface being 20 s for wagon 4, Axle 4, Trailing at the lowest temperature –20 ºC).

For cast iron material, Figure 46, the time delays generally range between 4 s and 8 s, with only exception being Axle 2 Trailing with two data points around 11 s occurring at high UIC index and lowest temperature (–10 ºC).

For the organic composite blocks, see Figure 47, it can again be noticed that the data for axles 1 and 2 are for a very narrow range of temperatures (between –4 ºC and +4 ºC). For these two axles, the time delays are all below 10 s. There are however some tendencies for increasing time delays for decreasing temperature and higher UIC indices. Axles 3 show some tendencies for increasing time delays for lower temperatures when combined with high UIC indices, which is also the case for Axle 4, Trailing. Axle 4, Leading show rather consistent time delays with no clear trends.

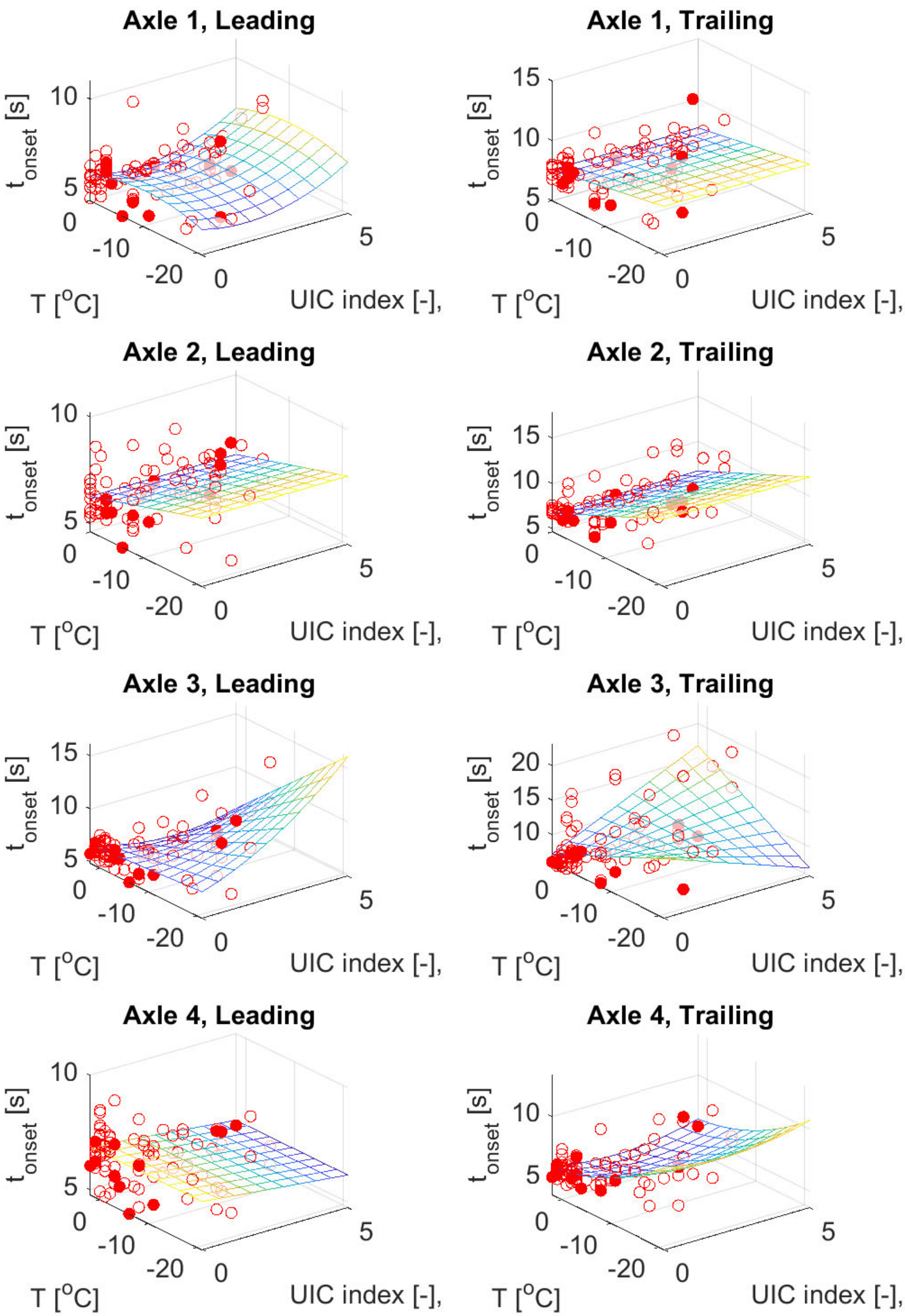

Figure 44 Sinter brake blocks: Calculated time delay until onset of brake friction forces for hanger links pertaining to given axles and positions on wagon 2 as function of air temperature and UIC winter index. Axle 1 is leading axle of wagon and axle 4 is trailing. A filled marker indicate that the datum point comes from a braking cycle just after the train changed its travelling direction.

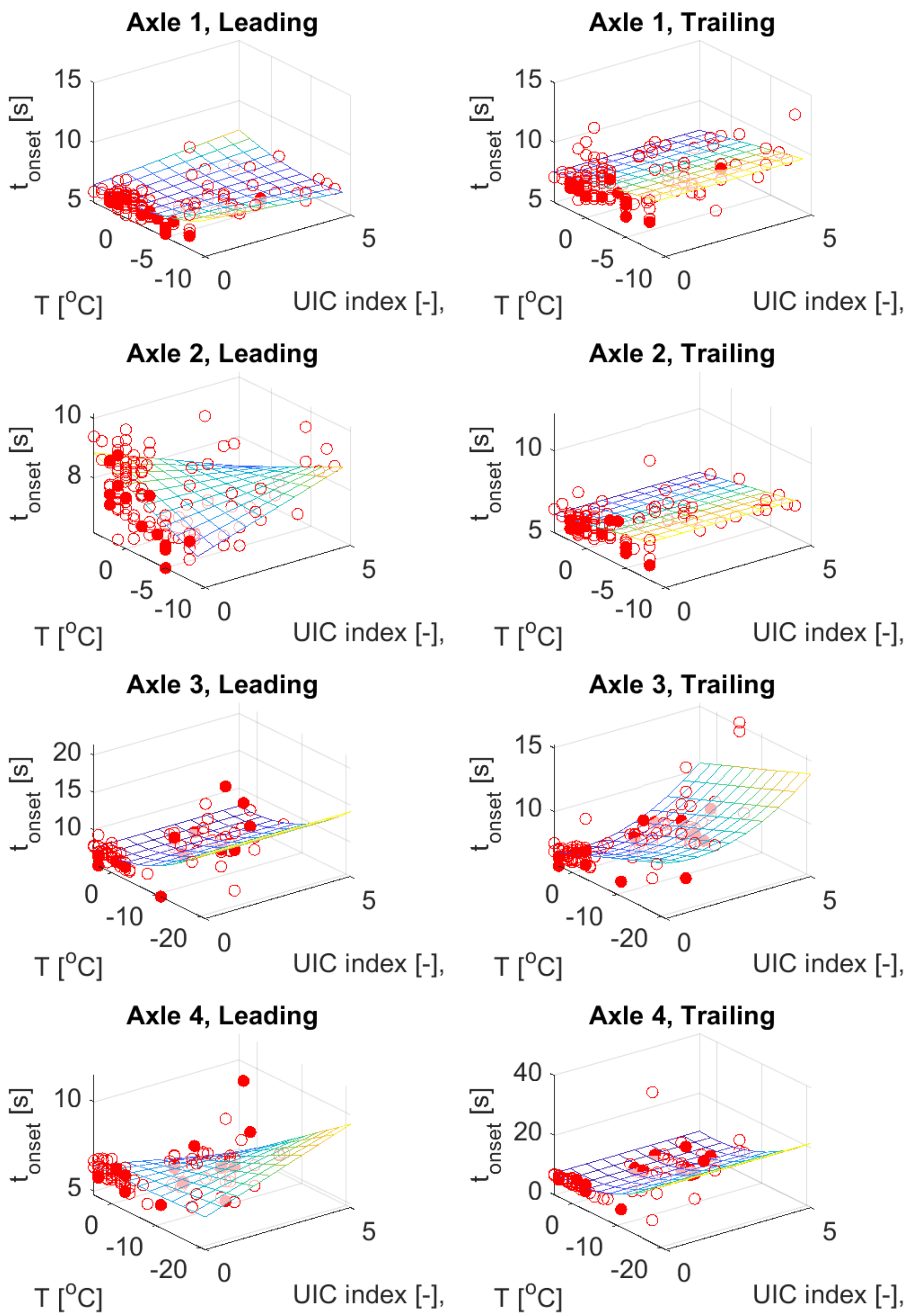

Figure 45 Sinter brake blocks: Calculated time delay until onset of brake friction forces for hanger links pertaining to given axles and positions of wagon 4 as function of air temperature and UIC winter index. Axle 1 is leading axle of wagon and axle 4 is trailing. A filled marker indicate that the datum point comes from a braking cycle just after the train changed its travelling direction.

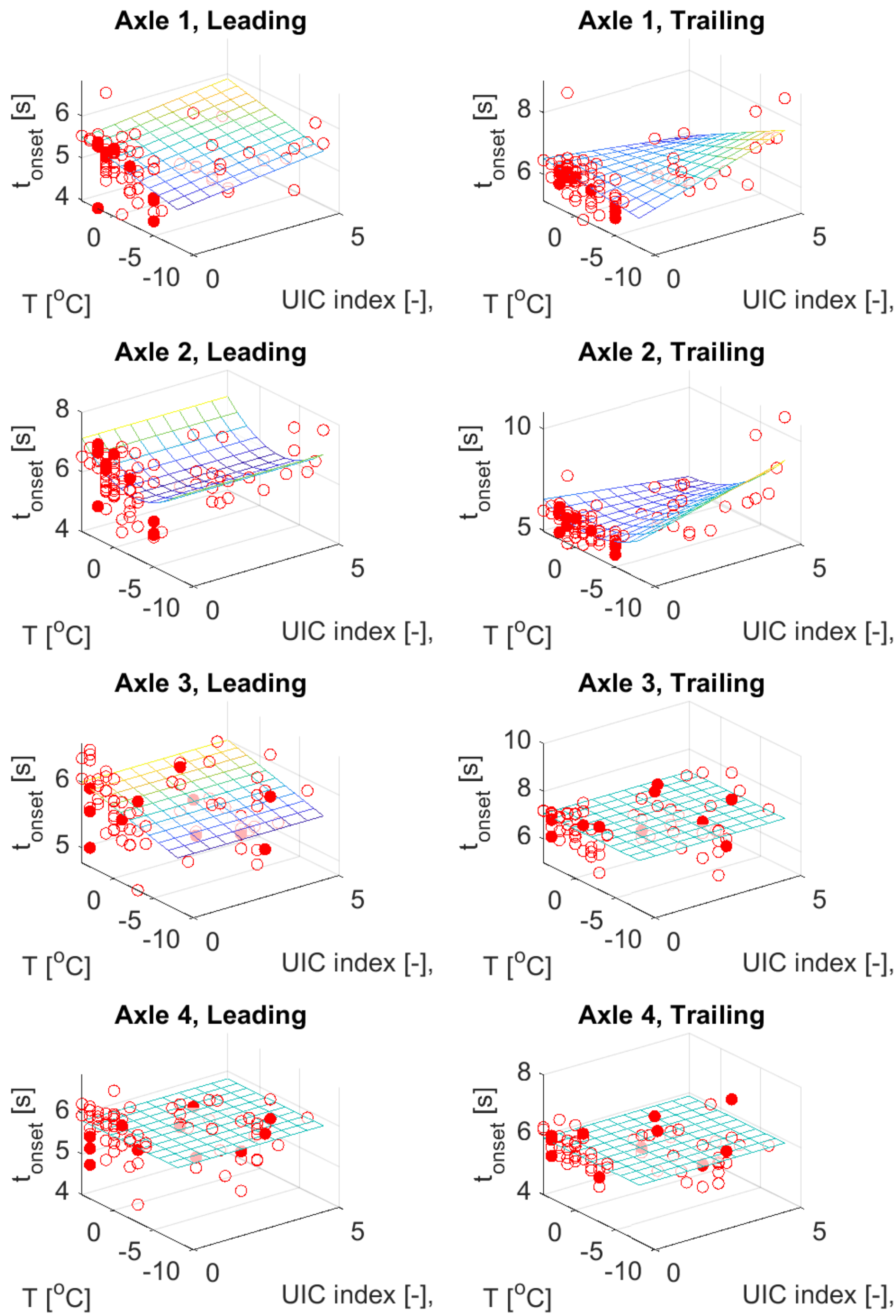

Figure 46 Cast iron brake blocks: Calculated time delay until onset of brake friction forces for hanger links pertaining to given axles and positions of wagon 2 as function of air temperature and UIC winter index. Axle 1 is leading axle of wagon and axle 4 is trailing. A filled marker indicate that the datum point comes from a braking cycle just after the train changed its travelling direction.

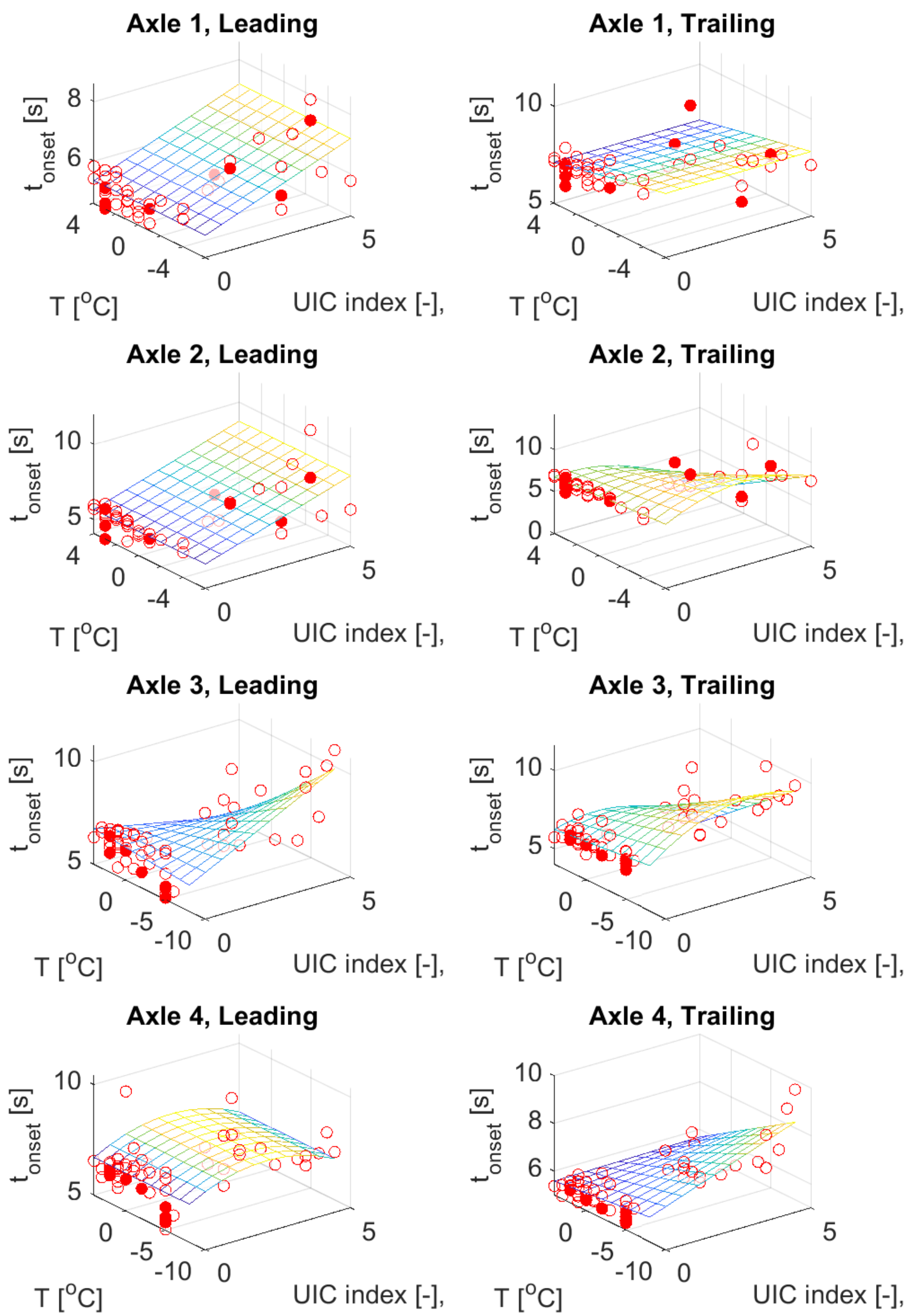

Figure 47 Organic composite brake blocks: Calculated time delay until onset of brake friction forces for hanger links pertaining to given axles and positions of wagon 2 as function of air temperature and UIC winter index. Axle 1 is leading axle of wagon and axle 4 is trailing. A filled marker indicate that the datum point comes from a braking cycle just after the train changed its travelling direction.

4.3. Comparison of winter seasons 2016–2017 up to 2019–2020

The winter season 2019–2020 is by Swedish citizens being remembered as a mild one. In an effort to demonstrate the different metrological conditions for the past four winters, data has been compiled using the data provided by Trafikverket for station 2553, located at Niemisel near test site 2 in the northern part of Sweden. The average monthly temperatures are shown in Figure 48. It shows that the average temperatures during November, December and January have been substantially higher (warmer) than the three years prior, with a lowest average temperature of –8.6 ºC. Lowest average temperatures are for the three earlier years –9.3, –13.5 and –15.5 ºC, respectively.

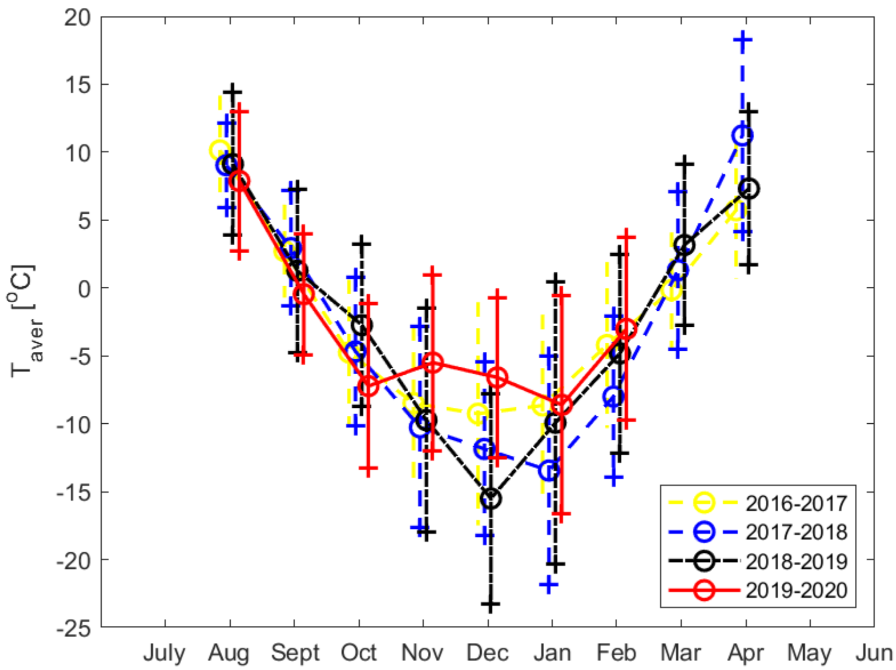

Figure 48 Overview of average temperatures indicated by circles during months August to May for the four past seasons. Vertical intervals indicate standard deviation of temperatures.

Additional information is provided in Appendix B. In Figure 62 and Figure 63, three-dimensional histograms show the number of occasions of ranges of snow-fall intensities in millimetres per 30 minutes vs air temperature. A first observation is that the lengths of the winter seasons are 185 days (days from first snow to last falling of snow), 161, 189 and 146, sequentially for the four considered winter seasons. The total durations of snowfall (recalculated into days) are 29, 47, 33 and 28 days. Thus, the winter 2019–2020 was somewhat shorter and also had less time of snowing than the others. One can see that most of the snowfall for the recent winter of 2019-2020 has occurred with a low intensity (0 – 1 mm / 30 min) in combination with a temperature of about 0 ºC (between –2 ºC and +2 ºC). For air temperatures below –10 ºC, there were few occasions (92 registered half-hours, any intensity) of snowfall during 2019–2020 as compared to previous winters with 140, 629 and 515 respectively. Focusing on snow-fall intensities higher than 1 mm / 30min, this is additionally presented in Figure 64. Here, it is clearly shown that the winter 2019–2020 has substantially less snowfall at lower temperatures than the two previous ones, but also somewhat less than 2016-2017. For temperatures below –15 ºC, there are nil occasions for

2019–2020, whereas for the previous years it is 11, 101 and 163 occasions. Similarly, when studying the possibility for snow-drift given in Figure 65, it is found that the winter 2019–2020 stands out since the number of occasions with possible snow drift at temperatures below –10 ºC are substantially lower than for the three other winters (1220 as compared to 1720, 2858 and 2672 occasions). Looking at the coldest temperature range, colder than –20 ºC, the differences are even more pronounced (129 as compared to 322, 735 and 1053 occasions).

5. Summary and Conclusions

The test campaign was performed using five tread braked and instrumented empty wagons and an unbraked locomotive in the most northern part of Sweden. The tests campaign had two main parts. The first consisted of stop brake tests with uniform block types (first organic composite blocks and later sinter blocks) and the second one featured one bogie with cast iron blocks and another bogie with organic composite blocks which were introduced with the remaining sinter block braked bogies. Early in the tests a small data acquisition system was employed, only capturing pneumatic brake data from the wagons. Later a larger system was installed that allowed for measurement also of braking forces (via instrumented hanger links and brake triangles) and temperatures of wheels and blocks. The results were analysed with respect to braking distances in the first part of the report and with a focus on braking forces in the second part. In addition to measured data, also metrological data has been acquired from Trafikverket for use in the data analysis.

5.1. Braking distances

The braking distance tests reported in Part 1 of the report show that the sinter brake blocks generally perform well for the encountered conditions (R0 up to W5), with average braking distances ranging between 750 m and 780 m. There were some longer stopping distance found for R0 reference conditions early in the tests (the first 30 stops exhibit a trend with decreasing braking distances) that tentatively indicate that the sinter blocks require thorough bedding in before they reach their full braking capacity.

The braking distances of the organic composite blocks show a trend with increasing braking distances for situations with snow whirling around the train than for reference conditions R0. For instance, the braking distance for UIC winter condition W3, the average braking distance has increased from 720 m at R0 up to 900 m (increase by 25%). A few brake cycles reach braking distances of around 1000 m. By employing regression models, a trend was discovered that indicate that the braking distance increases as the air temperature drops for high UIC winter indices, i.e. for conditions when there are substantial amounts of snow whirling around the wagons of the train. The fitted regression surfaces indicate that braking distances of about 1100 m could be resulting for UIC index 5 at –15 ºC, which was the lowest temperature for tests of the organic composite blocks.

In an effort to give an indication of nominal braking distance of the test train, a calculation was performed using information in UIC leaflet 544-1. Special considerations were made to consider the unbraked locomotive, the high efficiency of the braking systems of the test wagons, the longer filling time of the brake cylinders, and finally, the short length of the test train. Based on this, a nominal braking distance of 881 m was calculated for the test train.

The results presented above must be judged with care, keeping in mind the relatively mild winter weather experienced during the test campaign. For the organic composite blocks, the lowest temperature was –15 ºC, which can be deemed as a rather high temperature when considering normal conditions in the northern part of Sweden. A study of the metrological winter conditions during the four latest winters shows that the winter season 2019–2020 was a very mild one, with substantially higher temperatures than for earlier winters and it also shows less days of snowfall. Especially, the combination of snowfall at really low temperatures are less common than for previous years.

The trend for the organic composite brake blocks that point towards an increase in braking distances with a lowering of temperature for high UIC indices is problematic and could possibly indicate a safety problem for the blocks at very low temperatures of, say –30 ºC.

5.2. Brake friction forces

Later in the test campaign, presented in Part 2 of the report, forces of hanger links and of brake triangles are measured. Brake friction forces can be assessed based on estimated brake rigging geometries. The fact that a part of the brake normal force is taken by the hanger link, creating an offset superimposed on the friction force, means that the measurements are sensitive to the precise geometry around each hanger link. This geometry is affected by the wear state of the brake blocks, which is deemed only to change rather insignificantly during the test campaign, but also by the compression state of the primary suspensions of the wheelsets. To this end, the offsetting force (and the pertaining geometry) for each of the hanger links was determined by a comparative study for reference conditions in which the wagons were running in two different directions.

Braking performance results are presented on bogie level (friction forces and friction work for half a bogie) and for single hanger links (friction forces, friction work and time delay until onset of braking). Focus is on trends that could indicate deteriorated braking for winter conditions which are investigated by fitting of response surfaces by an automated procedure.

A first observation was that the braking friction force and also the brake work for a bogie show larger variations, indicated by larger standard deviations, for braking with cast iron blocks than for braking with the two LL type brake blocks.

For sinter blocks on bogie level, there are some such trends that point towards decreasing braking performance at high UIC indices for low temperatures (say, between –10 ºC and -15 ºC). However, there are very few data points from testing that fall into that category. Moreover, there are no such trends that could be observed from the brake distances when having uniform brake blocks on all wagons, for which even lower testing temperatures occurred. For single hanger links, only weak dependencies on temperature and UIC indices are generally found. For some of the hanger links there are some trends that indicate less braking performance at lower temperature and higher UIC indices, but again some also show increasing braking friction forces when the temperature drops. Regarding the time delay until onset of braking, assessed using a friction work criterion[25], half of the 8 studied inserts have time until onset ranging between 5 and 10 s, while the remaining ones show some higher time delays, with the highest time delays being found for either low temperatures or high UIC indices.

The results for cast iron blocks and organic composite blocks are even more limited when it comes to lowest testing temperatures compared to the tests with sinter blocks. This is a result of the fact that they were introduced later into the test campaign when milder winter temperatures prevailed. For this reason, no data points are available for cast iron blocks or for the organic composite material below –8 ºC.

The trends for the cast iron material is mixed, but often somewhat increasing braking performance with increasing UIC index or with decreasing temperature is found. However,

[25] Criterion that 10% of braking energy is consumed by the brake block insert for the considered hanger link.

there are also examples of the opposite. The time delays until onset of braking, generally fall range between 4 s and 8 s, with only exception being two data points around 11 s occurring at high UIC index and lowest temperature (–10 ºC).

For the organic composite material, there are mixed trends when it comes to temperature dependence, however over a narrow range of temperatures. There are some trends with decreasing braking performance towards higher UIC indices, but there is no consistency in the trends. Again, when it comes to time delays until onset of braking, there are some tendencies for increasing time delays for decreasing temperature and higher UIC indices, but the time delays are generally below 10 s.

APPENDIX A DETAILED INFORMATION WHEN BRAKING WITH UNIFORM BLOCK TYPE ON TRAIN

For each data category, the upper figure gives information on conditions for all brake cycles and the second top one gives information for those braking cycles that have braking distances larger than 833 m (> 833 m), the second bottom one is for > 900 m and the bottom one is for > 950 m.

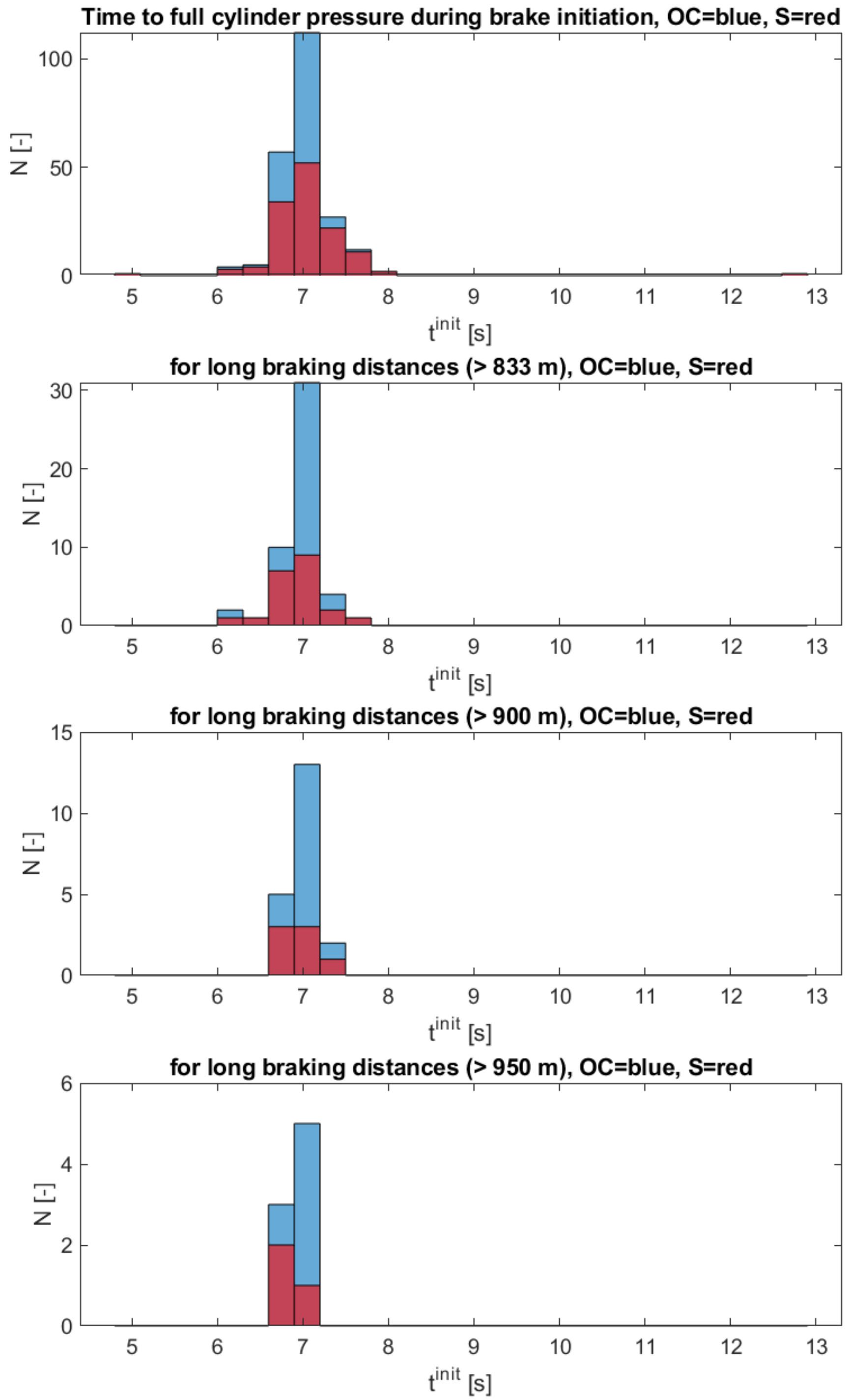

Figure 49 Time delay from initial pressure peak in brake cylinder until 90 %of maximum cylinder pressure is reached. Top: All cycles, second top cycles > 833 m, second bottom > 900 m and bottom > 950 m. Sinter is red and organic is blue.

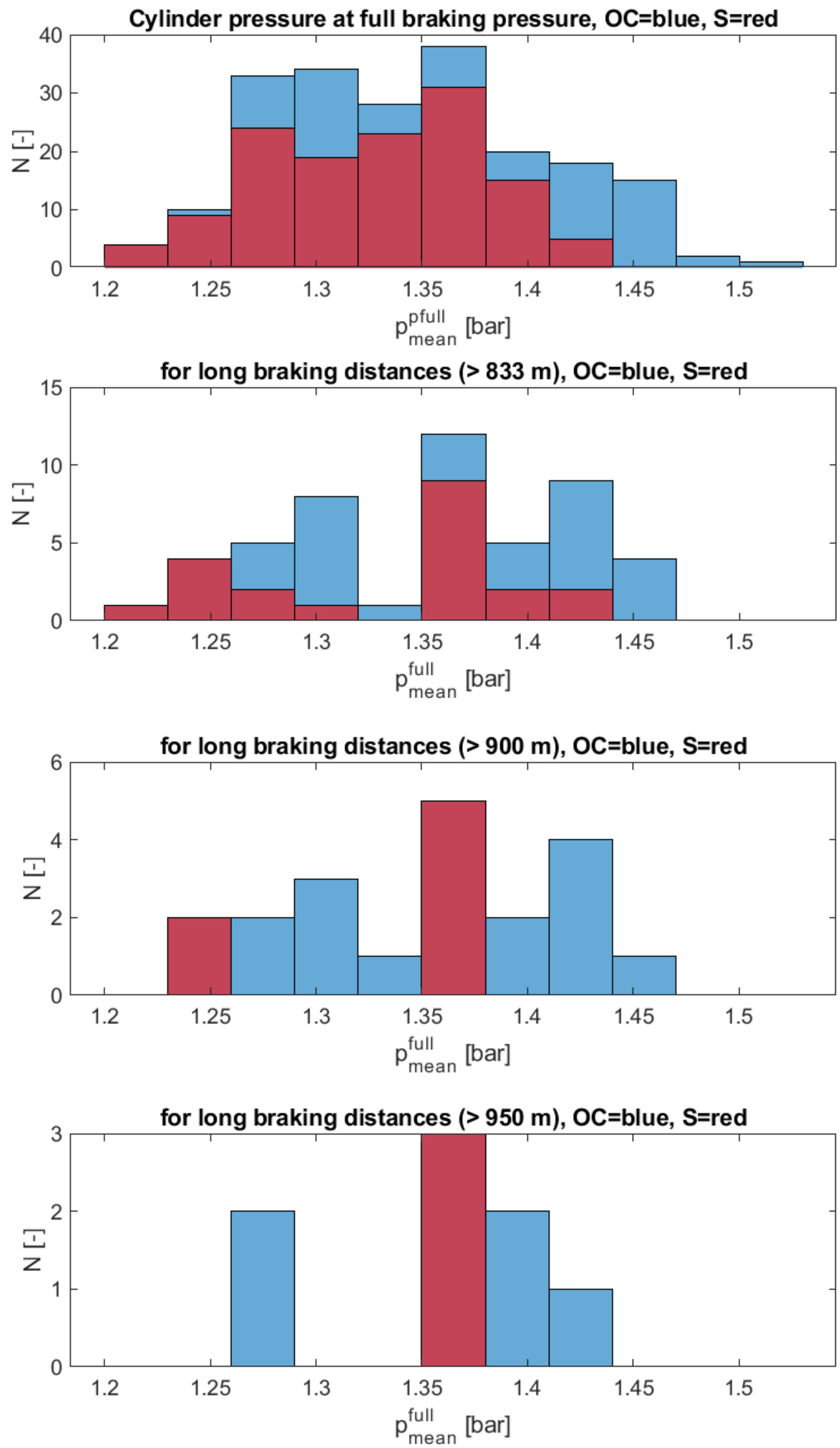

Figure 50 Overview of average full cylinder pressures. Top: All cycles, second top cycles > 833 m, second bottom > 900 m and bottom > 950 m. Sinter is red and organic is blue.

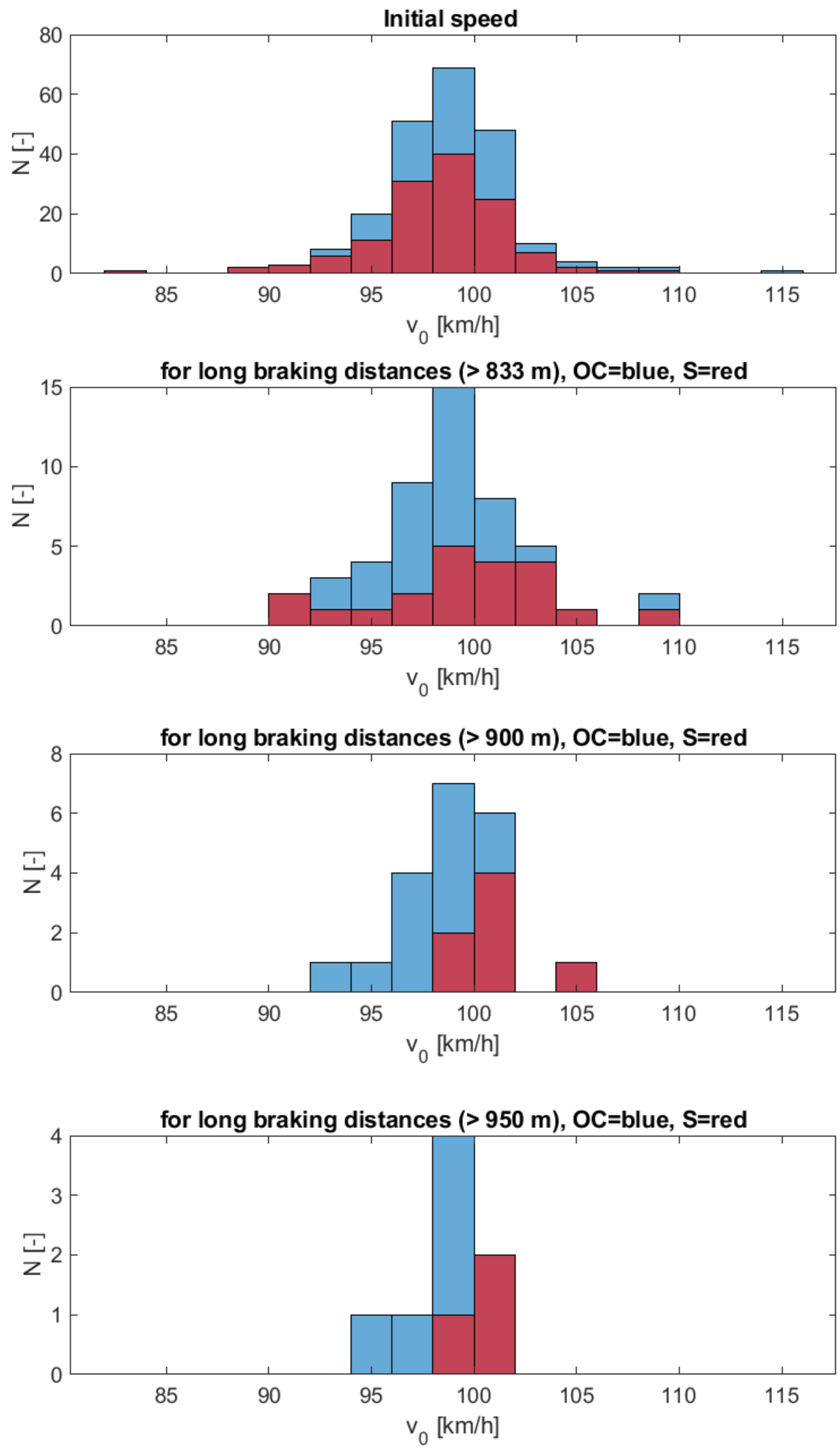

Figure 51 Overview of initial speeds. Top: All cycles, second top cycles > 833 m, second bottom > 900 m and bottom > 950 m. Sinter is red and organic is blue.

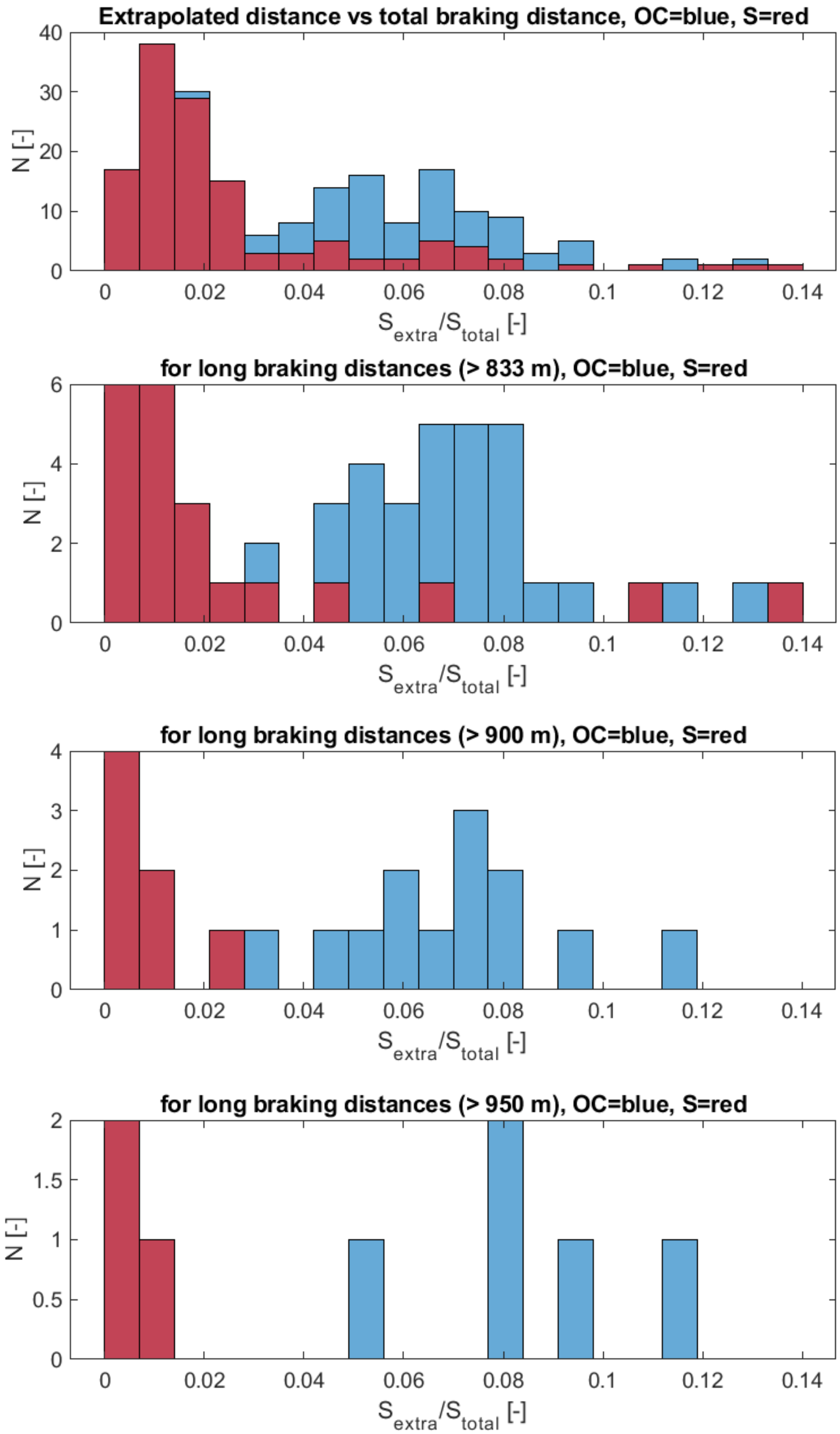

Figure 52 Overview of ratio between extrapolated distance and total braking distance. Top: All cycles, second top cycles > 833 m, second bottom > 900 m and bottom > 950 m. Sinter is red and organic is blue.

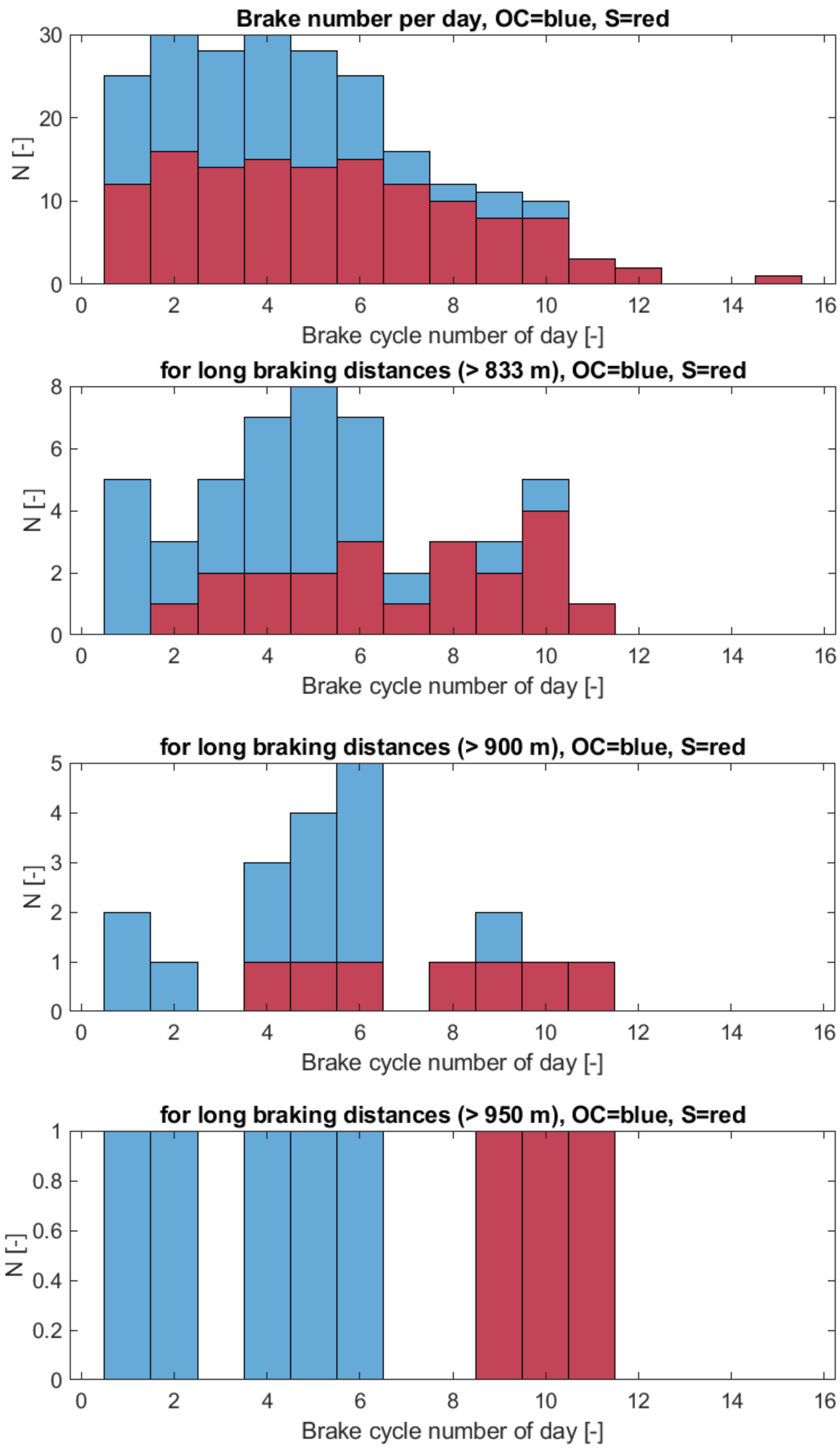

Figure 53 Overview of number of braking cycles pertaining to brake number of each day. Top: All cycles, second top cycles > 833 m, second bottom > 900 m and bottom > 950 m. Sinter is red and organic is blue.

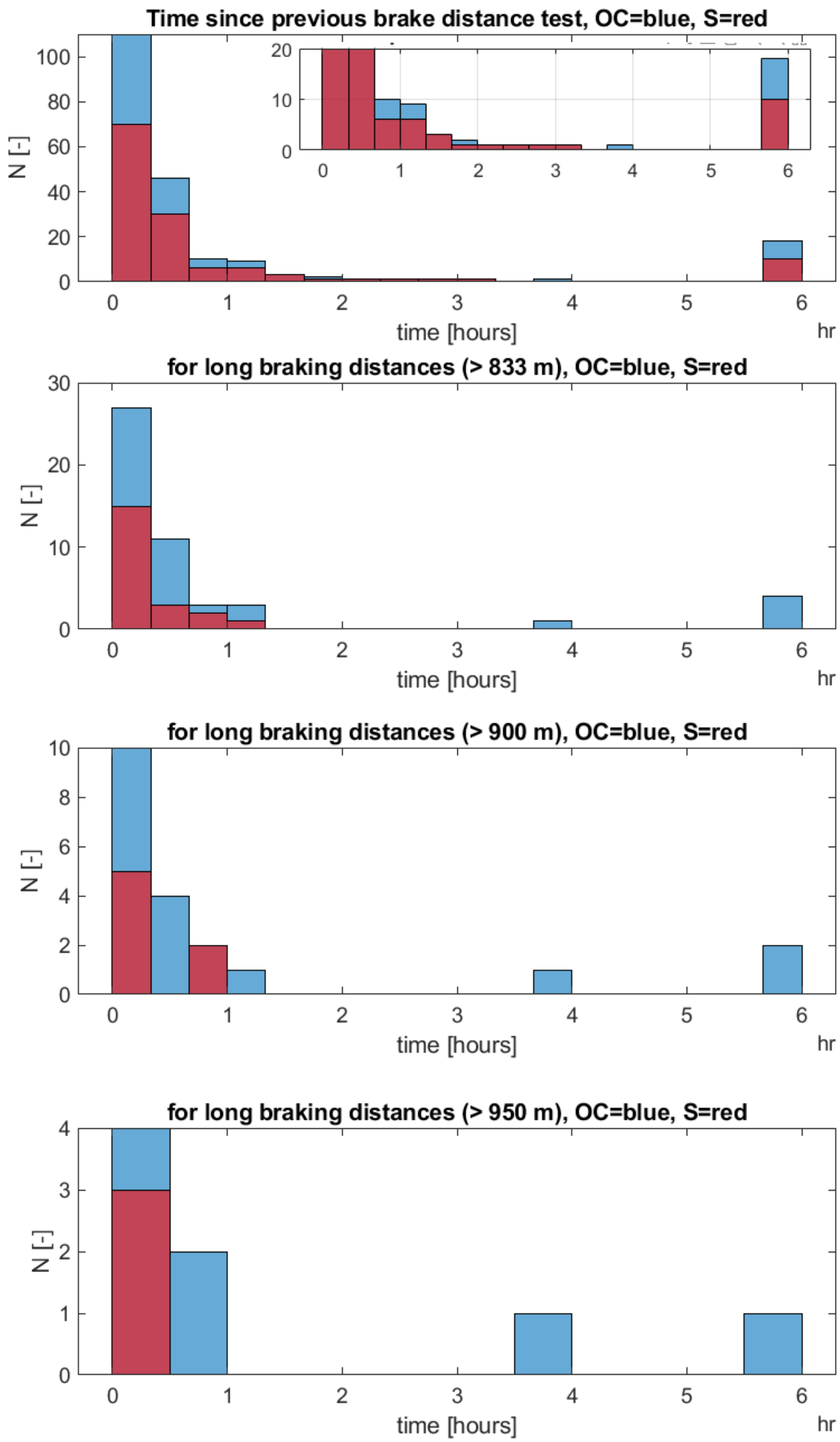

Figure 54 Overview of number of occurrences of time period from studied braking cycle to previous braking test. Maximum considered time gap is 6 h and time gaps larger than this have been categorized as 6 h. Top: All cycles, second top cycles > 833 m, second bottom > 900 m and bottom > 950 m. Sinter is red and organic is blue.

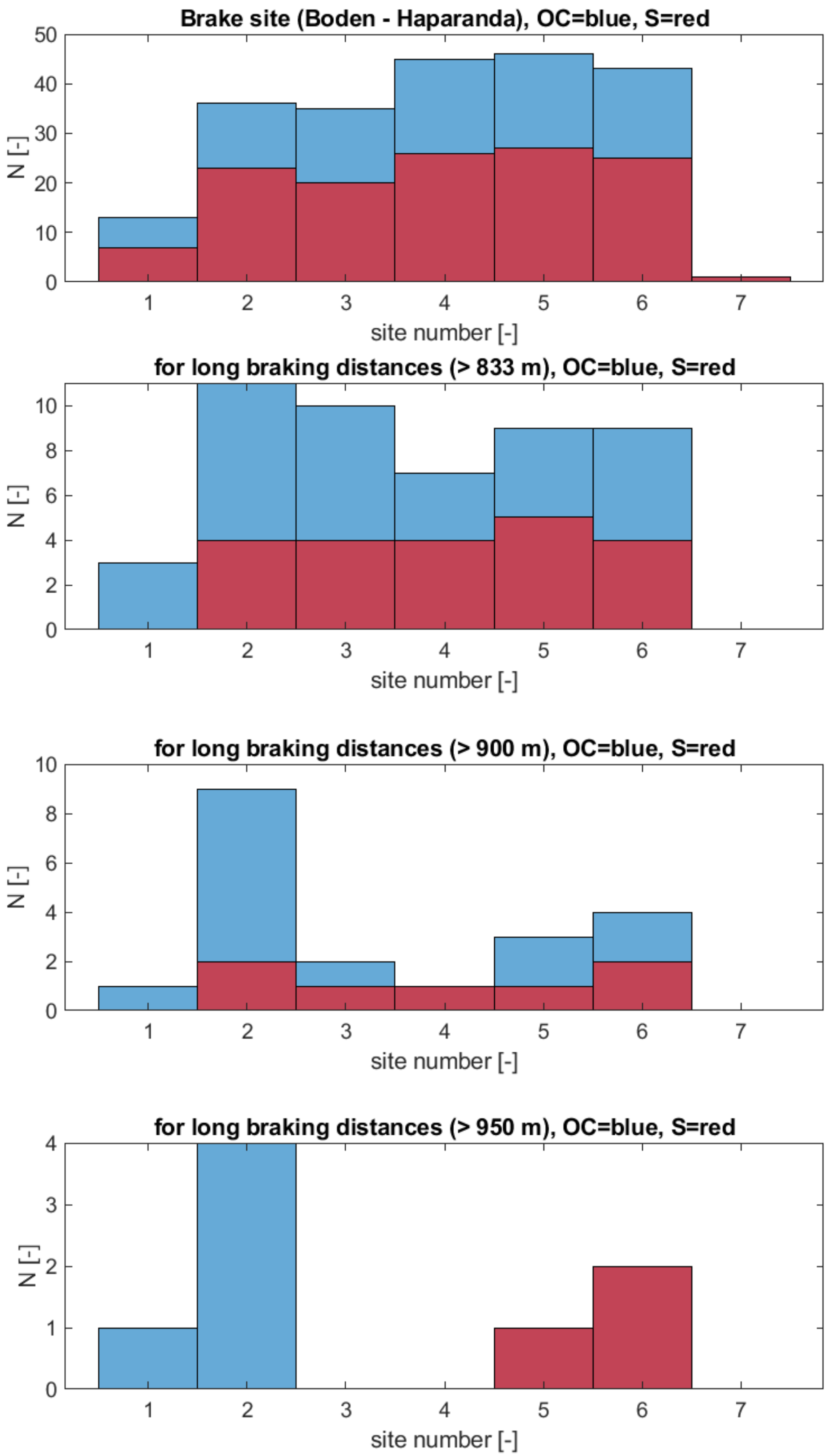

Figure 55 Overview of number of braking cycles per brake site. Top: All cycles, second top cycles > 833 m, second bottom > 900 m and bottom > 950 m. Sinter is red and organic is blue.

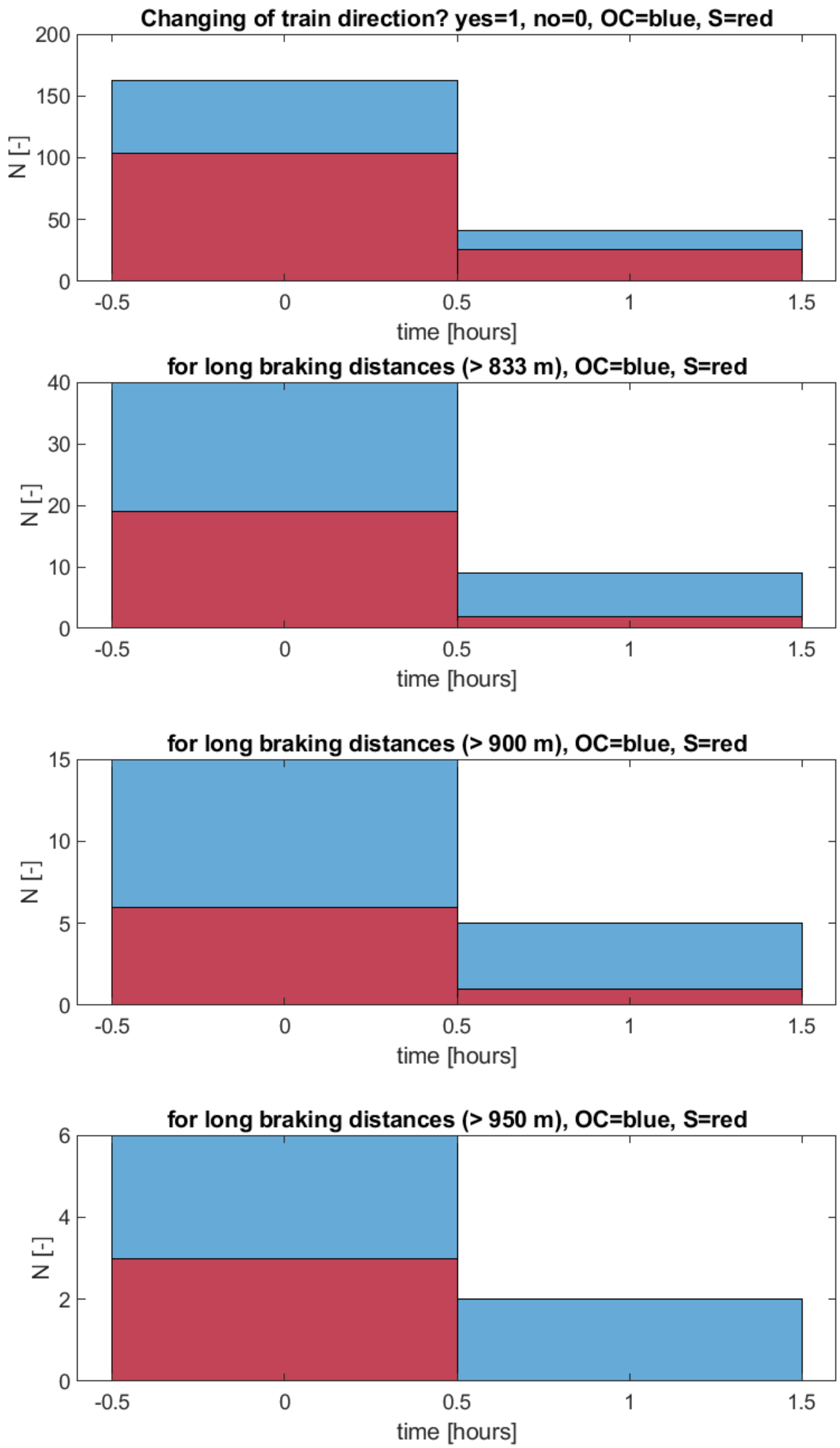

Figure 56 Overview of braking cycles directly after changing direction of test train. Top: All cycles, second top cycles > 833 m, second bottom > 900 m and bottom > 950 m. Sinter is red and organic is blue.

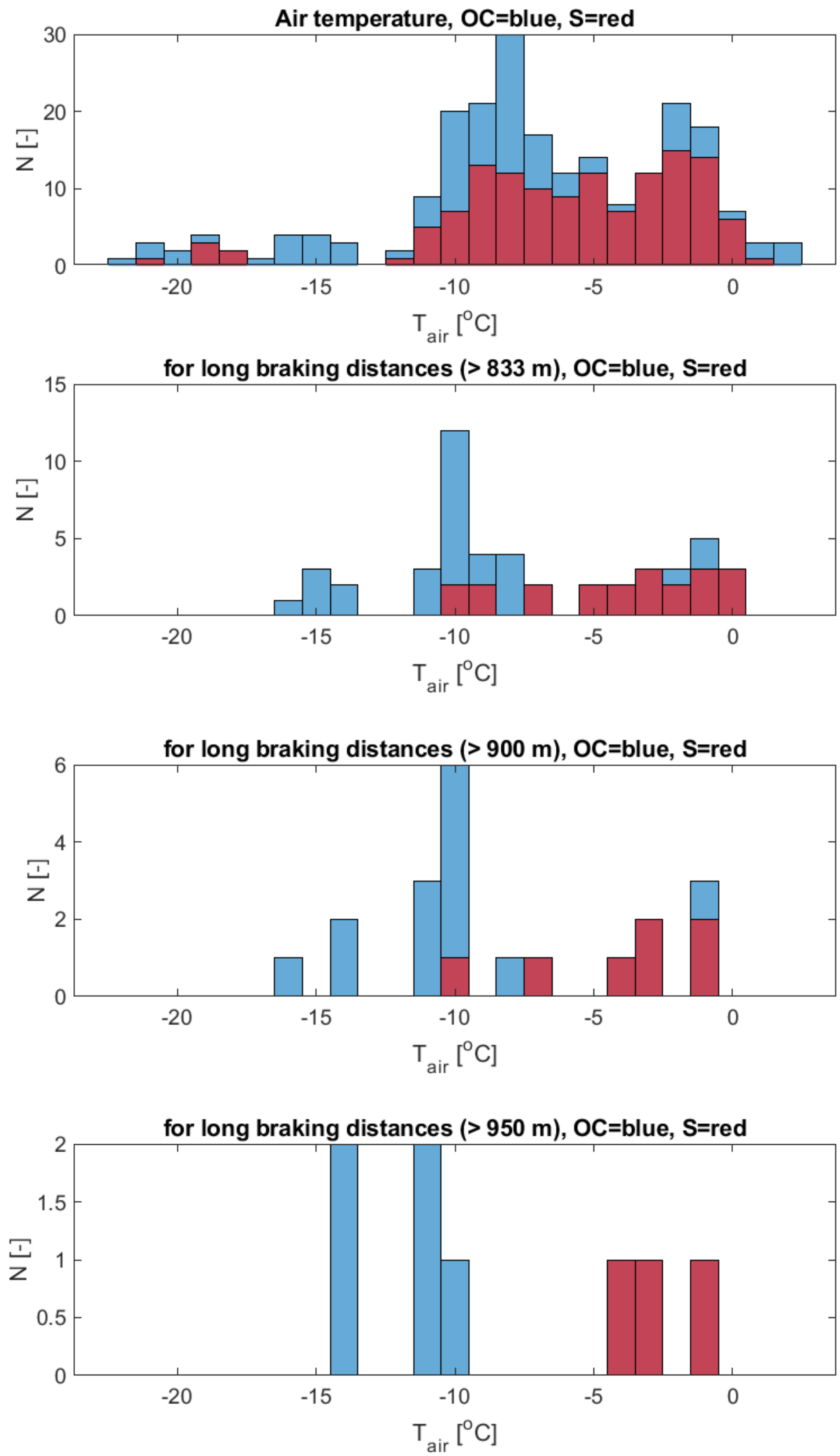

Figure 57 Overview of number of brake cycles for given air temperature ranges. Top: All cycles, second top cycles > 833 m, second bottom > 900 m and bottom > 950 m. Sinter is red and organic is blue.

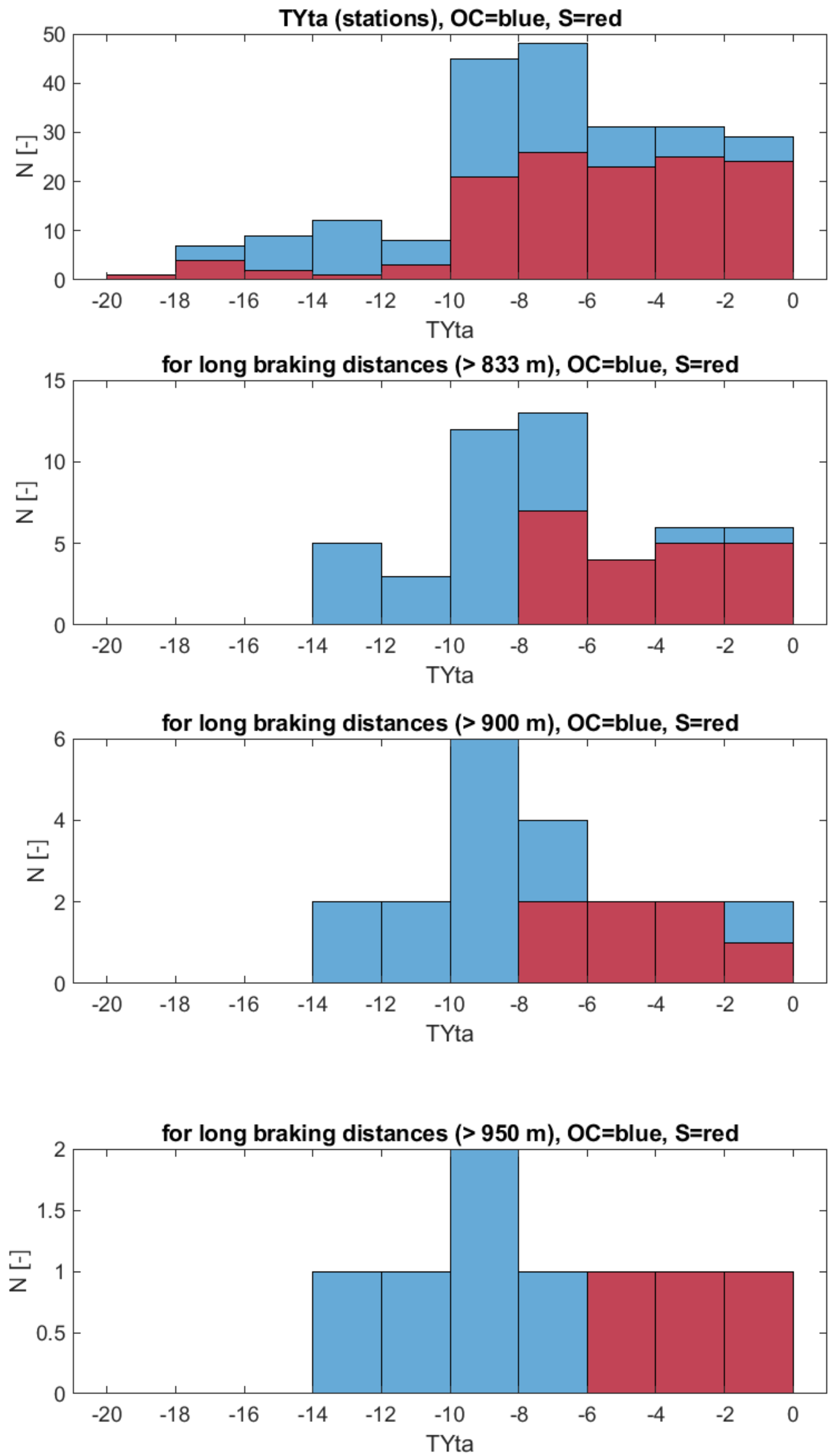

Figure 58 Overview of number of brake cycles for given surface temperature ranges. Top: All cycles, second top cycles > 833 m, second bottom > 900 m and bottom > 950 m. Sinter is red and organic is blue.

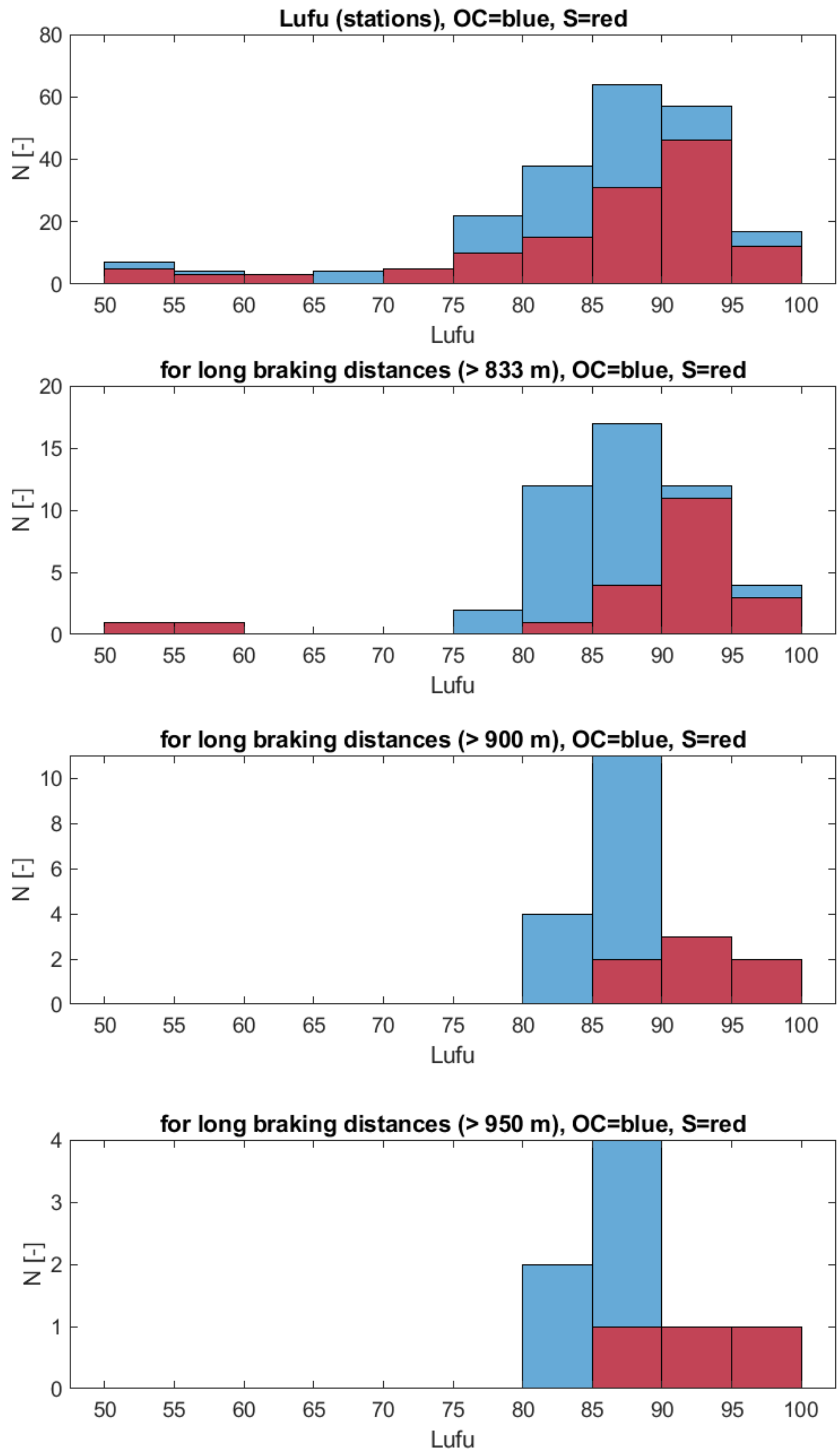

Figure 59 Overview of number of brake cycles for given air humidity ranges in [%]. Top: All cycles, second top cycles > 833 m, second bottom > 900 m and bottom > 950 m. Sinter is red and organic is blue.

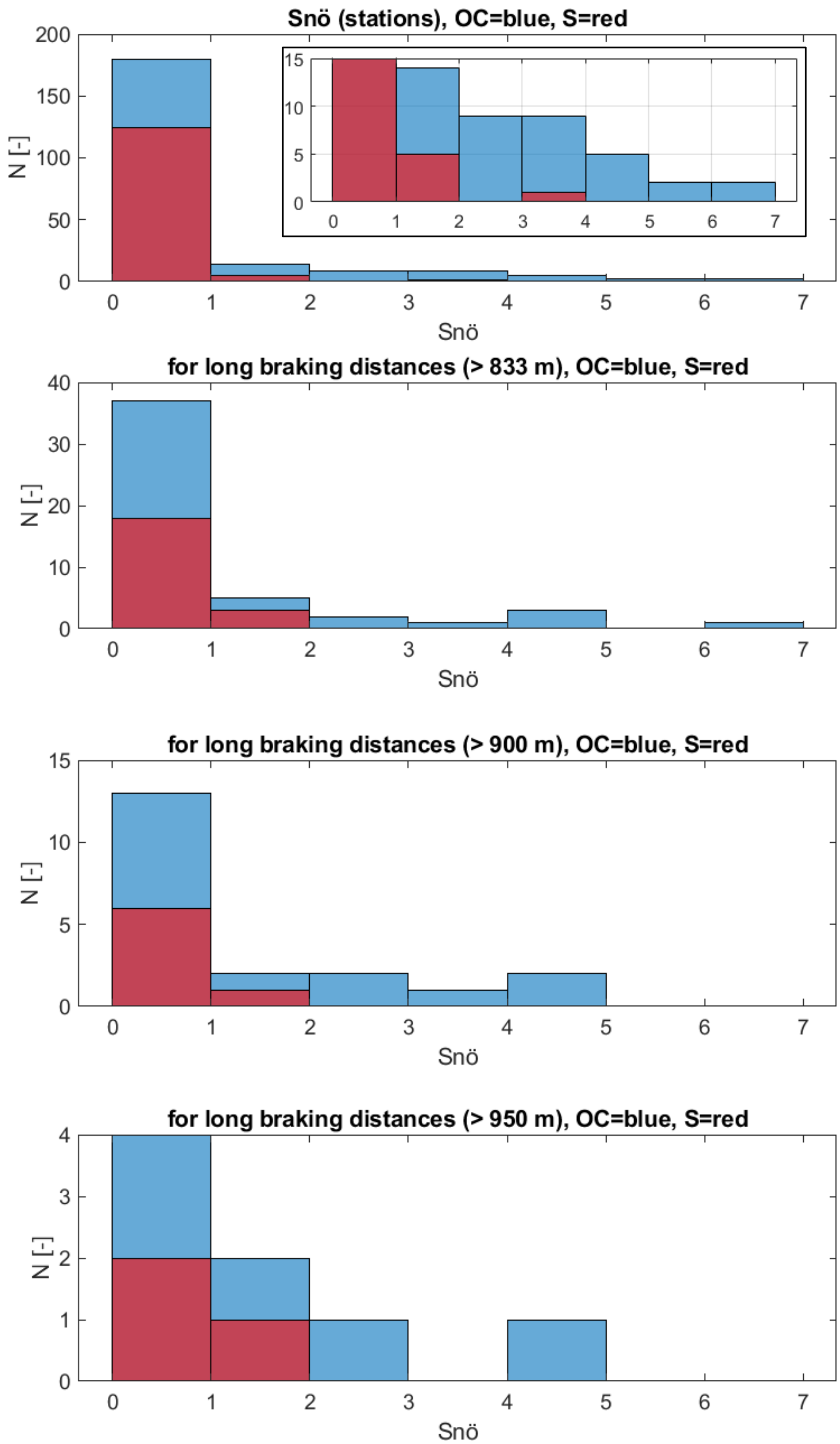

Figure 60 Overview of number of brake cycles for given snow intensity (mm / 30 min) ranges. Top: All cycles, second top cycles > 833 m, second bottom > 900 m and bottom > 950 m. Sinter is red and organic is blue.

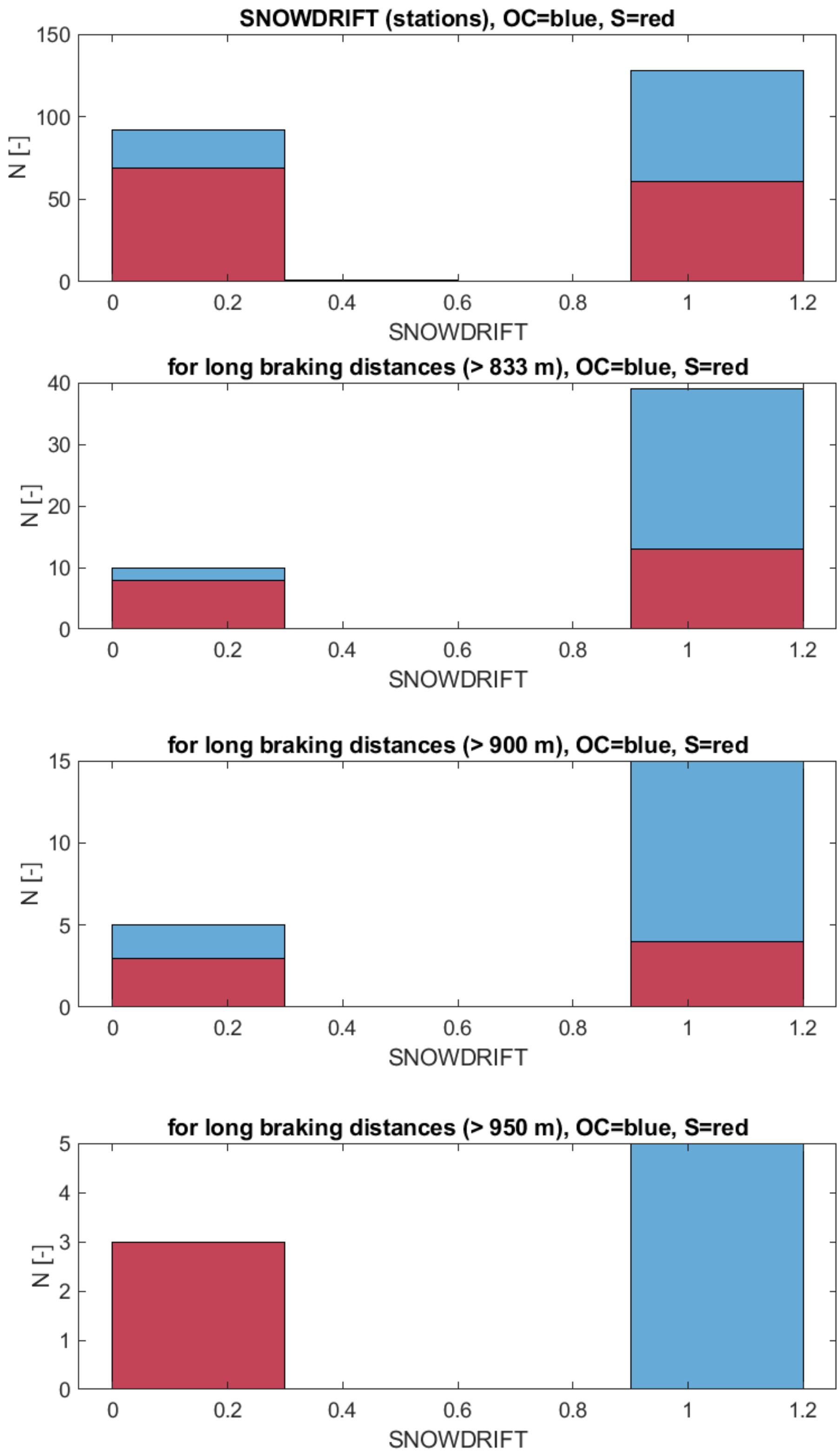

Figure 61 Overview of number of brake cycles for snow drift ranges (only values are "0" no risk of snow drift and "1" with risk of snow drift). Top: All cycles, second top cycles > 833 m, second bottom > 900 m and bottom > 950 m. Sinter is red and organic is blue.

APPENDIX B OVERVIEW OF WEATHER CONDITIONS FOR WINTERS 2016-2017 UP TO 2019-2020

Comparison of winter conditions for four past winters. Data from station 2553, Niemisel near brake site 2.

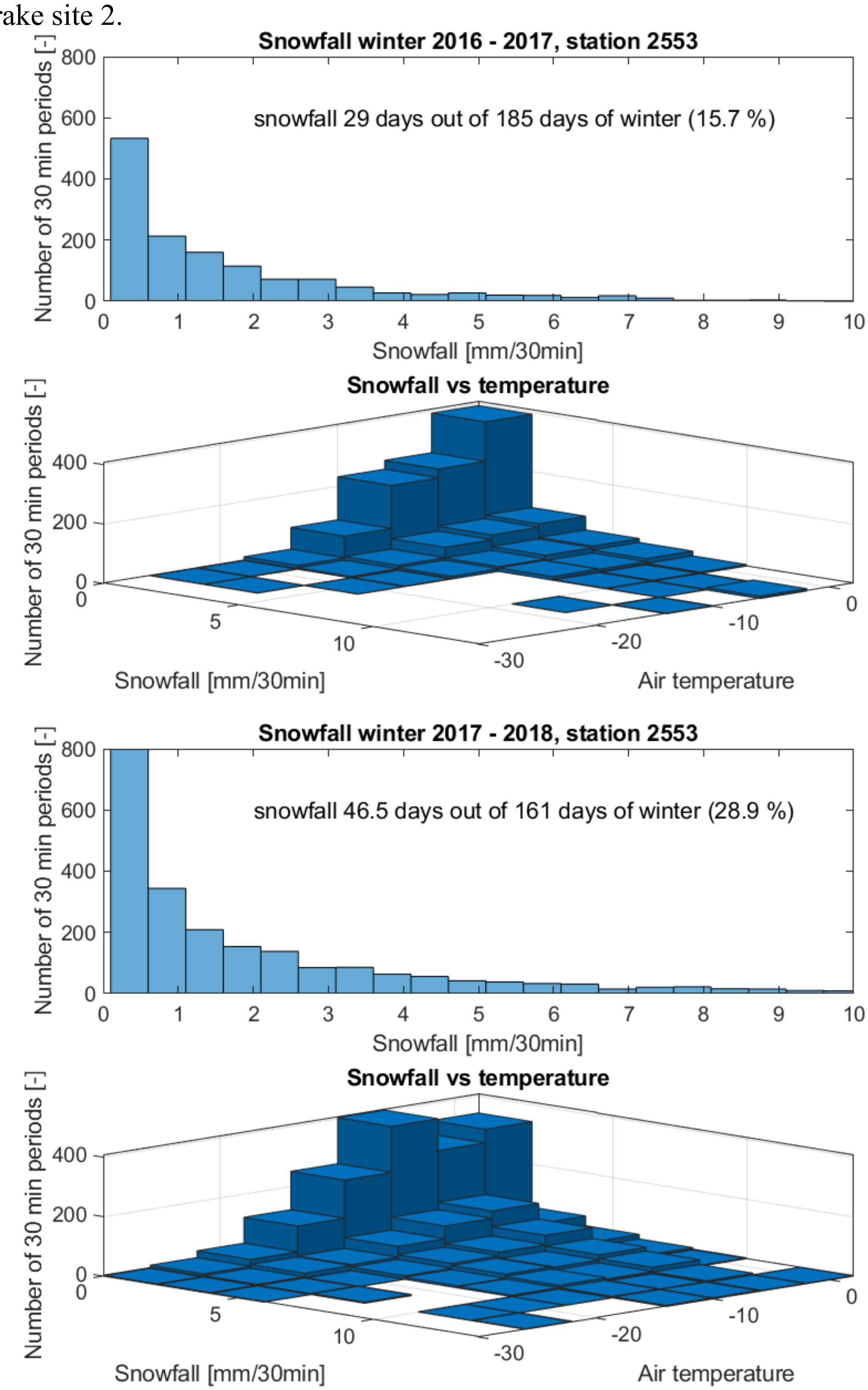

Figure 62 Snowfall and temperatures, winter 2016-2017 above and winter 2017-2018 below.

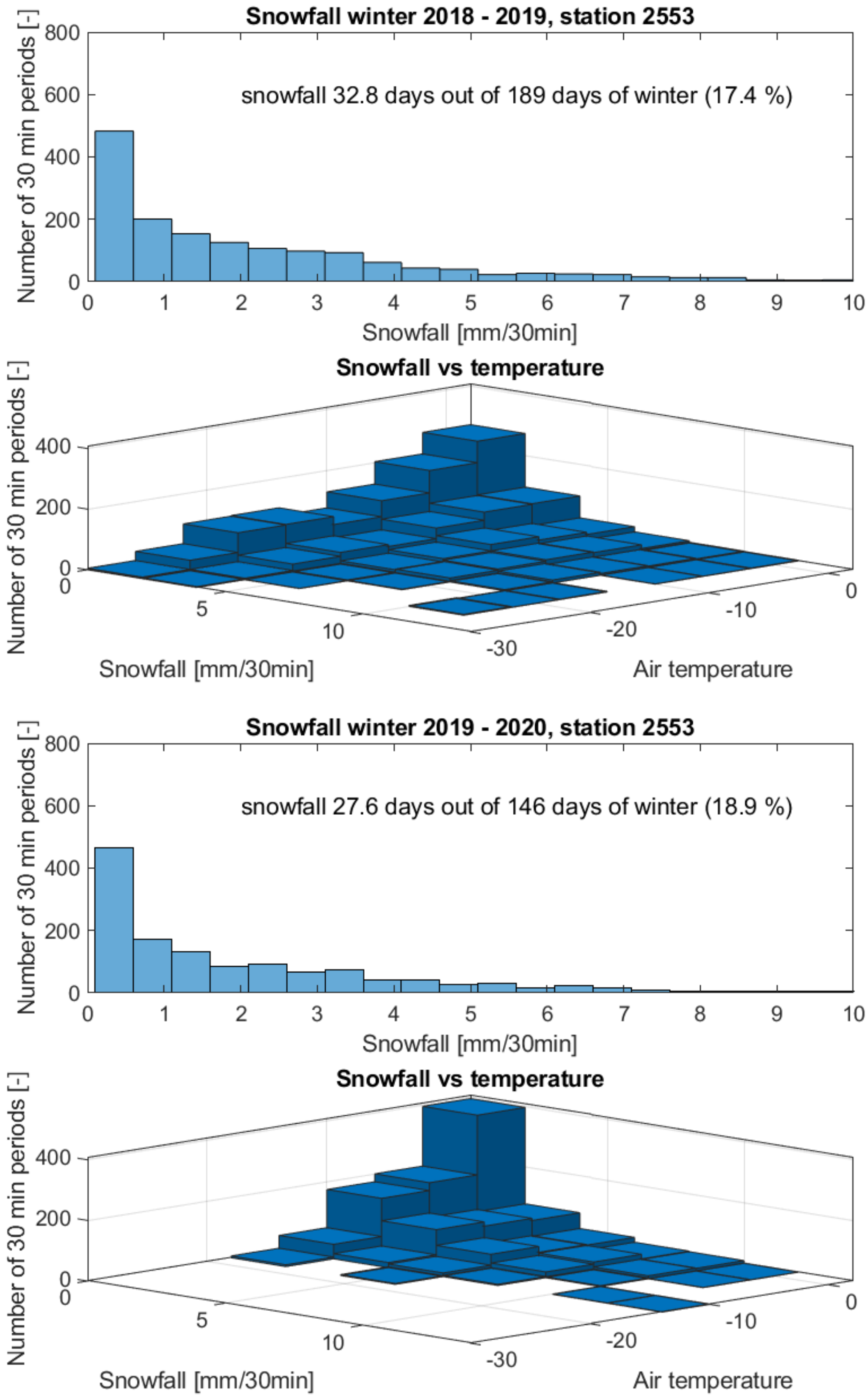

Figure 63 Snowfall and temperatures, winter 2018-2019 above and winter 2019-2020 below.

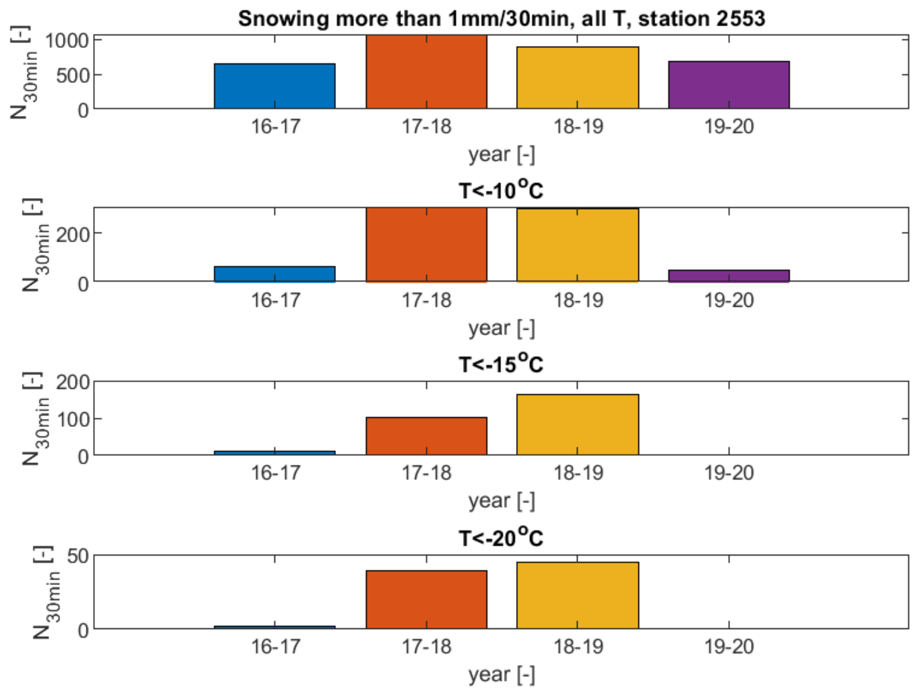

Figure 64 Snowfall of more than 1mm / 30 min and temperatures for winters 2016-2017 until 2019-2020. Number of occasions (i.e number of 30 min periods) in total (above), number of occasions of snowing when temperature was below -10 ºC (second top), below -15ºC (second bottom), and below -20 ºC (bottom).

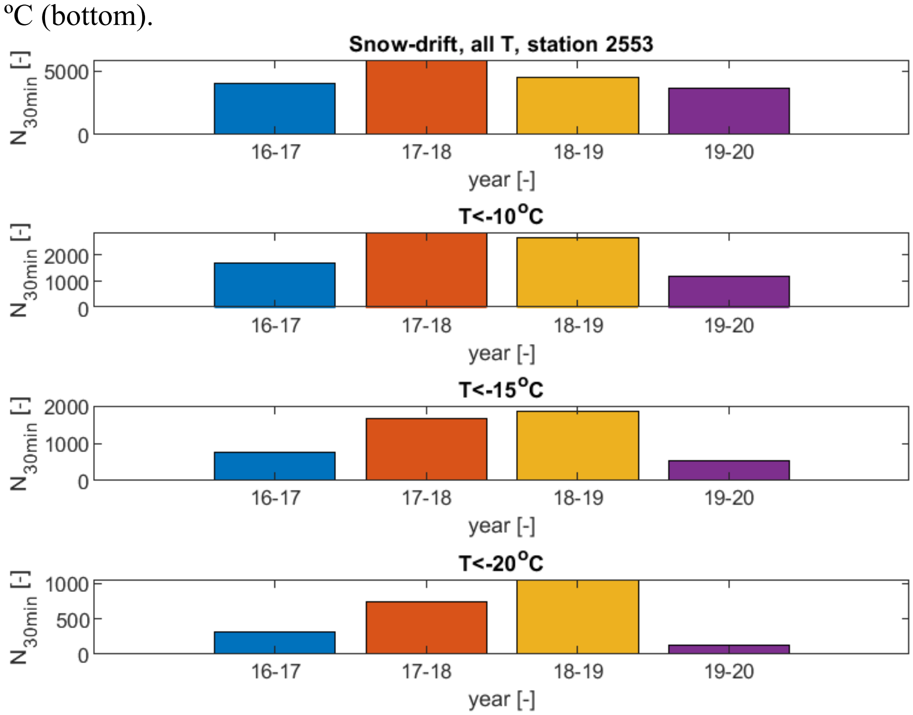

Figure 65 Snowdrift and temperatures for winters 2016-2017 until 2019-2020. Number of occasions (i.e number of 30 min periods) in total (above), number of occasions of snowing when temperature was below -10 ºC (second top), below -15 ºC (second bottom), and below -20 ºC (bottom).

APPENDIX C BRAKE CYLINDER VALVE MALFUNCTIONING

It was noted during testing that there for some brake cycles were no increase of brake cylinder pressure for one or two of the wagons. Upon further control, a total of 18 stops showed nil brake cylinder pressures for one or two of the wagons. All of these are for braking with sinter brake blocks and occurred for 5 consecutive stops on 20 February and after this for another 13 stops on 26-27 February. During the former period, the problems concerned wagon 2 and wagon 4 and for the latter mainly wagon 2. For the latter period, it was noted by the locomotive driver at the end of the 27 February that the handle for controlling the brakes on wagon 2 had been shifted to a position so that the braking was switched off. It was hypothesized that the handle had been hit by a piece of ice during operation on that same day, since braking had stopped working during operation on that day (as registered by pressure sensor). For the remaining brake cycles with problems, they constitute the first braking cycles in the morning of a cold day. The first registered temperatures for the mornings was -22ºC, -22ºC, and -16ºC respectively for the 20, 26 and 27 February. For all these occasions, when the air temperature later increased to about -10 ºC, the brakes on all wagons were again in operation.

The detection of non-braking wagons builds on evaluation of acquired brake cylinder pressures and brake triangle forces on the wagons. For the first 65 stops on sinter out of a total of 130 stops, a small DAQ system was employed and it was not possible to make such a detection. The resulting acceleration values at full braking is shown in Figure 66 for braking with sinter blocks, with separate markers for braking with the small DAQ system, the large DAQ system and for disregarded cycles. In the figure also a surface has been fitted to the results and the resulting fit is given in the plots as a line. The markers for disregarded stops (blue pentagrams) clearly stand out as outliers for W1-W5, being the only cycles with average deceleration being less than 0.5 m/s^2. For R0 the situation it is not that clear, but the disregarded cycles still are outliers as compared to the remaining data. The spread in data points acquired with the small DAQ system is similar to the one acquired with the large system, which is an indication that there should have been no wagon braking problems during brake testing with this small DAQ system.

The deceleration results are given in Figure 67 for the organic blocks. Here, all data were acquired with the small DAQ system. Noteworthy is that there seemingly are now outliers in the data for R0 or for W3-W5. There is a consistent spread in data that go well together with brake cycles at similar ranges of temperature. For W2 there could be two outliers at the warmest conditions, one at about 1 °C and another one at about 2.2 °C. For information: these two are for the fifth and the sixth brake cycles performed during the entire test campaign.

Upon detection of the problems with the non-existent build-up of brake cylinder pressures on some wagons, a workshop was booked for 29 February, at the EuroMaint facility in Luleå. It was then found that there were large quantities of Kemetyl antifreeze alcohol in the brake valves on some of the wagons. A EuroMaint brake expert stated that braking on a wagon may fail entirely if there are too much alcohol in the brake valve. The brake valves on all wagons were properly drained at the workshop in Luleå.

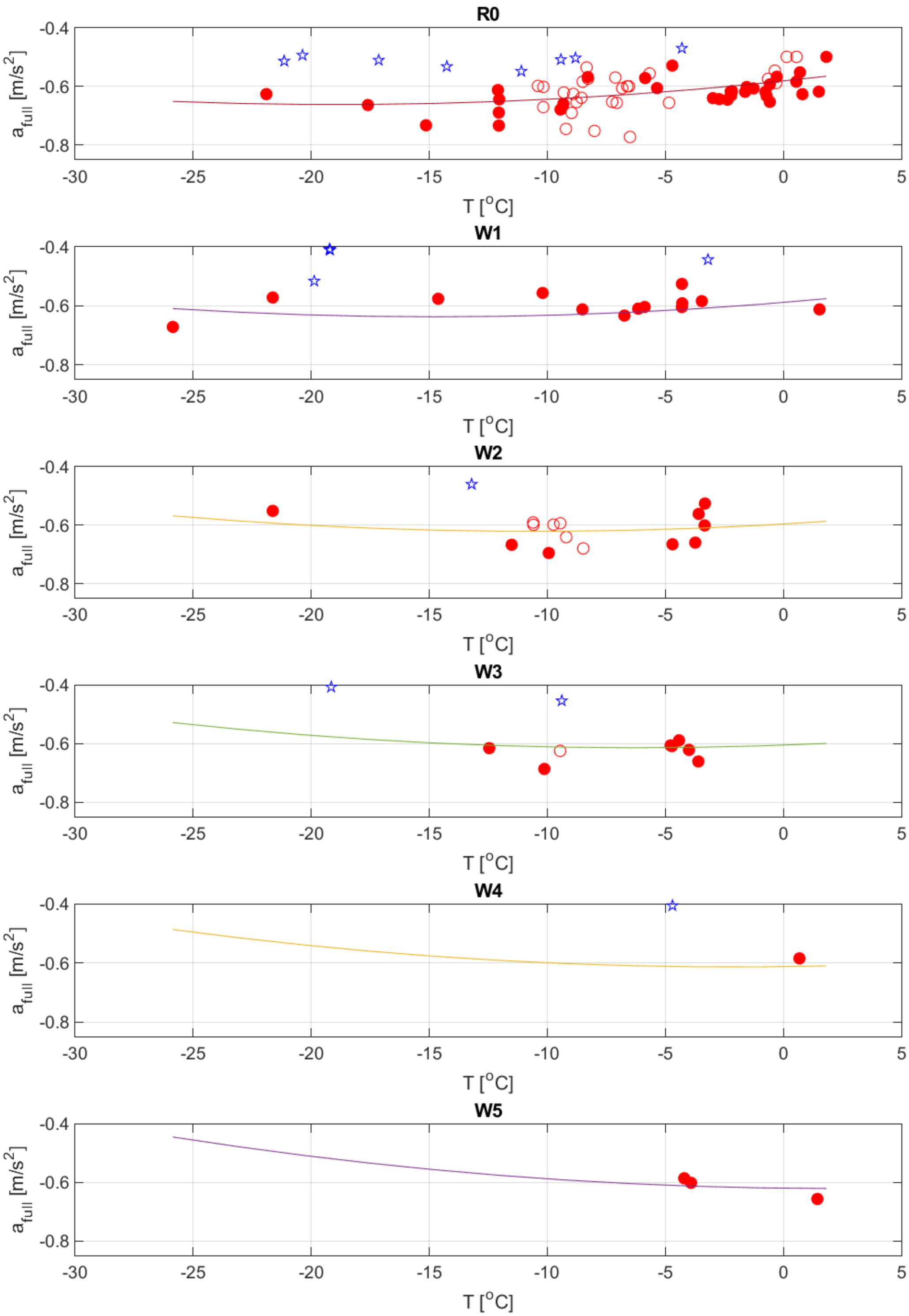

Figure 66 Results for sinter blocks. Average acceleration during period from time point at which 90% of maximum brake cylinder pressure is first reached until time point during brake pressure decrease at which deceleration is maximum. From top to bottom the plots are in sequence for UIC winter condition R0 to W5. Results from time period when using the small DAQ system are marked with red circles and results for the large DAQ system are marked with red dots. Results for otherwise disregarded brake cycles are marked with blue pentagram markers (i.e. stars).

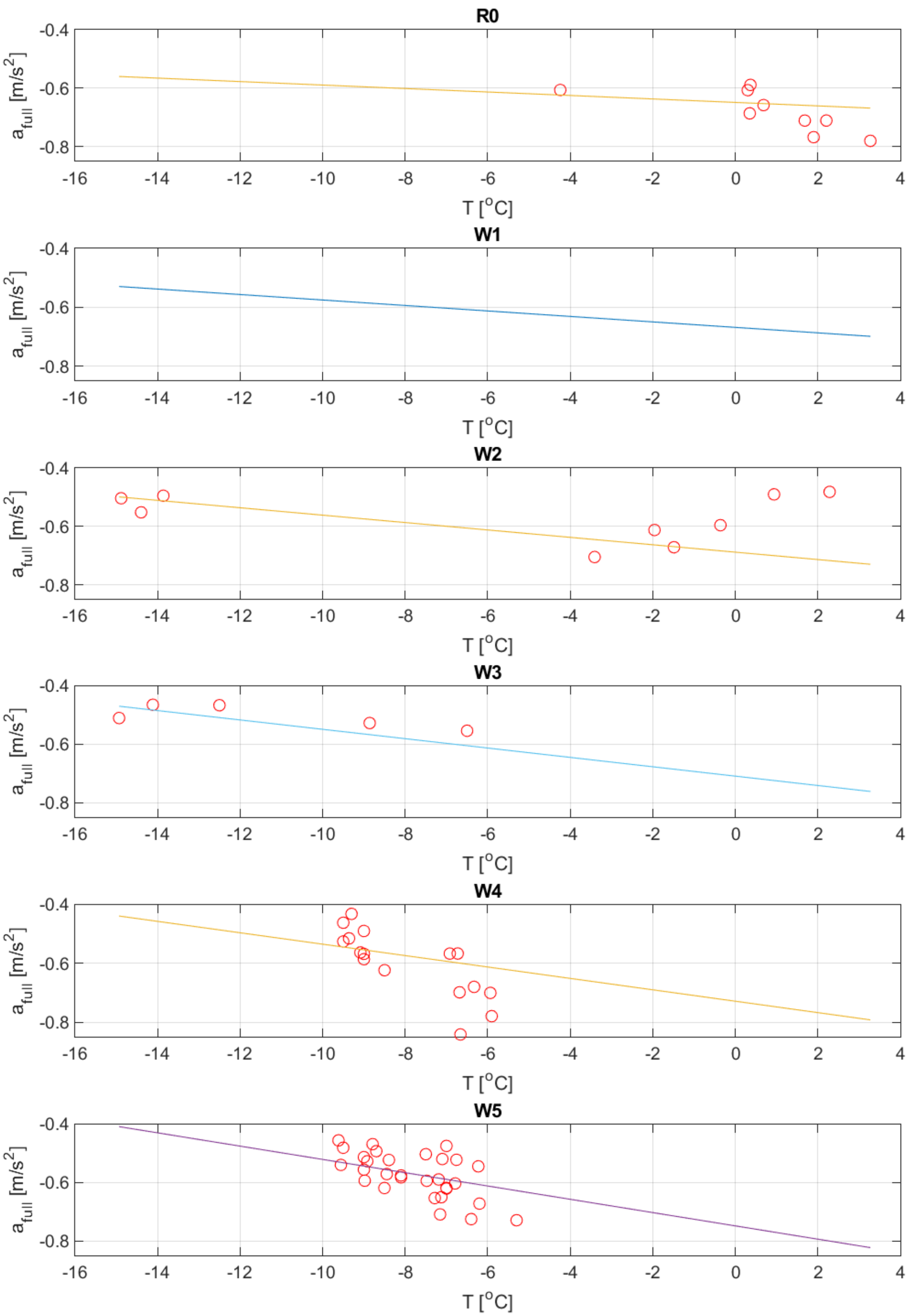

Figure 67 Results for organic composite blocks. Average acceleration during period from point at which 90% of maximum brake cylinder pressure is first reached until time point during brake pressure decrease at which deceleration is maximum. From top to bottom the plots are in sequence for UIC winter condition R0 to W5. Results from time period when using the small DAQ system are marked with red circles. There are no cycles for the large DAQ system and there are no disregarded cycles (thus no red dot or blue pentagram markers).